

On the Causality Verification and Enforcement of Signal Power Integrity Models

A Thesis

Presented in Partial Fulfillment of the Requirements for the

Degree of Master of Science

with a

Major in Electrical Engineering

in the

College of Graduate Studies

University of Idaho

by

Md Aminul Hoque

Major Professor: Ata Zadehgol, Ph.D.

Committee Members: Herbert Hess, Ph.D.; Karen Frenzel, Ph.D.

Department Administrator: Mohsen Guizani, Ph.D.

May 2017

Authorization to Submit Thesis

This thesis of Md Aminul Hoque, submitted for the degree of Master of Science with a major in Electrical Engineering and titled “On the Causality Verification and Enforcement of Signal Power Integrity Models,” has been reviewed in final form. Permission, as indicated by the signatures and dates given below, is now granted to submit final copies to the College of Graduate Studies for approval.

Major Professor: _____ Date _____
Ata Zadehgol, Ph.D.

Committee
Members: _____ Date _____
Herbert Hess, Ph.D.

_____ Date _____
Karen Frenzel, Ph.D.

Department
Administrator: _____ Date _____
Mohsen Guizani, Ph.D.

Abstract

The ever-growing development in high-speed digital systems in speed and complexity is greatly facilitated by creating macro-model for representing electronic packages. Signal Integrity (SI) engineers extensively use macro-model of digital systems in electronic circuit simulators to verify the validity and integrity of different circuits and their behavior upon simulation. When creating the macro-models for future simulation and design, verifying the stability, passivity, and causality of the data is a very important task. In this thesis, we primarily focus our discussion on causality of the system.

Causality verification of linear interconnect system in high speed digital systems is of paramount importance. A real physical system is always causal, but the measured S-parameter of such systems may contain causality violations. Different techniques of causality detection have been introduced in literature over time. We analyze some of these techniques and focus on their merits and demerits. A new method for checking causality in frequency-domain is proposed along with two ways of enforcing causality on original data. We compare error in these methods after enforcement.

Analysis of proposed techniques and conclusions brought about on these techniques are supported by appropriate numerical examples. We performed tests on both artificial systems and actual physical system models for verification. Additionally, we demonstrated tests in both time domain and frequency domain for verification and enforcement of causality.

Acknowledgements

The success of any project depends largely on the encouragement and guidance of many others. I take this opportunity to express my gratitude to the people who have been instrumental in the successful completion of this project.

I would like to express my special appreciation and thanks to my adviser Professor Dr. Ata Zadehgo, who has been a tremendous mentor for me. I would like to thank him for encouraging my research and for allowing me to conduct independent research with brilliant support. His advice on both research as well as on my career have been priceless.

I would also like to thank my committee members, Professor Herbert Hess and Professor Karen Frenzel for serving as my committee members and providing valuable feedback.

I would also like to thank my parents for keeping their faith on me. Especially I want to extend my gratitude towards my lovely wife, Nuzhat, without your support and encouragement nothing was possible.

I would also like to thank my fellow lab members: Protap, Venkatesh and Nuzhat for your generous effort in moving forward with the research. It would not be possible without the long group discussions and brain-storming that we have had among ourselves.

Lastly, I would like to acknowledge Brent Keeth, Ph.D., Sr. Fellow at Micron Technology, Inc., for supporting my research in the ACEM-SPI lab at the University of Idaho.

Table of Contents

Authorization to Submit Thesis	ii
Abstract	iii
Acknowledgements	iv
Table of Contents	v
List of Tables	viii
List of Figures	ix
1 Introduction	1
1.1 Objective	1
1.2 Overview	1
2 Literature Review	3
2.1 Introduction	3
2.2 Definition of Causality	4
2.2.1 Causality and Dispersion	5
2.2.2 Kramer-Krönig Relations	6
2.3 Causality of Sampled Data	12
2.3.1 The S-matrix	12
2.3.2 Challenges of Determining Causality of Sampled Data	13
2.3.3 Dispersion Relation With Subtractions	14
2.4 Different Methods of Causality Verification	15
2.4.1 Direct Hilbert Transform	17
2.4.2 Generalized Dispersion Relations	17
2.4.3 Minimum Phase and All-pass Decomposition	19

2.4.4	Causality Check by Analog Integration.....	20
2.4.5	Estimation of Causality Metric	21
2.4.6	Low Pass Filtering Approach	21
2.5	Enforcement of Causality.....	24
2.5.1	Causality Enforcement in Numerical Solutions of Maxwell's Equations..	24
2.5.2	Causality Enforcement by Hilbert Transform.....	24
2.5.3	Causality Enforcement by Delay Extraction	25
2.5.4	Causality Enforcement by Iterative FFT and IFFT.....	25
2.5.5	Causality Enforcement by Extracting Dominant Delay	26
2.5.6	Causality Enforcement by Extrapolation of Spectrum.....	26
2.5.7	Phase Perturbation Technique of Causality Enforcement	27
2.5.8	Stable Recursive Method for Causality Enforcement	27
2.6	Summary and Discussion	30
3	Causality Verification by Filtering	31
3.1	Introduction	31
3.2	Formulation.....	32
3.2.1	Scattering parameters.....	32
3.2.2	Filtered Fourier Transform	32
3.2.3	Error Threshold.....	34
3.3	Numerical Example.....	34
3.3.1	Analytic Example	34
3.3.2	Practical case.....	44
3.4	Summary.....	47
4	Causality Verification by Generalized Hilbert Transform	48
4.1	Generalized Dispersion Relations.....	48
4.2	Location of Subtraction Points	49

4.3	Reconstruction Operation	52
4.4	Numerical Integration	53
4.5	Error Thresholds	55
4.5.1	Truncation Error	55
4.5.2	Discretization Error	56
4.6	Numerical Simulation and Discussion	56
4.6.1	Analytic Example	57
4.7	Summary	70
5	Causality Verification and Enforcement of Signal Power Integrity Models by Filtered Hilbert Transform on Extrapolated Systems	71
5.1	Introduction	71
5.2	Dispersion Relations and the Hilbert Transform	73
5.3	The Low-pass Filter Approach	77
5.3.1	Minimum Phase Filter	77
5.3.2	Error Estimation	81
5.4	Numerical Extrapolation	83
5.4.1	Linear Extrapolation	83
5.4.2	Three Point Extrapolation	86
5.5	Detecting Causality Violation	89
5.6	Effect of Filter Parameters	92
5.7	Causality Enforcement	92
5.8	Summary	103
6	Summary and Conclusions	104
	References	106

List of Tables

5.1 Poles and residues for realizing the causal system $H(s)$	74
---	----

List of Figures

2.1	Time Domain response of the Causal Signal	8
2.2	Hilbert Transform of the Frequency response of the Causal Signal	9
2.3	Time Domain response of the Non-Causal Signal	10
2.4	Hilbert Transform of the Frequency response of the Non-Causal Signal	11
2.5	Causality Verification approaches	16
2.6	Causality Enforcement approaches	23
2.7	Modification of Impulse Response according to Reference [1]	29
3.1	Impulse response obtained from the filtered frequency responses given in (3.9). The dashed lines denote the threshold error bound. (Source: Md Aminul Hoque, Ata Zadehgol, On the Sensitivity of Causality Filter Parameters. Copyright ©2016, IEEE Electrical Design of Advanced Packaging and Systems (EDAPS) Symposium 2016.)	36
3.2	Impulse response obtained from the modified filtered frequency responses given in (3.9), leaving out the non-causal part. It is observed that the impulse response stays within the threshold limit for $t < 0$. (Source: Md Aminul Hoque, Ata Zadeh- hgol, On the Sensitivity of Causality Filter Parameters. Copyright ©2016, IEEE Electrical Design of Advanced Packaging and Systems (EDAPS) Symposium 2016.)	37
3.3	As a result of increased cut-off frequency, the time response stays within the threshold value, even though it is non causal, given in (3.9).(Source: Md Aminul Hoque, Ata Zadehgol, On the Sensitivity of Causality Filter Parameters. Copy- right ©2016, IEEE Electrical Design of Advanced Packaging and Systems (EDAPS) Symposium 2016.)	39

3.4	Decreasing the cut-off frequency yields non-causal characteristic of a purely causal sequence. (Source: Md Aminul Hoque, Ata Zadehgo, On the Sensitivity of Causality Filter Parameters. Copyright ©2016, IEEE Electrical Design of Advanced Packaging and Systems (EDAPS) Symposium 2016.)	40
3.5	Impulse response of the functions in (3.9). Clearly the $H_{22}(j\omega)$ is non-causal but it can not be detected when ω_m is reduced to $2\pi*40$ rad/s. (Source: Md Aminul Hoque, Ata Zadehgo, On the Sensitivity of Causality Filter Parameters. Copyright ©2016, IEEE Electrical Design of Advanced Packaging and Systems (EDAPS) Symposium 2016.)	42
3.6	Impulse response of the functions in (3.9) when ω_m is increased to $2\pi*60$ rad/s. The anticipation factor of $H_{22}(j\omega)$ is left out, so all functions are causal. But the result displays causality violation for $H_{11}(j\omega)$. (Source: Md Aminul Hoque, Ata Zadehgo, On the Sensitivity of Causality Filter Parameters. Copyright ©2016, IEEE Electrical Design of Advanced Packaging and Systems (EDAPS) Symposium 2016.)	43
3.7	Impulse response of the elements of S-matrix for the 1351 frequency point S-parameters. It is observed that the impulse response stays within the threshold limit for $t < 0$ up to $t = -25s$. (Source: Md Aminul Hoque, Ata Zadehgo, On the Sensitivity of Causality Filter Parameters. Copyright ©2016, IEEE Electrical Design of Advanced Packaging and Systems (EDAPS) Symposium 2016.)	45
3.8	Impulse response of the elements of S-matrix. Causality violation is seen at $t = -37s$ and $t = -58s$ as the time response of the S_{11} and S_{22} go beyond the threshold value. (Source: Md Aminul Hoque, Ata Zadehgo, On the Sensitivity of Causality Filter Parameters. Copyright ©2016, IEEE Electrical Design of Advanced Packaging and Systems (EDAPS) Symposium 2016.)	46
4.1	Truncation error bound vs. normalized angular frequency with $\epsilon = 0.1$	51
4.2	Real and Imaginary part of the input transfer function	58

4.3	Reconstructed Real part of the input transfer function. Since the reconstructed output stays within the threshold, the system is causal	59
4.4	Reconstructed Imaginary part of the input transfer function. Since the reconstructed output stays within the threshold, the system is causal	60
4.5	Real and Imaginary part of the input transfer function, with Gaussian perturbation	62
4.6	Reconstructed Real part of the input transfer function. Since the reconstructed output goes beyond the threshold, the system is non-causal	63
4.7	Reconstructed Real part of the input transfer function (in log scale). Since the reconstructed output does not go beyond the threshold, the system is causal . .	65
4.8	Reconstructed imaginary part of the input transfer function (in log scale). Since the reconstructed output does not go beyond the threshold, the system is causal	66
4.9	Reconstructed Real part of the input transfer function (in log scale) with the perturbation. The reconstructed output can be used as the causality enforced response	68
4.10	Reconstructed imaginary part of the input transfer function (in log scale) which shows causality violation.	69
5.1	Comparison of imaginary part of $H_c(j\omega)$ and the Hilbert Transform of the real part of $H_c(j\omega)$. Although the function is causal, reconstructed imaginary does not match with the original.	75
5.2	Comparison of real part of $H_c(j\omega)$ and the Hilbert Transform of the imaginary part of $H_c(j\omega)$. Although the function is causal, reconstructed real does not match with the original.	76
5.3	Comparison of imaginary part of $H_c f(j\omega)$ and the Hilbert Transform of the real part of $H_c f(j\omega)$. The reconstruction error is much less than Fig. 5.2, but still significant close to ω_{max}). Here, $nn = 3$ and $rp = 3$ dB.	79
5.4	Comparison of imaginary part of $H_c(j\omega)$ and the Hilbert Transform of the imaginary part of $H_c(j\omega)$. Here, $nn = 3$ and $rp = 3$ dB.	80

- 5.5 Comparison of imaginary part of $H_{cf}(j\omega)$ and the Hilbert Transform of the real part of $H_{cf}(j\omega)$ using Linear extrapolation. The reconstruction error in the vicinity of ω_{max} is removed. Filter parameters: $nn = 3$ and $rp = 3$ dB. Here, $\omega_{max} = 8000$ rad/s, $\omega_{ex} = 12000$ rad/s 84
- 5.6 Comparison of imaginary part of $H_{cf}(j\omega)$ and the Hilbert Transform of the real part of $H_{cf}(j\omega)$ using Linear extrapolation. Here, $nn = 3$ and $rp = 3$ dB and $\omega_{max} = 8000$ rad/s, $\omega_{ex} = 12000$ rad/s. 85
- 5.7 Comparison of imaginary part of $H_{cf}(j\omega)$ and the Hilbert Transform of the real part of $H_{cf}(j\omega)$ using Three-point extrapolation. The reconstruction error in the vicinity of ω_{max} is removed. Filter parameters: $nn = 3$ and $rp = 3$ dB. Here, $\omega_{max} = 8000$ rad/s, $\omega_{ex} = 12000$ rad/s 87
- 5.8 Comparison of imaginary part of $H_{cf}(j\omega)$ and the Hilbert Transform of the real part of $H_{cf}(j\omega)$ using Three-point extrapolation. Here, $nn = 3$ and $rp = 3$ dB and $\omega_{max} = 8000$ rad/s, $\omega_{ex} = 12000$ rad/s. 88
- 5.9 Comparison of imaginary part of $H_{ncf}(j\omega)$ and the Hilbert Transform of the real part of $H_{ncf}(j\omega)$ using linear extrapolation. The reconstruction goes beyond the threshold around 2500 rad/s, where the non-causal pole location is located. It is more clearly visible in the zoomed box. Filter parameters: $nn = 3$ and $rp = 3$ dB. Here, $\omega_{max} = 8000$ rad/s, $\omega_{ex} = 12000$ rad/s 90
- 5.10 Comparison of real part of $H_{ncf}(j\omega)$ and the Hilbert Transform of the imaginary part of $H_{ncf}(j\omega)$ using linear extrapolation. The reconstruction goes beyond the threshold around 2500 rad/s, where the non-causal pole location is located. It is more clearly visible in the zoomed box. Filter parameters: $nn = 3$ and $rp = 3$ dB. Here, $\omega_{max} = 8000$ rad/s, $\omega_{ex} = 12000$ rad/s. 91
- 5.11 Hilbert Transform performed on real part of $H_{fc}(j\omega)$ with filter parameters: $nn = 6$ and $rp = 6$ dB. Here linear extrapolation is used with $\omega_{max} = 8000$ rad/s, $\omega_{ex} = 12000$ rad/s. 93

5.12 Hilbert Transform performed on real part of $H_{fnc}(j\omega)$ with filter parameters: $nn = 2$ and $rp = 3$ dB. Here linear extrapolation is used with $\omega_{max} = 8000 \text{ rad/s}$, $\omega_{ex} = 12000 \text{ rad/s}$ 94

5.13 Enforcing causality by Option A using Linear Extrapolation. That imaginary part is again used for generating the real part, which is shown here and we observe a full match. Filter parameters: $nn = 3$ and $rp = 3$ dB. Here, $\omega_{max} = 8000 \text{ rad/s}$, $\omega_{ex} = 12000 \text{ rad/s}$ 96

5.14 Enforcing causality by Option A using Thre-point Extrapolation. That imaginary part is again used for generating the real part, which is shown here and we observe a full match. Filter parameters: $nn = 3$ and $rp = 3$ dB. Here, $\omega_{max} = 8000 \text{ rad/s}$, $\omega_{ex} = 12000 \text{ rad/s}$ 97

5.15 Enforcing causality by Option B using Linear Extrapolation. Here, the reconstruction does not fully match, but stays within the threshold limit. Filter parameters: $nn = 3$ and $rp = 3$ dB. Here, $\omega_{max} = 8000 \text{ rad/s}$, $\omega_{ex} = 12000 \text{ rad/s}$. 98

5.16 Enforcing causality by Option B using Thre-point Extrapolation. Here, the reconstruction does not fully match, but stays within the threshold limit. Filter parameters: $nn = 3$ and $rp = 3$ dB. Here, $\omega_{max} = 8000 \text{ rad/s}$, $\omega_{ex} = 12000 \text{ rad/s}$. 99

5.17 Absolute error reported from Enforcing causality by Option A (Both linear and three-point extrapolation. Filter specification are as in Fig. 5.15. 101

5.18 Absolute error reported from Enforcing causality by Option B (Both linear and three-point extrapolation. Filter specification are as in Fig. 5.16. 102

CHAPTER 1

Introduction

1.1 Objective

Modern industry standards are constantly aiming at reaching higher speeds with lower power consumption. Naturally, these attempts increase the complication of electrical interfaces. Henceforth, the role of signal integrity analysis is growing continuously. Electrical signals have to travel between I/O through packages, connectors, traces, and vias of the printed circuit boards, backplanes, and more. The goal of signal integrity analysis is to provide an accurate assessment of electrical link-paths, connecting a set of transmitting and receiving devices to estimate the reliability of the link for signal propagation. This process is facilitated by using macro-model of digital systems in electronic circuit simulators to verify the validity and integrity of the circuits. Stability, passivity and causality are the fundamental criteria for ensuring an appropriate model that portrays the actual structure.

The objective of this thesis is to investigate different methods of causality test and address some issues associated with these. We propose some modifications of the existing techniques and discuss the results we obtain after improvising these modifications. The main part of the thesis proposes a new method of causality verification and enforcement in frequency-domain by applying direct Hilbert Transform on filtered data. We show that the method overcomes some fundamental issues associated with previously proposed techniques in literature. We also investigate some sensitivities of the proposed method on detecting causality accurately and specify an appropriate range for detecting causality violation correctly.

1.2 Overview

We have organized the thesis into several chapters. We begin with literature review - starting from the initial development on causality to the state of the art. Different methods of

causality verification and enforcement have been introduced over time, which are mentioned and analyzed in chapter 2. In the next chapter, we focus on existing issues with a newly proposed technique of causality verification in time-domain by applying minimum-phase low-pass filters. We investigate thoroughly with test cases which raises the validity of the technique in different scenarios. In the fourth chapter we discuss the frequency-domain approach for causality test and emphasize on sensitivities of some key parameters (location of subtraction points, number of subtraction points etc.) on this method. In chapter 5, we propose a new technique for causality verification and enforcement that solves some of the issues with the previously mentioned time-domain and frequency-domain approaches. Finally, we conclude in chapter 6 with suggestions on future prospects of this research work.

CHAPTER 2

Literature Review

Causality verification has been an existing problem for a long time. We can trace back to mid-twentieth century for early developments on causality, mostly found in physics and optical science. In this chapter, we describe a chronological discussion on causality verification and enforcement. In our analysis, we critically discuss advantages and shortcomings of different approaches found in literature.

2.1 Introduction

The ever-growing advancement in enhanced rendering digital systems in rapidity and complexity simultaneously is greatly advanced by creating macromodel presentation of electronic packages. Signal Integrity (SI) engineers extensively use macromodel of digital systems in electronic circuit simulators to verify the validity and integrity of different circuits and their behavior upon simulation [2], [3]. When creating the macromodels for future simulation and design, verifying the stability, passivity and causality of the data is a very important task [4].

For model extraction, engineers employ a common procedure that involves two main steps. First, the frequency domain response of a structure under test is obtained through numerical simulation or measurement. For example, we can consider the scattering matrix of any interconnect system [4]. It creates a set of responses of the structure under investigation in the frequency domain, in discrete sampled form. The later step involves developing a suitable model to represent the system and to further analyze or modify the system. Following these steps, a model that represents the measured data is obtained, although that does not ensure the convergence of simulation [5]. In order to take into account of these concerns, we must consider model behavioral checking which involves passivity, stability and causality verification. In this chapter, we focus on causality verification and enforcement of electrical interconnect models.

Through rigorous effort and research, it is widely validated that models containing causality violations lead to artifacts upon transient simulations. These artifacts may include early arrival of the signal, inaccurate amplitude and delay. If the modelling is inaccurate in the sense of frequency dependent losses, it may produce non-causal results [6–8]. The other possible factors that may lead to the development of a non-causal model includes improper choice of criteria of convergence, sample frequency and additional options for setup [9]. As a result, causality verification of models is of tremendous importance. All physical systems are by nature causal, but the models used for simulation and design may possess causality violations at certain frequencies. To get appropriate result from simulation, the models must be checked for causality violation and modified - if there is any violation, keeping the change to a minimum level. This thesis addresses each of these subjects in a chronological fashion.

We have organized this chapter into several sections, starting with the formal definition of causality in section 2.2. The time domain and frequency domain characteristics along with dispersion relations are described here. We describe the validity of Scattering parameters in section 2.3, along with the challenges associated with causality verification of band-limited sampled data. In section 2.4, we discuss different methods of checking causality in physical systems. Section 2.5 deals with several techniques of causality enforcement.

2.2 Definition of Causality

Causality is referred to the cause and effect characteristic of physically realizable systems. A system is causal if any response of that system does not arise before applying an input that generates the response. Any output occurring before the cause is referred to as non-causal [10]. Every physical structure has to abide by this definition. Causality is defined when a system with an impulse response $h(t)$, is zero whenever $t < 0$, in time domain. In other words, any change in its output is not visible till there is a change in the input signal.

2.2.1 Causality and Dispersion

While discussing causality, another physical phenomenon arises inevitably, which is 'Dispersion'. Dispersion refers to the relation between phase velocity and frequency. When a wave is propagating in a medium that is dispersive in nature, the shape of the time-localized wave can change. The initial development on the relationship between phase velocity and frequency was demonstrated in the solutions of spring coupled point masses in vibration [11, 12]. Early in the 1870s, dependence between attenuation and dispersion was established. Later, Krönig [13] and Kramers [14] argued that, the real and imaginary part of the refraction electromagnetic index (i.e., $c_0/c_p(\omega)$, the ratio between the speed of light and phase velocity) are related to the Hilbert transform of each other, as a result of causality and linearity. This concept was developed in the 1920s. The fact that the dispersion and loss are related to each other - is the significance of this relationship. The term "Kramers-Krönig relations" (or K-K relations) is broadly referred to the dependency among quantities that are mathematically represented by Hilbert transforms. One simple example could be when the two quantities may be considered as the real and imaginary parts of a complex function. In this case, we can express each pair as the integral over the other. Let us assume $H(j\omega)$ is the Fourier transform of $h(t)$, which is defined as the transfer function. Then, the following expressions (2.1a)-(2.1b) show a pair of Kramers-Krönig (K-K) relations for a complex function $H(j\omega)$ [10, 13–15]:

$$U(\omega) = \frac{1}{\pi} \int \frac{V(\omega')}{\omega - \omega'} d\omega' \quad (2.1a)$$

$$V(\omega) = -\frac{1}{\pi} \int \frac{U(\omega')}{\omega - \omega'} d\omega' \quad (2.1b)$$

where $H(j\omega) = U(\omega) + jV(\omega)$. These equations express the dependence between real and imaginary part of the transfer function and they are valid for all causal systems. An im-

portant finding from these relationships is that, to determine $\text{Re}\{H(j\omega)\}$ (or $\text{Im}\{H(j\omega)\}$) at any specific frequency, information of $\text{Im}\{H(j\omega)\}$ (or $\text{Re}\{H(j\omega)\}$) at all frequencies is needed. Hilbert transform can be performed in many different ways such as direct numerical integration [16,17] or interpolating indirectly using different kernels such as Hermitan [18], sinc [19] and rational [20] functions.

2.2.2 Kramer-Krönig Relations

Since their discovery, the K-K relations have occupied a significant role in the research of almost all forms of wave propagation. Some of the imporant areas of application are electromagnetics and optics [21], particle physics [10], electronics [22], quantum mechanics [23], nuclear magnetic resonance [24], and acoustics [25,26]. Initially, this type of dispersion relations were considered as general restrictions on physical theories. We can test the validity of the basic assumptions such as causality by comparing these dispersion relations with experiment [10].

We can assume a simple causal and non-causal function pair $f_c(t)$ and $f_{nc}(t)$ for validating the K-K relations, which are defined as:

$$f_{nc}(t) = u(t+1)u(-t+2) \quad (2.2a)$$

$$f_c(t) = u(t)u(-t+3) \quad (2.2b)$$

The frequency domain response of the signals are obtained by taking Fourier Transform of the equations (2.2a)-(2.2b) that can be expressed as:

$$F_{nc}(\omega) = \frac{\cos \pi\omega \sin 3\pi\omega}{\pi\omega} - j \frac{\sin \pi\omega \sin 3\pi\omega}{\pi\omega} \quad (2.3a)$$

$$F_c(\omega) = \frac{\sin 6\pi\omega}{2\pi\omega} - j \frac{\sin (3\pi\omega)^2}{\pi\omega} \quad (2.3b)$$

Then we determine the Hilbert Transform the real part of F_{nc} and F_c and compare them with the imaginary part of F_{nc} and F_c , respectively. According to the K-K relationships, the two functions should match only if the original signal is causal. We can clearly see in Figure 2.2 that the two curves match perfectly in case of a causal signal. On the other hand, the responses does not match when the original signal is non-causal as in Figure 2.4.

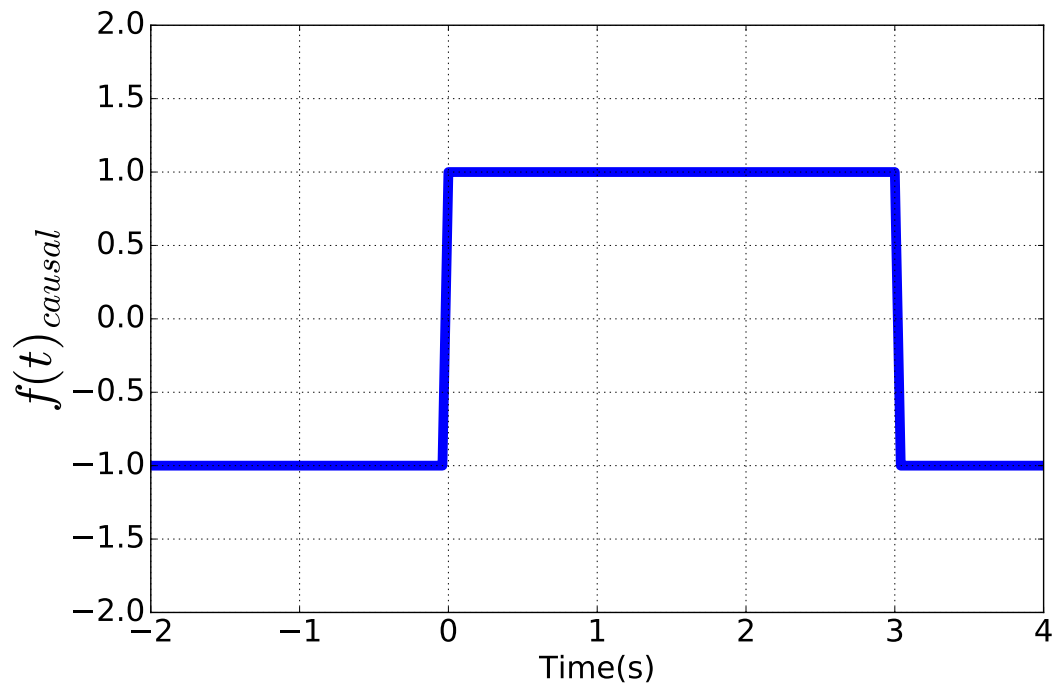


Figure 2.1: Time Domain response of the Causal Signal

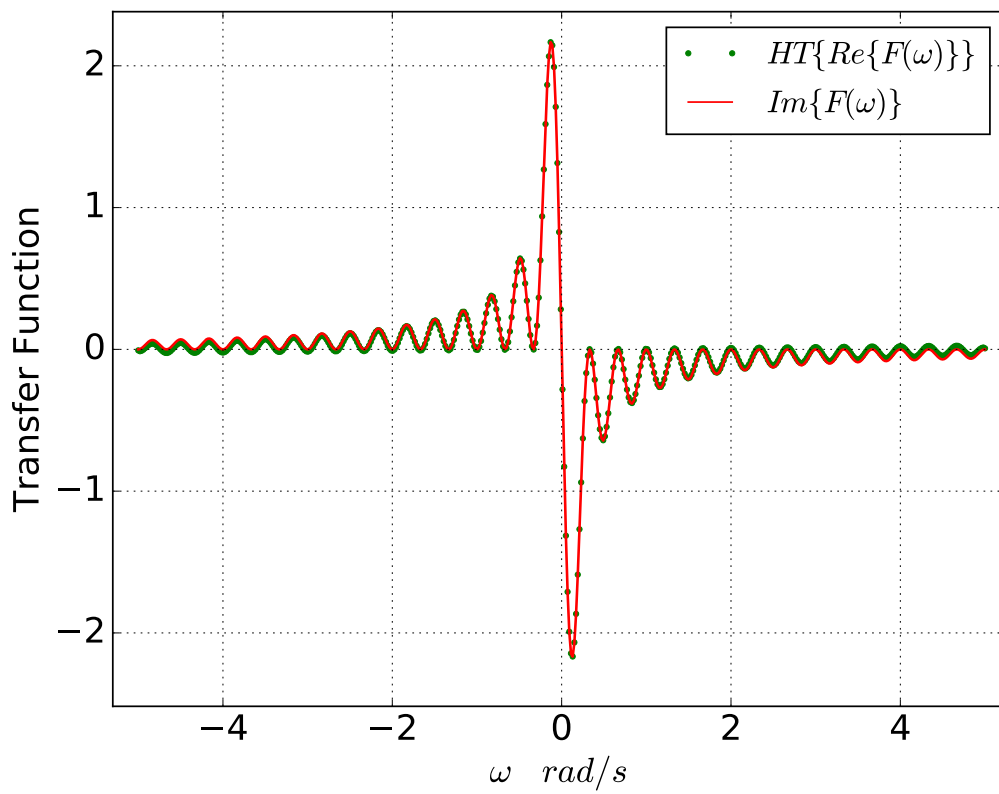


Figure 2.2: Hilbert Transform of the Frequency response of the Causal Signal

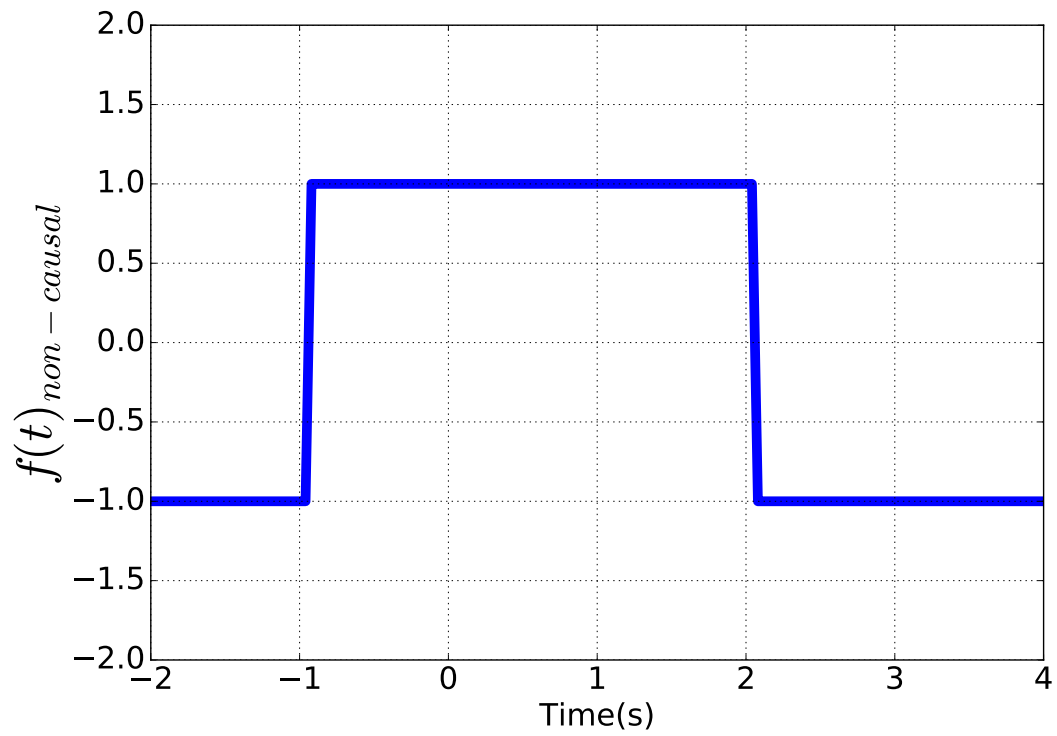


Figure 2.3: Time Domain response of the Non-Causal Signal

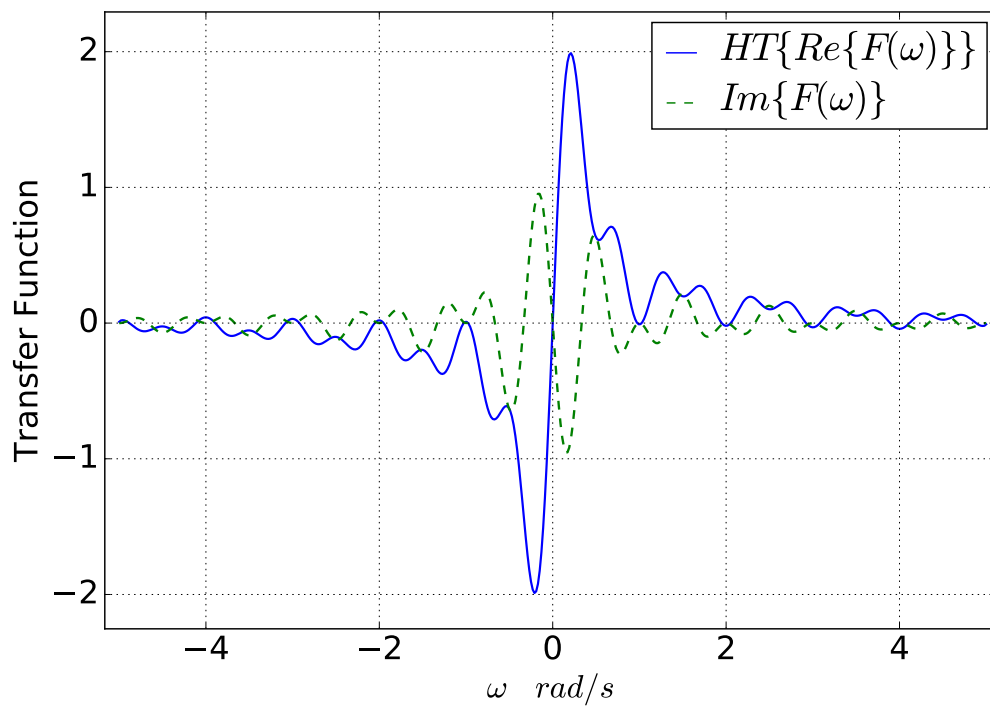


Figure 2.4: Hilbert Transform of the Frequency response of the Non-Causal Signal

In this work, we primarily focus on the effect of dispersion relations on determining causality of high-speed interconnect models. As interconnects are all real physical systems, they must be causal in nature, hence the dispersion relations should be validated in these systems. One way of checking the causality of the system under consideration is to validate the dispersion relations on them. If these relations hold for the model, then we can assume that the model is causal and therefore, shows consistency with the actual physical system.

2.3 Causality of Sampled Data

2.3.1 The S-matrix

In the early work on causality of dispersive systems, notable contribution by Heisenberg [27] and Wheeler [28] led to the development of the concept of Scattering matrix or S-matrix. The basic idea is that the interaction of the particles in a dispersive media can be represented by the S-matrix. Such interactions are observed by allowing particles to collide, which may result in several possible outcomes. Conceptually the collision process can be divided into three stages. The representation of the S-matrix is incorporated in the transition as:

$$initial\ stage \xrightarrow{S\text{-matrix}} final\ stage$$

The S-matrix stores all the information needed for computing any observable quantity in the system. The causality condition is the fundamental assumption for the system to hold. By rigorous effort and mathematical analysis, causality conditions are described in literature in many different aspects. The K-K relations are one of the conditions that is widely used for verifying causality of physical systems. Titchmarsh's theorem [15] provides us with four statements that are equivalent, i.e., if any one of them is true, the others will definitely be true. Later on, Schützer and Tiomno [29] formulated a causality condition for the scattering of nonrelativistic particles, which implies regularity of the S-function in the upper half of the

complex energy plane.

2.3.2 Challenges of Determining Causality of Sampled Data

While developing the dispersion relation of $H(j\omega)$, it was assumed to be a square integrable function, which may not be valid in practice. As the argument presented in [10], if $H(j\omega)$ is bounded, then for any input $X(\omega)$ that is a causal transformation will generate an output $Y(\omega)$ that is also a causal transformation. This does not imply that $H(j\omega)$ is causal. For instance, if $H(j\omega) = B$, where B is a constant, satisfies above statements. On the other hand, $\text{Re}\{H(j\omega)\}$ and $\text{Im}\{H(j\omega)\}$ could be totally unrelated and equation (2.1a)-(2.1b) would be meaningless for this choice of $H(j\omega)$. As a solution, an arbitrary constant K must be specified before relating $\text{Re}\{H(j\omega)\}$ and $\text{Im}\{H(j\omega)\}$.

A different formulation of the causality condition in nonrelativistic scattering was proposed by Van Kampen [30], which refers to the conservation of probability. His work suggests that the maximum probability of detecting a particle outside of the scatterer at any given moment is unity. Although Van Kampen's causality condition readily led to more detailed information about the analytic behavior of the S-function than Schützer and Tiomno's condition, it still does not exclude singularities other than the poles from the negative real axis, nor does it nullify the probability of analytic discontinuation to the lower half-plane. Therefore, only partial results can be extracted from this proposal.

Reference [17] addressed the Hilbert transformation as a means of verifying causality of measured continuous-wave data. In this section, a numerical formulation of the Hilbert transformation is demonstrated with several examples. Assuming a real valued signal $f(t)$, the spectrum $F(j\omega)$ has the following property [31]:

$$F(-j\omega) = F^*(j\omega) \quad (2.4)$$

This implies $\text{Re}\{H(j\omega)\} = U(\omega)$ is an even function of ω and $\text{Im}\{H(j\omega)\} = V(\omega)$ is

an odd function of ω . In this case, which is restrictive but practical at the same time, the Hilbert transform can be written as follows [32]:

$$U(\omega) = \frac{2}{\pi} \int_0^{\infty} \frac{\omega' V(\omega')}{(\omega^2 - \omega'^2)} d\omega' + K \quad (2.5a)$$

$$V(\omega) = -\frac{2\omega}{\pi} \int_0^{\infty} \frac{U(\omega')}{(\omega^2 - \omega'^2)} d\omega' \quad (2.5b)$$

As a result, we can determine one part of the transform within a range given by a constant K , if the other part is known. Using these equations, the reconstruction of a waveform is possible for determining transient response from the spectral data, which is also minimum phase. The outcome of this procedure is accurate only if the original data is minimum phase. Although, for real system data, we can not be certain that the reconstruction will be excellent [17]. However, the numerical evaluation of the Hilbert transformation involves integral over a singular point, which may lead to large errors. It is important to add the contribution of values at higher frequencies to the total integral. If the high frequency components are neglected, it can result in significant errors in the phase at high frequencies.

Two major challenges emerge when equation (2.1a)-(2.1b) are used numerically for scattering parameters (S-parameters). Firstly, integrals have to be approximated to the limited frequency range, which creates a large truncation error. Secondly, these relations are valid only for square-integrable functions as they decay to zero as frequency increases, which is not the case for general S-parameters [33].

2.3.3 Dispersion Relation With Subtractions

Considering these facts, alternate methods have been applied for direct causality check on sampled data (readily available as S-parameters). These methods are derived from the original dispersion relations (2.1a)-(2.1b) and based on approximations and assumptions related to the situation at hand. One of the early proposed method for causality check is

Dispersion Relations with Subtractions [34, 35].

As we mentioned before regarding the constant K that appears for relating $\text{Re}\{H(j\omega)\}$ and $\text{Im}\{H(j\omega)\}$, it is specified by giving the value of $H(j\omega)$ for some real frequency $\omega = \omega_0$. Using the mathematical operations on the dispersion relation around $\omega = \omega_0$ as described in [10], we come up with the modified dispersion relation:

$$H(j\omega) = H(j\omega_0) + \frac{\omega - \omega_0}{\pi j} \int \frac{[H(\omega') - H(\omega)]}{\omega' - \omega_0} \frac{d\omega'}{\omega' - \omega} \quad (2.6)$$

This relation is a typical dispersion relation for a function $H(j\omega)$ that satisfies the boundedness condition. It requires the subtraction of the constant $H(j\omega_0)$, therefore is named *Dispersion Relations with one Subtraction*. The usual practice is to choose the reference frequency at $\omega_0 = 0$, as such the subtracting constant is the static value of $H(j\omega_0)$. However, the method can be extended to more than one subtraction [36, 37]. In literature, this technique has been widely used for causality verification by distributing ω_0 frequencies over the entire bandwidth [38].

2.4 Different Methods of Causality Verification

Since the introduction of S-parameters in the field of science and engineering, different methods of causality verification and enforcement have been introduced. In this section, we try to summarize some of the important methods of verifying and enforcing causality. We begin with early developments and gradually introduce more recent updates on causality check. We can graphically represent the classification of causality check as shown in Fig. 2.5.

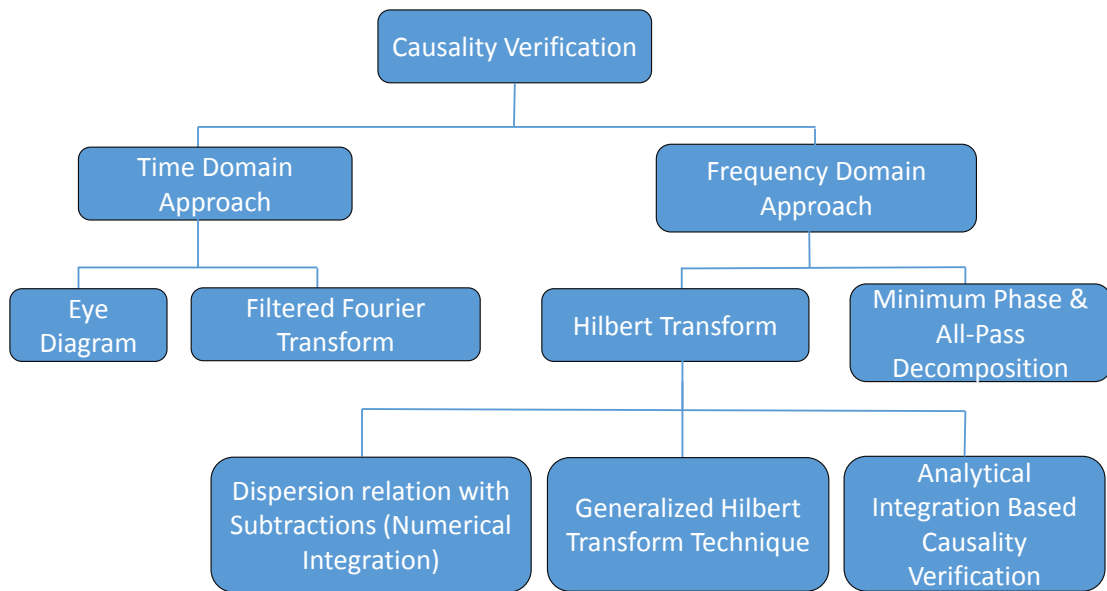


Figure 2.5: Causality Verification approaches

2.4.1 Direct Hilbert Transform

In the novel work by Antonini [16], direct Hilbert Transform is used to verify causality of sampled S-parameters. Numerical examples given in this work shows small but distributed error along the entire bandwidth. The root mean square (rms) value is used to verify causality (i.e., rms error less than 5% is assumed to be causal). In this method, the reconstructed responses (both magnitude and phase) fail to match the original at the borders because of the inherent approximations of the numerical application of Hilbert Transform. To minimize the error at upper boundary values, the measured bandwidth should be chosen in a way that the network function is measured beyond the frequency of interest. However, no rigorous estimate of the error bound is defined in this work.

2.4.2 Generalized Dispersion Relations

In order to overcome the challenges that arise when K-K relations are directly applied on S-parameters, causality verification for tabulated data using dispersion relation with subtractions was first demonstrated in reference [39]. An explicit error bound calculation technique was presented in this novel work. Additionally, a detailed analysis regarding the resolution of the proposed method is described. The validation of the method is further established in [40]. The direct discretization of (2.1a)-(2.1b) fails because of the finite bandwidth of the sampled data and finite number of discrete samples. Therefore, an error arises when trying to correlate the real and imaginary part of the data. The most significant contribution of this work is to formulate the error bound. Instead of directly using equations (2.1a)-(2.1b), a modified pair of dispersion relations are used [39]:

$$U(\omega) = \alpha_U(\omega) + \frac{\omega^n}{\pi} \int \frac{V(\omega') - \alpha_V(\omega')}{(\omega')^n} \frac{d\omega'}{\omega - \omega'} \quad (2.7a)$$

$$V(\omega) = \alpha_V(\omega) - \frac{\omega^n}{\pi} \int \frac{U(\omega') - \alpha_U(\omega')}{(\omega')^n} \frac{d\omega'}{\omega - \omega'} \quad (2.7b)$$

where

$$\alpha_U(\omega) = \sum_{V=0}^{n-1} \frac{U^{(V)}(0)}{V!} \omega^V, \quad \alpha_V(\omega) = \sum_{V=0}^{n-1} \frac{V^{(V)}(0)}{V!} \omega^V$$

Here, the number of subtractions is given by n . These expressions are extracted using two steps. First step involves subtracting the n -th order Taylor polynomial from $H(j\omega)$ and dividing the result by ω^n . Afterwards, the Hilbert Transform is applied on the result to get the expressions in equation (2.7a)-(2.7b). Although numerical evaluation of these relations requires the n -th order Taylor polynomial, which gets ill-conditioned for sampled data. This problem is solved in reference [39] by distributing the roots of the polynomial ω^n at frequencies other than $\omega = 0$:

$$U(\omega) = \beta_U(\omega) + \frac{\prod_{q=1}^n (\omega - \bar{\omega}_q)}{\pi} \int \frac{V(\omega') - \beta_V(\omega')}{\prod_{q=1}^n (\omega' - \bar{\omega}_q)} \frac{d\omega'}{\omega - \omega'} \quad (2.8a)$$

$$V(\omega) = \beta_V(\omega) - \frac{\prod_{q=1}^n (\omega - \bar{\omega}_q)}{\pi} \int \frac{V(\omega') - \beta_V(\omega')}{\prod_{q=1}^n (\omega' - \bar{\omega}_q)} \frac{d\omega'}{\omega - \omega'} \quad (2.8b)$$

where $\beta_F(\omega) = \sum_{q=1}^n l_q(\omega) F(\bar{\omega}_q)$ for $F = \{U, V\}$ and $l_q(\omega) = \prod_{p=1, p \neq q}^n \frac{(\omega - \bar{\omega}_p)}{(\bar{\omega}_q - \bar{\omega}_p)}$ (Lagrange Interpolation Polynomial). The optimal placement of the subtraction points is ensured by implying a Chebyshev distribution, which guarantees minimal truncation error. A bound for the truncation error is estimated assuming $|H(j\omega)| \leq 1$. Using these assumptions, causality verification is done by reconstructing the imaginary part and comparing it to the raw data. Examples in reference [39] shows excellent resolution of the causality check.

A similar approach with more practical examples is stated in [41]. Comparison with previous methods have been presented and it clearly shows the effectiveness of the proposed method mainly because the generalized Hilbert transform was utilized instead of the Hilbert transform. Moreover, the inaccuracy because of the truncation error was minimized and the effect of discretization error was reduced. A rigorous upper limit of the truncation error made the reduction of truncation error possible. Lastly, the difference of result in two different

methods of numerical integration (namely, Simpson’s rule and Trapezoidal rule) were used to take care of the numerical error associated with integration.

However, the causality check given in [41] and [39] has some limitations. The strategies depicted beforehand might be oversensitive while deciding causality infringement, consequently they may falsely declare an input as non-causal, which may not result in an erroneous transient simulation. Likewise, the testing strategies that actualize the current definition numerically are delicate to false-positive results (i.e., causal data inaccurately announced as non-causal).

More recently, in [5], [42] sampled S-parameters are to be guaranteed for causality prior to macromodeling, trying to diminish faulty result. The method described here are based on Hilbert Transform as given in [39,41]. Unfortunately, this method can likewise dispose of S-parameters that might not have brought about a mistaken transient simulation on account of the oversensitive way of the causality check. The reason behind the oversensitivity of the current method is that the threshold for the detection of violation is sometimes fixed at a littler number than required for acceptable transient simulation [43]. Thus, violations that would not have brought about a wrong transient simulation might be accounted for by the current detailing. Although, it is suggested in references [5, 42] that isolated single point causality violations may arise when the error threshold of the reconstructed data is small or model frequency points are widely spread. In most cases, ignoring the single point violations does not affect the convergence of simulation [5]. Additionally, the experiments in [5] suggests that it is more challenging to generate causal models having lower loss dielectrics.

2.4.3 Minimum Phase and All-pass Decomposition

Another approach based on minimum phase and all-pass decomposition was introduced in reference [44]. By using the locations of the poles and zeros of the all-pass function, we can obtain the phase plot graphically. According to the argument presented in [44], stable poles (confined within the unit circle) for a causal system results in a monotonically diminishing

and negative phase plot. On the other hand, if the model is non-causal by nature, it would be positive. Numerical examples and one practical case is demonstrated that follows this claim. This method is less susceptible to the available bandwidth of the system and more able to withstand numerical blunders because of inadequate data and Gibbs phenomenon. However, in some cases the method could fail if too few information are given. The authors did found non-causality report on some loss-less cases, which are obviously incorrect, which suggests that the proposed method might require improvements.

2.4.4 Causality Check by Analog Integration

A couple of new testing techniques were introduced in [43,45,46] to decrease false-positive test results. It was achieved by carefully taking the discretization error bound into account while approximations were made on the sampled data by interpolation/approximation functions. The principal difference between the method described in [45] and that in [41] is that, in this work, cubic splines are utilized to interpolate the frequency response. The causality test is performed on the analytic function obtained by cubic spline, rather than the actual sampled data. Because of achieving Generalized Hilbert Transform analytically, the run time of the operation is reduced with good accuracy.

The amount of non-causality detectable by this method, as in reference [45], is also larger than the previous methods because of applying analytic integration – thus overcoming the sensitivity problems of previous methods. However, the technique in [45] can prompt unbounded results in the presence of large non-uniform frequency steps in the tabulated data (e.g., logarithmic spaced frequency samples). In [46], this problem is resolved by improving the algorithm by using a global (i.e., non-piecewise) rational function approximation for tabulated frequency responses, whether piecewise cubic spline interpolation technique was applied in [45]. However, the speed might be compromised for data that has large delays.

2.4.5 Estimation of Causality Metric

In practical cases and simulations, causality is to be considered as a metric quantity, not an absolute property, as described in [47], [48]. A polar plot of the sampled data can be used to estimate the Causality Measure (CM) of a system. It is calculated as the proportion of clockwise rotation to aggregate rotation in percentage. Although the algorithm is consistent for numerical models, but not as effective for measured data due to noise.

According to recent works by Tsiklauri, [1,49] physical systems should not only be causal, they should be delay causal. Therefore, a signal should arrive at the output after system delay. Considering this concept, causality is considered to be a metric quantity, instead of an absolute property, as the proportion of energy that arrives before delay to the total energy. It is demonstrated in these papers that using little phase perturbation, causality property can be changed significantly. The major challenge is however to minimize numerical error brought about by band limited nature of the measured data.

2.4.6 Low Pass Filtering Approach

The methods described so far analyzes the system in frequency domain, although causality is characterized in the time space more explicitly. As mentioned above, frequency domain analysis of causality is complicated and sometimes misleading. Therefore a time domain approach is described in [50], where a sampled scattering parameter is passed through a low-pass filter to attenuate truncation error. The technique is further extended and justified in [51], [52] where the application of the filtering is rigorously validated.

Although the method is effective in detecting causality violations in most cases, it is also sensitive to the filter specification to a major extent [53]. The paper focuses on the reduction of numerical error by attenuating out-of-band frequency region, but does not specify the filter parameters. Investigation shows that the method yields different result when filter parameters (such as knee frequency, filter order and pass-band ripple etc.) are varied [53].

There should be a relationship to the error bound and filter parameters that is yet to be determined. Therefore, the choice of the appropriate filter is still an area of research.

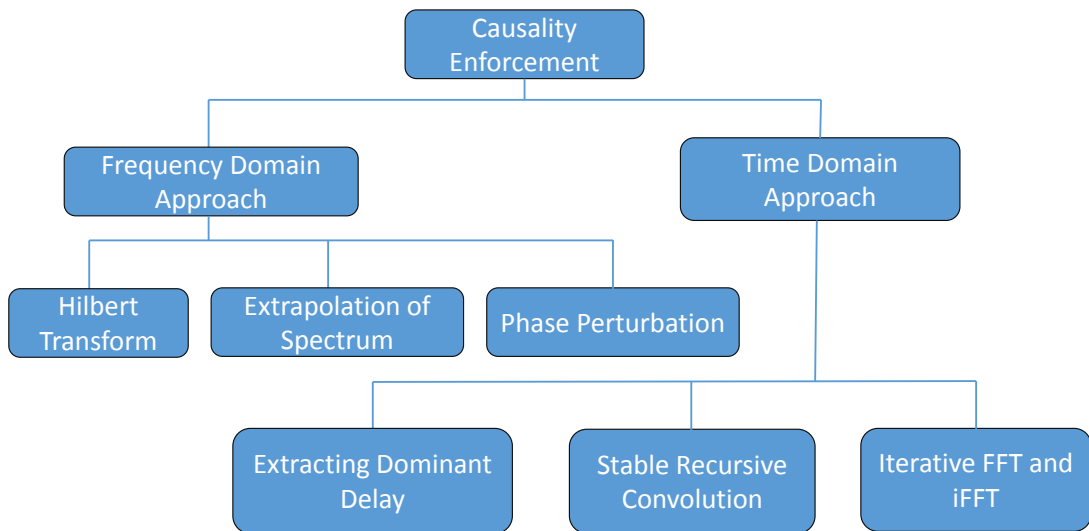


Figure 2.6: Causality Enforcement approaches

2.5 Enforcement of Causality

The enforcement of causality is as equally important for reliable time domain simulation as detection. Often the frequency domain characteristic of the system is modified to meet the causality condition. Recently, time domain modification algorithms have been developed and successfully implemented for enforcing causality in systems, which have been reported for causality violation. An illustration showing different methods of enforcing causality is presented in Fig. 2.6.

2.5.1 Causality Enforcement in Numerical Solutions of Maxwell's Equations

Perhaps the first attempt of enforcing causality was made by Clapp [54]. According to the novel work, the causality condition is fulfilled if the Maxwell hypothesis is presented in integral-equation form, with alteration embedded in the integrands. At exactly that point, a solution utilizing numerical integration will be physically realizable. The argument presented here is strictly confined to numerical solutions of Maxwell's equations.

2.5.2 Causality Enforcement by Hilbert Transform

Later in 1993, a novel work by Arabi in reference [55] utilized the Hilbert transform for enforcing causality on the EM fields for high speed digital systems. This technique uses the minimum phase portion of the system to calculate the causal transfer function. Finally, the total phase of the transfer function is obtained by the summation of the linear and non-linear minimum phase functions. Similar approaches have been applied in literature (see in reference [17, 56–58]). Although it is shown in these papers that the method works, one should be careful while implementing this method on measured spectra with a positive phase [17].

2.5.3 Causality Enforcement by Delay Extraction

Another technique based on port-to-port delay extraction is described in reference [59]. At first, a technique to extract delay from S, Y and Z parameters is explained and demonstrated. After extracting the port-to-port delay of the system, the determined impulse response in time domain can be adjusted so that the delay in the system can be correctly measured. Afterwards the impulse response is transferred back to frequency domain data via Fourier Transform. Numerical examples are presented to validate this technique. Alternatively, the 'base delay' for a device under test can be considered. The 'base delay' is the first time instant in the positive time axis at which emergence of the output is expected [60]. There are several approaches to get the 'base delay', although it is a function of frequency, that means the delay actually varies with frequency.

However, if we consider a distributed network with delays that are not closely grouped, this methodology may not produce accurate results [61]. A general distributed network that has more than one delays no longer acts as a minimum phase response because of the significant phase contributions of each delay elements. Consequently, applying Hilbert transform could result in incorrect estimation of the system [17]. Moreover, since this technique discards transient response before delay, there is loss of energy for the signal.

2.5.4 Causality Enforcement by Iterative FFT and IFFT

An improved method using iterative Fast-Fourier Transform (FFT) and Inverse Fast-Fourier Transform (IFFT) was introduced in reference [62]. This advanced method is able to preserve the energy of the signal more accurately. However, both of the methods in reference [59, 62] deals with causality violations in interconnects. A new method of causality enforcement by magnitude equalization was introduced in the novel work of Song et. al., (see [63]). As the magnitude equalizer does not have any physical length, the equalizer's phase is obtained using DHT assuming no delay. The errors from non-causal responses are adjusted by

applying the synthesized phase to the simulation. Although being a straightforward method, because of the IFFT, a convolution is applied numerically for the transient simulation that involves complex higher order calculations. This complexity can be reduced by adopting fast convolution methods [64].

2.5.5 Causality Enforcement by Extracting Dominant Delay

An alternative method given in reference [65] seeks to calculate the losses due to attenuation of the transfer function as sampled data utilizing a Hilbert transform approach and then the outcome of the Hilbert transform is used to estimate the largest delay. This technique specifically upholds the finite delay for the excitation to go from the input to the output, providing more appropriate results compared to the direct application of IFFT. However, like the previous approaches, this method could also produce inaccurate results when a network with more than one unextracted higher order delays is put to test.

2.5.6 Causality Enforcement by Extrapolation of Spectrum

According to the novel work by Rao et. al. (see [66]), one of the most effective, general purpose method for time-domain simulation and analysis is the time-domain convolution. This work demonstrates the requirement for another model for impulse response and proposes a system for its consideration in transient simulation, which is described in details in the patent [67]. In this method, optimized extrapolation is used to extend the truncated spectrum beyond the maximum sample frequency. This reduces the difference between computed and original imaginary part in the in-band frequency range, therefore ensuring a causal impulse response that accurately represents the original spectrum.

2.5.7 Phase Perturbation Technique of Causality Enforcement

It is possible to form Kramers-Krönig relations among amplitude and phase of the transfer function [68, 69]. Therefore, phase can be completely reconstructed by attenuation. Moreover, if magnitude is frequency dependent, delay causal system cannot have perfectly linear phase [70]. In reference [49], these principles are used to show that if there is causality unfulfillment for the system, a small alteration in phase makes significant improvement to the causality condition, keeping the change in magnitude to a minimum level.

If we consider a system $H(\omega) = e^{-\alpha(\omega) - j\theta(\omega)}$, where $\theta(\omega)$ is the phase and $\alpha(\omega)$ is the attenuation. Then the following system of equations can be used for phase reconstruction [49]:

$$\theta(\omega) = \frac{\omega}{\pi} \int \frac{\alpha(\omega')}{\omega^2 - \omega'^2} d\omega' \quad (2.9a)$$

$$\alpha(\omega) = \alpha(0) - \frac{\omega^2}{\pi} \int \frac{\theta(\omega')}{\omega'(\omega^2 - \omega'^2)} d\omega' \quad (2.9b)$$

where $\alpha(0)$ is a constant. The principal value integrals can be numerically computed by dispersion relations with subtractions as mentioned previously. The method produces same numerical error, which requires optimum number of subtractions to minimize numerical error.

2.5.8 Stable Recursive Method for Causality Enforcement

Recently another approach for causality enforcement has been adopted by Tsiklauri et. al. (see [1], which involves a stable recursive convolution in time-domain. The enforcement technique ensures a delay causal response. Actual physical systems have delay, therefore the system should be delay causal. Mathematically, if the impulse response of a system is $h(t)$, then condition for delay causality is: $h(t) = 0$, for $t < \tau$; where τ is the system delay. Causality is enforced by taking the part of impulse response before the delay and adding its mirror image regarding the delay point to the part after the delay. Finally, the part before

the delay is set to zero. The technique used in this work is to decompose the original impulse response into even and odd functions, then applying the following operation [1]:

$$h_{enforced}(t) = h_e(t) + \text{sign}(t - \tau)h_e(t) \quad (2.10)$$

where $h_e(t)$ is the even part of the impulse response. To illustrate the procedure, we take a fictitious impulse response $h_{nc}(t)$, which is not delay causal. We assume the delay time of the system is 0.5s. We obtain the enforced delay causal impulse response $h_c(t)$ according to the formula given in equation (2.10). The two responses are depicted in Fig. 2.7. A stable recursive algorithm is given in reference [1] that produces good result on measured S-parameters. Although the work is novel and efficient in implementation, it heavily depends on detecting the delay time accurately for the system.

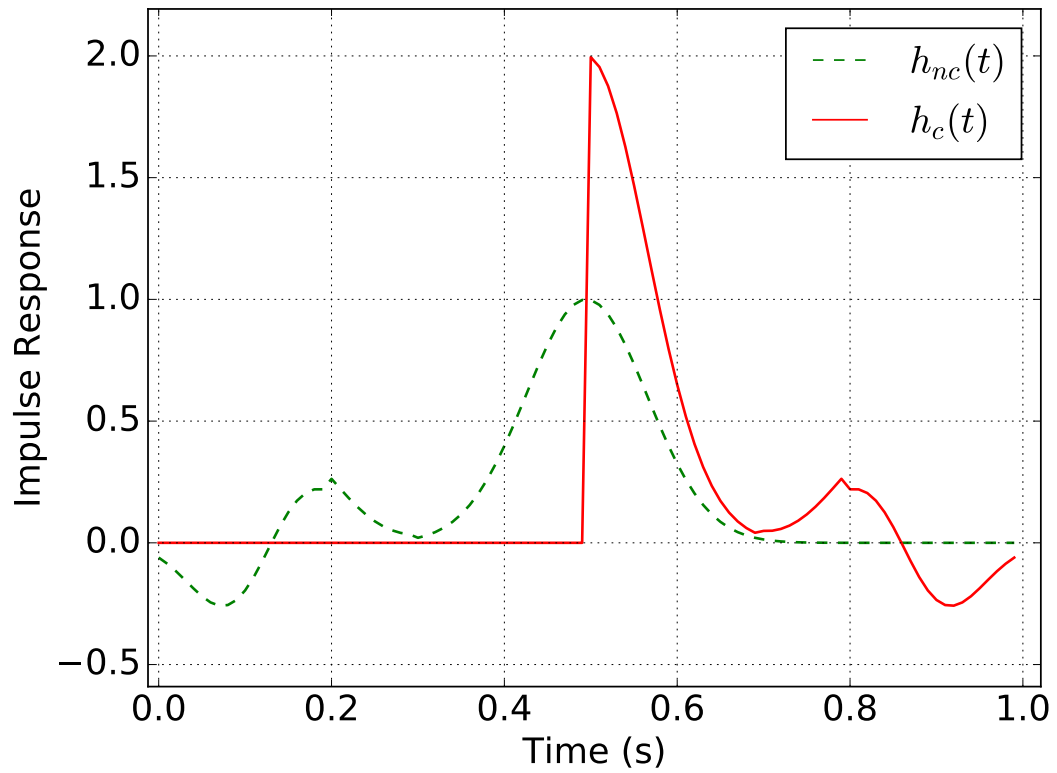


Figure 2.7: Modification of Impulse Response according to Reference [1]

2.6 Summary and Discussion

We reviewed an important physical characteristic of high speed interconnect system with wide applications in modern technology. The importance of causality in macro-models developed for future modeling, design and simulation is described. We start our discussion with early development on the concept of causality in chronological order that shows different steps of development towards state of the art techniques for causality verification and enforcement. As it is an immensely important property of data that describes real-world systems, violation of this property usually leads to erroneous results.

In our discussion, we focus on important milestones in achieving advanced techniques. Perhaps the most important criterion for causality is the Kramers-Krönig dispersion relations. Many of the techniques for verifying causality are some derivative of the original dispersion relations. Although causality is defined in time-domain, the K-K relations are specified in frequency domain, which make them appropriate for the sampled data that are the most available. However, each method have some advantages/disadvantages over others that are critically analyzed throughout this work. Causality enforcement is also treated the same way - we have discussed different methodologies in chronological order to focus on the gradual development of causality enforcement.

CHAPTER 3

Causality Verification by Filtering

Among different methods, in this chapter we concentrate on a time domain approach for detecting causality violation. Although simple in implementation, the method is sensitive to certain filter parameters. The detailed analysis with numerical examples are presented in this chapter.

3.1 Introduction

Scattering parameters (S-parameters) are extensively used in the field of signal/power integrity to define components in the frequency domain. In order to obtain well-posed models for transient analysis, the raw frequency data must be causal, stable and passive [4]. The main focus in this chapter is on the sensitivity of parameters of a method used for detecting causality violations. Mathematically, a causal system having impulse response $h(t)$ must follow the condition [4]:

$$h(t) = 0 \quad \text{for } t < 0, \quad (3.1)$$

In frequency domain, the system under consideration must follow the Kramers-Krönig dispersion relationship [13, 14], which states a relation between real and imaginary part of the frequency response.

A method for causality check is described in [41], where a minimum-phase low-pass filter is used to reduce the truncation error. This chapter carefully examines some cases where the method produces inaccurate results. The following section refers to a method of checking causality as described in [41]. In section 3.3, through numerical examples we have shown the effect of choosing different filter parameters.

3.2 Formulation

3.2.1 Scattering parameters

Scattering parameters are widely used in microwave engineering to characterize linear devices such as transmission lines, microstrip filters, antennas and active devices operating in small-signal conditions [41]. It is common practice to treat the incident waves as the independent quantities; we denote these as a_n , and express their contributions to the reflected or outward traveling wave b_n at port N by a series of scattering coefficients. In matrix form:

$$\begin{bmatrix} b_1 \\ \vdots \\ b_n \end{bmatrix} = \begin{bmatrix} S_{11} & \cdots & S_{1n} \\ \vdots & \ddots & \vdots \\ S_{n1} & \cdots & S_{nn} \end{bmatrix} \cdot \begin{bmatrix} a_1 \\ \vdots \\ a_n \end{bmatrix} \quad (3.2)$$

For a two-port network, the S-parameter representation of the system in matrix form can be written as:

$$\begin{bmatrix} b_1 \\ b_2 \end{bmatrix} = \begin{bmatrix} S_{11} & S_{12} \\ S_{21} & S_{22} \end{bmatrix} \cdot \begin{bmatrix} a_1 \\ a_2 \end{bmatrix} \quad (3.3)$$

Generally, a scattering matrix is applied to represent the properties of a physical microwave junction; certain relationships exist within the scattering matrix as a result of the familiar laws of reciprocity and conservation of energy [71]. The condition of reciprocity requires that the S-matrix is symmetric.

3.2.2 Filtered Fourier Transform

Causality of a system can be determined by observing the impulse response in the time domain whether it meets the condition given in (3.1). From measured data, generally the frequency domain responses are available in form of scattering parameters up to a maximum frequency. If the sampled transfer function is given by $S(j\omega)$ for a single port system, the

corresponding time domain response can be calculated by inverse Fourier Transform of the samples [41]:

$$h(t) = \frac{1}{2\pi} \int_{-\omega_m}^{\omega_m} S(j\omega) e^{j\omega t} d\omega + \frac{1}{2\pi} \int_{|\omega_m| > \omega_m} S(j\omega) e^{j\omega t} d\omega, \quad (3.4)$$

where $j = \sqrt{-1}$, $\omega_m = \text{maximum frequency}$.

If the sampled data is available up to a certain frequency (ω_m), only the first part of the integral in (3.4) can be computed. Hence, the obtained impulse response differs from the actual response by a truncation error. Reference [41] addressed this issue through filtering the sampled response by a low-pass filter. The filtered response is obtained using following equations [41]:

$$H_{F_{i,j}}(j\omega) = F(j\omega)S_{i,j}(j\omega), \quad (3.5)$$

where $i, j \in \{1, 2\}$, and $F(j\omega)$ is the filter transfer function. Taking inverse Fourier Transform of these responses give us the time domain response as follows [41]:

$$h_{f_{i,j}}(t) = \frac{1}{2\pi} \int_{-\omega_m}^{\omega_m} H_{F_{i,j}}(j\omega) e^{j\omega t} d\omega + \frac{1}{2\pi} \int_{|\omega_m| > \omega_m} H_{F_{i,j}}(j\omega) e^{j\omega t} d\omega, \quad (3.6)$$

where $i, j \in \{1, 2\}$.

In this section, we have performed the inverse Fourier Transform by evaluating numerical integration using equation (3.6) for a two port network. The time parameter 't' is fed into the integral over the frequency range. Thus we are able to determine time domain response of the transfer function for any time instance, either in positive or negative axis. The theorem 1 described in [41] suggests that, if the filter is minimum phase, the causality of $h_{f11}(t)$, $h_{f12}(t)$, $h_{f21}(t)$ and $h_{f22}(t)$ are equivalent to the causality of the given S-parameter. The steps to follow the causality checking is given below:

Step 1: Acquiring band-limited samples of S-parameters

Step 2: Passing the samples through a minimum phase low-pass filter to attenuate out-of-

band samples

Step 3: Determining the error-threshold based on the filter parameters

Step 4: Performing inverse Fourier Transform of the filtered response to obtain time domain response

Step 5: Checking whether the response exceeds the error threshold in the region $t < 0$

3.2.3 Error Threshold

In this work, we have selected a Chebyshev low pass minimum phase filter because of its steeper roll-off characteristic. The error threshold (E) is obtained as in [41]:

$$E = M \frac{1}{2\pi} \int_{|\omega_m| > \omega_m} |F(j\omega)| d\omega \quad (3.7)$$

where $F(j\omega)$ is the frequency response of the minimum phase filter and M is the value of the frequency response of the system beyond $\omega > \omega_m$. We assume $M = 1$ for passive devices [41]. Therefore, the conditions for the S-parameter to be causal is [41]:

$$|h_{f_{i,j}}(t)| < E \quad \text{for } t < 0 \quad (3.8)$$

3.3 Numerical Example

3.3.1 Analytic Example

Through an analytic example, we can demonstrate the validity of causality checking of the S-matrix. At first, we consider a fictitious two port S-matrix, elements of which are known

as functions of frequencies beforehand. We define them as follows:

$$H_{11}(j\omega) = \frac{1}{j\omega + 20}; H_{12}(j\omega) = H_{21}(j\omega) = \frac{1}{j\omega^4 + 20}$$

$$H_{22}(j\omega) = \frac{1}{j\omega^5 + 15} + \frac{0.5}{j\omega + 1} e^{j\omega 10}$$

Clearly, $H_{11}(j\omega)$ and $H_{12}(j\omega)$ are causal and their time domain response should show causal properties as given in (3.1). On the other hand, $H_{22}(j\omega)$ is non-causal because of the presence of the anticipation factor $e^{j\omega 10}$. Since sampled data is used to obtain the time domain response, and samples are only available up to a maximum allowed frequency (in this case, we fixed it to $\omega_m = 2\pi*50$ rad/s), the time domain response of the two frequency responses are not exactly zero for negative time instances, but should be limited to an error bound given by (3.8).

Each of the frequency responses are sampled at 100 points up to ω_m . At first the time domain response is obtained for each elements of the S-matrix. A 4th order Chebyshev (type 1) low-pass filter is used with cut-off frequency $2\pi*25$ rad/s and pass-band ripple of 2 dB. The output graph of the impulse response (Fig. 3.1) shows causality violation of $H_{22}(j\omega)$. For further verification, we omit the $e^{j\omega 10}$ term from $H_{22}(j\omega)$ and perform the verification again. The results are shown in Fig. 3.2.

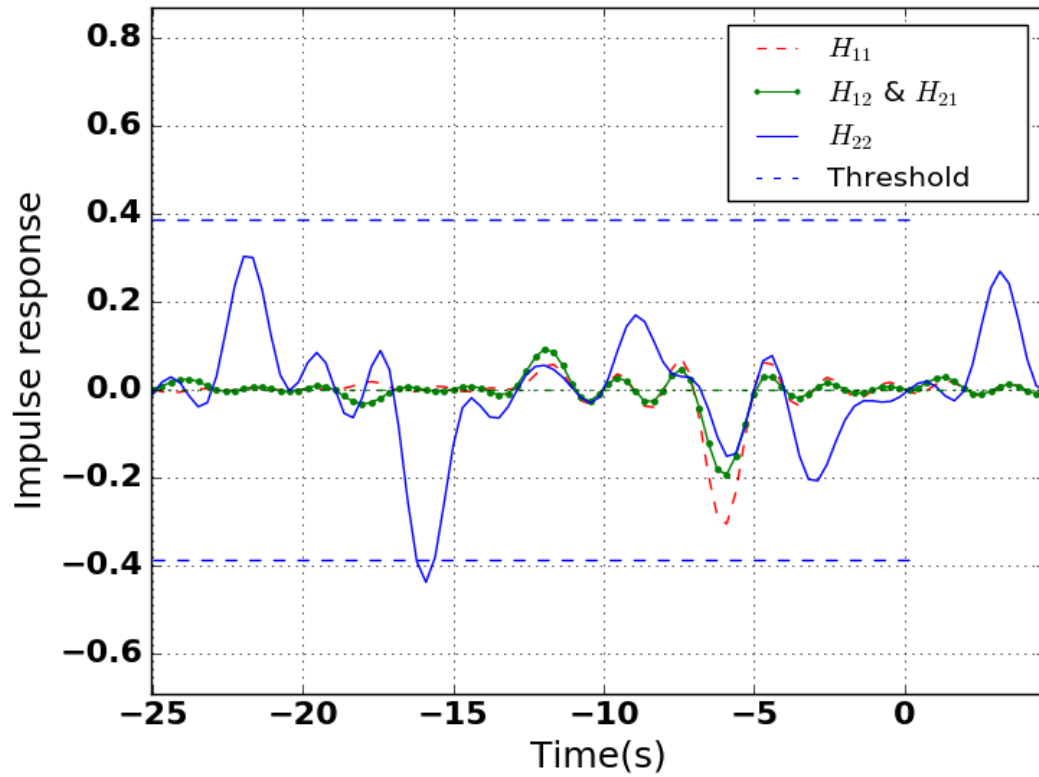


Figure 3.1: Impulse response obtained from the filtered frequency responses given in (3.9). The dashed lines denote the threshold error bound. (Source: Md Aminul Hoque, Ata Zadehgo, On the Sensitivity of Causality Filter Parameters. Copyright ©2016, IEEE Electrical Design of Advanced Packaging and Systems (EDAPS) Symposium 2016.)

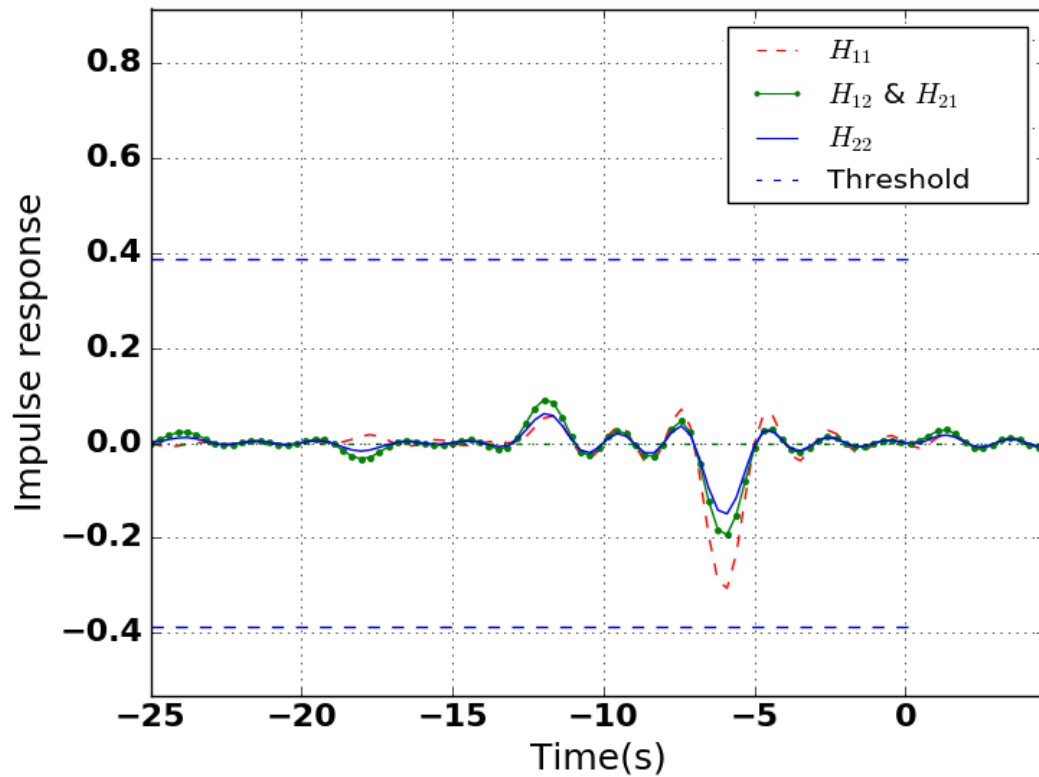


Figure 3.2: Impulse response obtained from the modified filtered frequency responses given in (3.9), leaving out the non-causal part. It is observed that the impulse response stays within the threshold limit for $t < 0$. (Source: Md Aminul Hoque, Ata Zadehgo, On the Sensitivity of Causality Filter Parameters. Copyright ©2016, IEEE Electrical Design of Advanced Packaging and Systems (EDAPS) Symposium 2016.)

However, the test is sensitive to the filter specification. If we increase the cut-off frequency to $2\pi*30$ rad/s, the test fails to detect violation (Fig. 3.3). We show another case where the filter cut-off frequency is reduced down to $2\pi*20$ rad/s, which declares a causal system to be non-causal (Fig. 3.4).

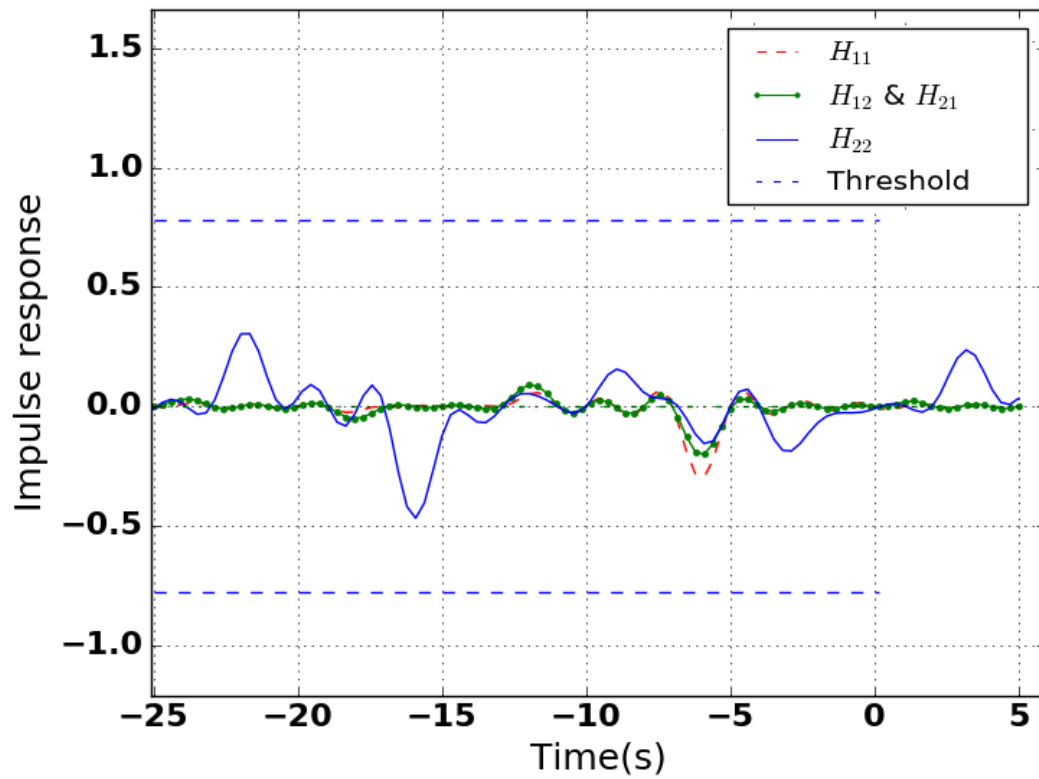


Figure 3.3: As a result of increased cut-off frequency, the time response stays within the threshold value, even though it is non causal, given in (3.9). (Source: Md Aminul Hoque, Ata Zadehgo, On the Sensitivity of Causality Filter Parameters. Copyright ©2016, IEEE Electrical Design of Advanced Packaging and Systems (EDAPS) Symposium 2016.)

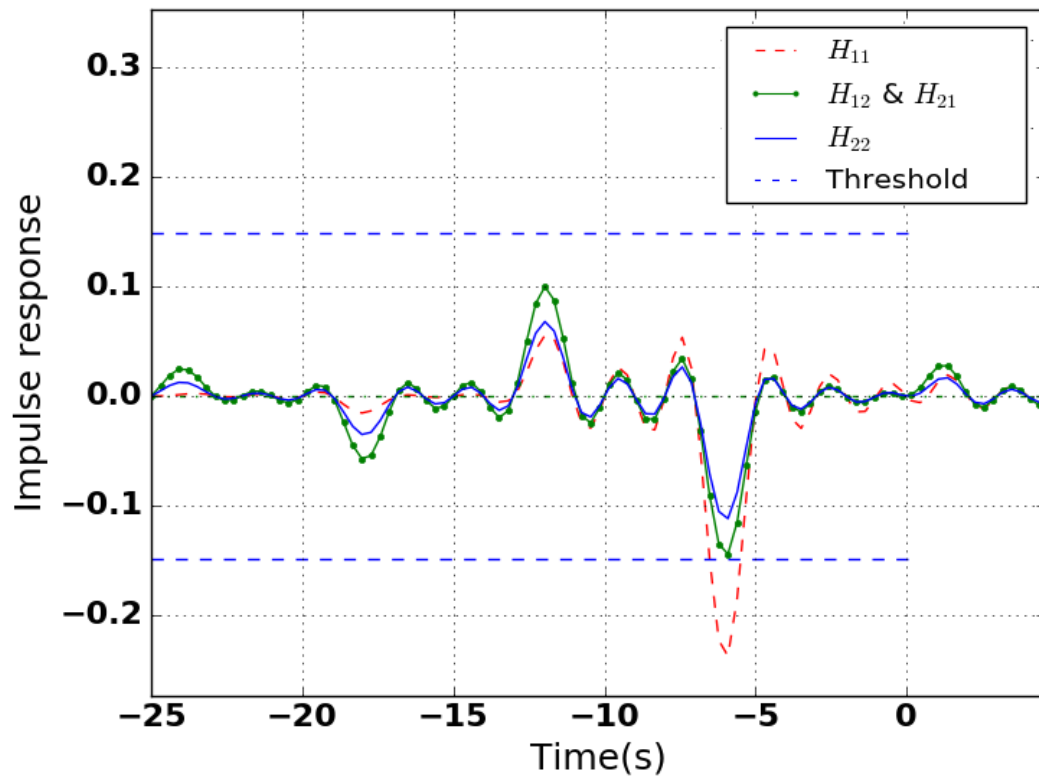


Figure 3.4: Decreasing the cut-off frequency yields non-causal characteristic of a purely causal sequence. (Source: Md Aminul Hoque, Ata Zadehgol, On the Sensitivity of Causality Filter Parameters. Copyright ©2016, IEEE Electrical Design of Advanced Packaging and Systems (EDAPS) Symposium 2016.)

Another important parameter to consider is the maximum frequency of the samples. If we consider the transfer functions in (3.9) and take the samples up to $\omega_m = 2\pi*40$ rad/s, the test fails to detect the causality violation as shown in Fig. 3.5. On the other hand, by increasing ω_m to $2\pi*60$ rad/s, causality check generates causality violations for causal functions, which is depicted in Fig. 3.6. There is no methodology provided in [41] regarding maximum frequency, although it clearly makes an impact on detection of causality violation. Therefore, relationship between the maximum frequency of samples, cut-off frequency of the filter, pass-band ripple and other filter parameters should be established.

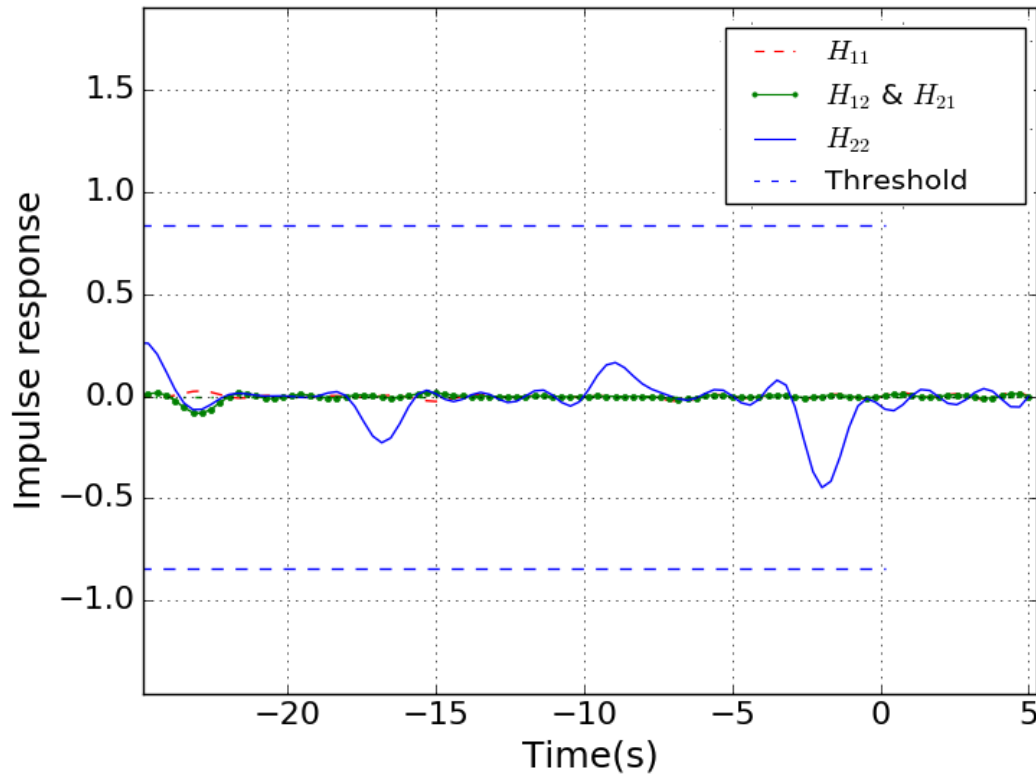


Figure 3.5: Impulse response of the functions in (3.9). Clearly the $H_{22}(j\omega)$ is non-causal but it can not be detected when ω_m is reduced to $2\pi*40$ rad/s. (Source: Md Aminul Hoque, Ata Zadehgo, On the Sensitivity of Causality Filter Parameters. Copyright ©2016, IEEE Electrical Design of Advanced Packaging and Systems (EDAPS) Symposium 2016.)

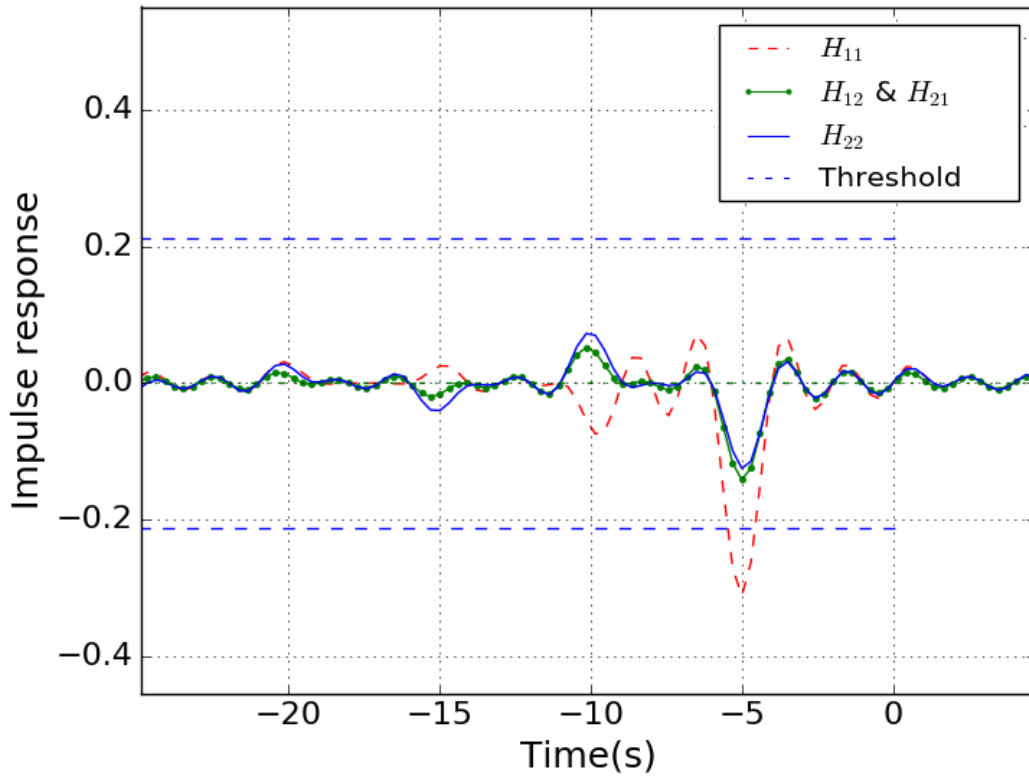


Figure 3.6: Impulse response of the functions in (3.9) when ω_m is increased to $2\pi*60$ rad/s. The anticipation factor of $H_{22}(j\omega)$ is left out, so all functions are causal. But the result displays causality violation for $H_{11}(j\omega)$. (Source: Md Aminul Hoque, Ata Zadehgo, On the Sensitivity of Causality Filter Parameters. Copyright ©2016, IEEE Electrical Design of Advanced Packaging and Systems (EDAPS) Symposium 2016.)

3.3.2 Practical case

Now we consider the 2-port S-parameters extracted for a set of power-plane that contains 1351 frequency points up to 5 GHz. The filter chosen in this case is a 4th order type 1 Chebyshev low-pass filter with pass band ripple of 7 dB and cut-off frequency at 2.8 GHz. Since the network is passive, $M = 1$ [41]. By checking each element of the S-matrix, we obtain the output in Fig. 3.7, which appears to be causal. However, one question remains, that is how much further we need to check in the negative time for causality violation? If we go further back into the negative time axis, causality violation does show up as depicted in Fig. 3.8.

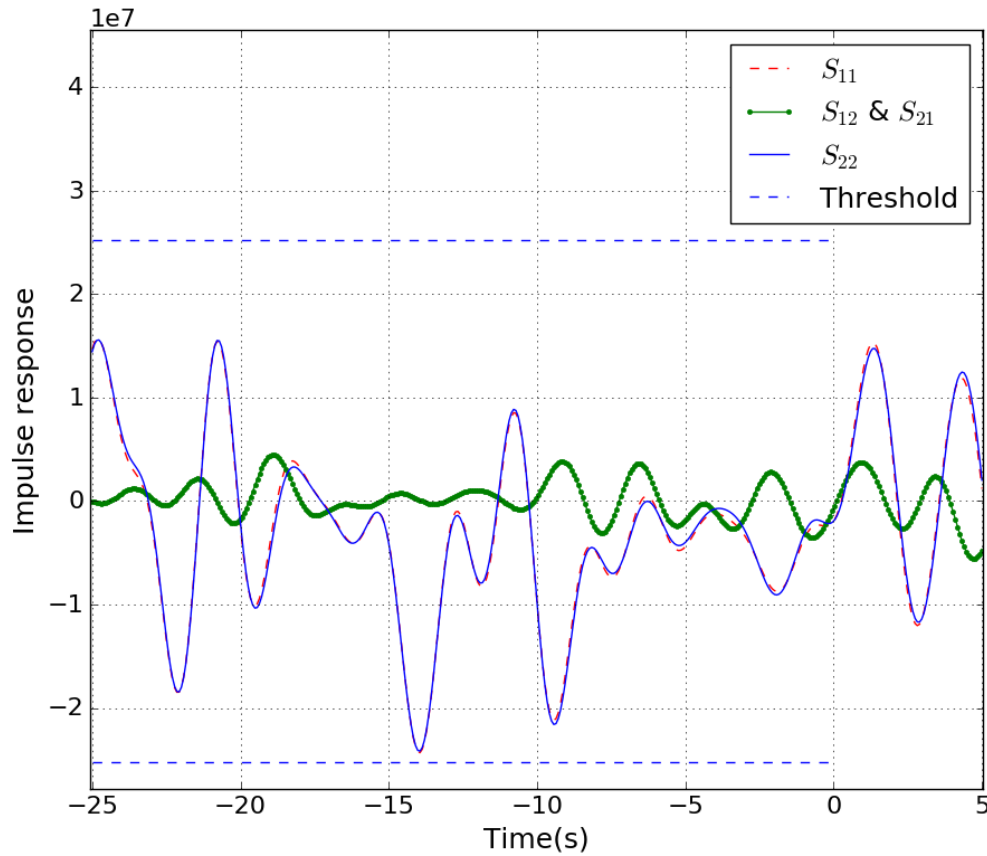


Figure 3.7: Impulse response of the elements of S-matrix for the 1351 frequency point S-parameters. It is observed that the impulse response stays within the threshold limit for $t < 0$ up to $t = -25$ s. (Source: Md Aminul Hoque, Ata Zadehgo, On the Sensitivity of Causality Filter Parameters. Copyright ©2016, IEEE Electrical Design of Advanced Packaging and Systems (EDAPS) Symposium 2016.)

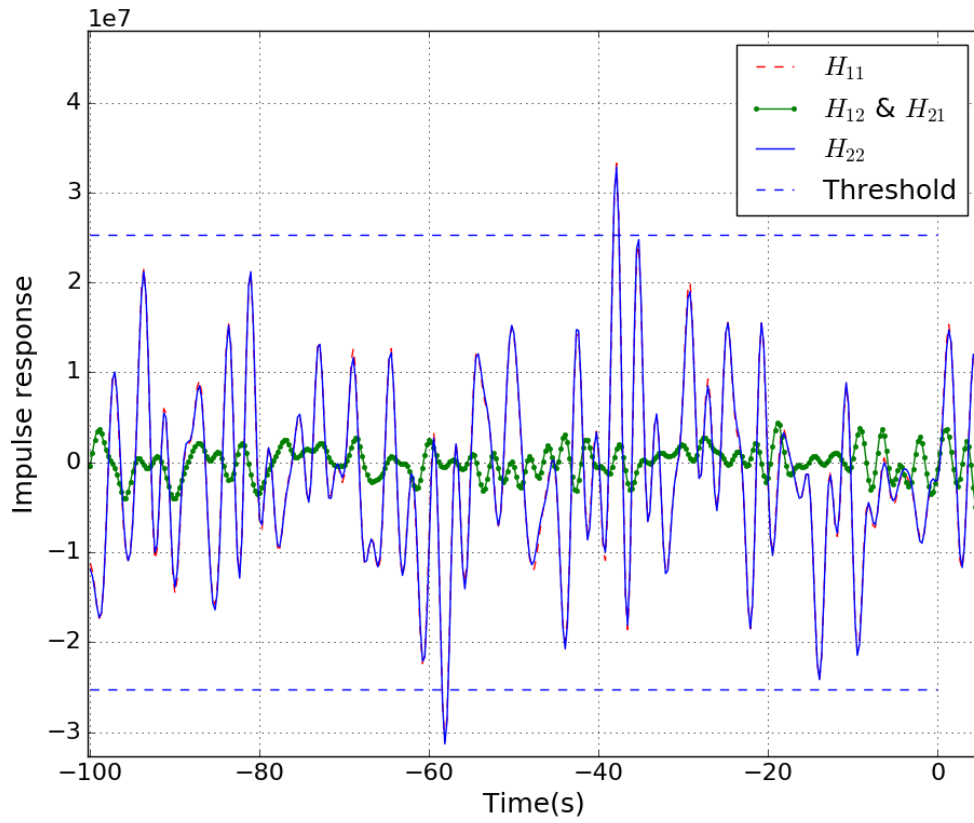


Figure 3.8: Impulse response of the elements of S-matrix. Causality violation is seen at $t = -37$ s and $t = -58$ s as the time response of the S_{11} and S_{22} go beyond the threshold value. (Source: Md Aminul Hoque, Ata Zadehgo, On the Sensitivity of Causality Filter Parameters. Copyright ©2016, IEEE Electrical Design of Advanced Packaging and Systems (EDAPS) Symposium 2016.)

3.4 Summary

We examine an existing proposed method [41] for verification of causality of sampled S-parameters. Our investigation reveals that while the proposed method is novel in its simplicity and ease of implementation, in practice it is quite sensitive to the filter parameters, the duration of negative time, and the maximum sampled frequency. Specifically, the choice of filter's knee frequency plays a significant role in the method's ability to accurately detect non-causality. Additionally, it is not clear how far back in negative time the impulse response must be checked to conclusively demonstrate causality. Moreover, the effect of maximum frequency available for sampled data can significantly affect the detection of non-causality. While the proposed method [41] appears promising, the above parameters must be precisely specified in order to make the method useful for solving practical problems.

CHAPTER 4

Causality Verification by Generalized Hilbert Transform

We have discussed about time domain approaches of causality verification in previous chapters. In this chapter, we discuss a frequency domain approach for the same purpose. The formulation is based on the original dispersion relations, but typical issues of applying the K-K relations are solved by using a modified formulation. The important parameters and their recommended values for generating fruitful result are discussed in details.

4.1 Generalized Dispersion Relations

Hilbert transform is applied on tabulated S-parameters that evokes a frequency domain causality test. It was first formulated in reference [10]. However, the complete implementation with practical examples are provided in reference [39]. An explicit error bound calculation technique was presented in this novel work. Additionally, a detailed analysis regarding the resolution of the proposed method is described. The validation of the method is further established in [40]. The direct discretization of the original dispersion relation (2.1a)-(2.1b) fails because of the finite bandwidth of the sampled data and finite number of discrete samples. Therefore, an error or mismatch is inevitable when trying to correlate the real and imaginary part of the data. One significant contribution of this work is the formulation of the error bound. Instead of directly using equations (2.1a)-(2.1b), a modified pair of dispersion relations are used [39]:

$$U(\omega) = \alpha_U(\omega) + \frac{\omega^n}{\pi} \int \frac{V(\omega') - \alpha_V(\omega')}{(\omega')^n} \frac{d\omega'}{\omega - \omega'} \quad (4.1a)$$

$$V(\omega) = \alpha_V(\omega) - \frac{\omega^n}{\pi} \int \frac{U(\omega') - \alpha_U(\omega')}{(\omega')^n} \frac{d\omega'}{\omega - \omega'} \quad (4.1b)$$

where

$$\alpha_U(\omega) = \sum_{V=0}^{n-1} \frac{U^{(V)}(0)}{V!} \omega^V, \quad \alpha_V(\omega) = \sum_{V=0}^{n-1} \frac{V^{(V)}(0)}{V!} \omega^V$$

Here, the number of subtractions is given by n . These expressions are extracted using two steps. First step involves subtracting the n -th order Taylor polynomial from $H(j\omega)$ and dividing the result by ω^n . Afterwards, the Hilbert Transform is applied on the result to get the expressions in equation (4.1a)-(4.1b). Although numerical evaluation of these relations requires the n -th order Taylor polynomial, which gets ill-conditioned for sampled data. This problem is solved in reference [39] by distributing the roots of the polynomial ω^n at frequencies other than $\omega = 0$:

$$U(\omega) = \beta_U(\omega) + \frac{\prod_{q=1}^n (\omega - \bar{\omega}_q)}{\pi} \int \frac{V(\omega') - \beta_V(\omega')}{\prod_{q=1}^n (\omega' - \bar{\omega}_q)} \frac{d\omega'}{(\omega - \omega')} \quad (4.2a)$$

$$V(\omega) = \beta_V(\omega) - \frac{\prod_{q=1}^n (\omega - \bar{\omega}_q)}{\pi} \int \frac{V(\omega') - \beta_V(\omega')}{\prod_{q=1}^n (\omega' - \bar{\omega}_q)} \frac{d\omega'}{(\omega - \omega')} \quad (4.2b)$$

where $\beta_F(\omega) = \sum_{q=1}^n l_q(\omega) F(\bar{\omega}_q)$ for $F = \{U, V\}$ and $l_q(\omega) = \prod_{p=1, p \neq q}^n \frac{(\omega - \bar{\omega}_p)}{(\bar{\omega}_q - \bar{\omega}_p)}$ (Lagrange Interpolation Polynomial).

4.2 Location of Subtraction Points

Placing the subtraction points is of great importance for this method to work. According to several references [36–38], a Chebyshev distribution ensures optimal placement of the subtraction points (also known as the anchor points). The subtraction points can be extracted by the zeros of the N -th order Chebyshev polynomial which can be written as:

$$\bar{\omega}_q = -\omega_{max}(1 - \epsilon) \cos \frac{(q-1)\pi}{n-1}, \quad q = 1, 2, \dots, n \quad (4.3)$$

Here, $\bar{\omega}_q$ are the subtraction points, ω_{max} is the maximum frequency in radians per second, and ϵ is an arbitrarily small number ($\epsilon \ll 1$). The number of subtraction points can be

increased or decreased based on the density of samples and variation in input. The increased number of subtraction points reduces the truncation error obtained from it. However, it also makes the test more sensitive in detecting causality violation. We shall discuss these issues in more details in later part of this chapter.

Because of the finite bandwidth of available samples, the reconstructed output does not perfectly match with the input. However, we can estimate the maximum deviation of the output caused by the bandlimited nature of data. A bound for the truncation error is estimated assuming $|H(j\omega)| \leq 1$. Using these assumptions, causality verification is done by reconstructing the imaginary part and comparing it to the raw data. The truncation error bound $T_n(\omega)$ is given as [40]:

$$T_n(\omega) = \frac{1}{\pi} \sum_{q=1}^n \left[\left| \ln \frac{\omega_{max} - \bar{\omega}_q}{\omega_{max} - \omega} \right| - (-1)^n \left| \ln \frac{\omega_{max} + \bar{\omega}_q}{\omega_{max} + \omega} \right| \right] \times \prod_{p=1, p \neq q}^n \frac{|\omega - \bar{\omega}_q|}{\bar{\omega}_p - \bar{\omega}_q} \quad (4.4)$$

However, the value of ϵ can lead to ambiguity, as it has an effect on placing the subtraction points. In the original paper, the only assumption on the value of ϵ is specified by $\epsilon \ll 1$, which does not give an insight on what the specific value should be. Based on our investigation, we found out that the test is sensitive to the value of ϵ . By setting the value of $\epsilon = 0.1$, we obtain truncation error bound that is depicted in Figure 4.1. The error bound is determined using equation (4.3), for three different values of subtraction points, $n = 4, 8, 12$. For most of our simulations afterwards, we shall choose 12 subtraction points as it gives lower truncation error bound.

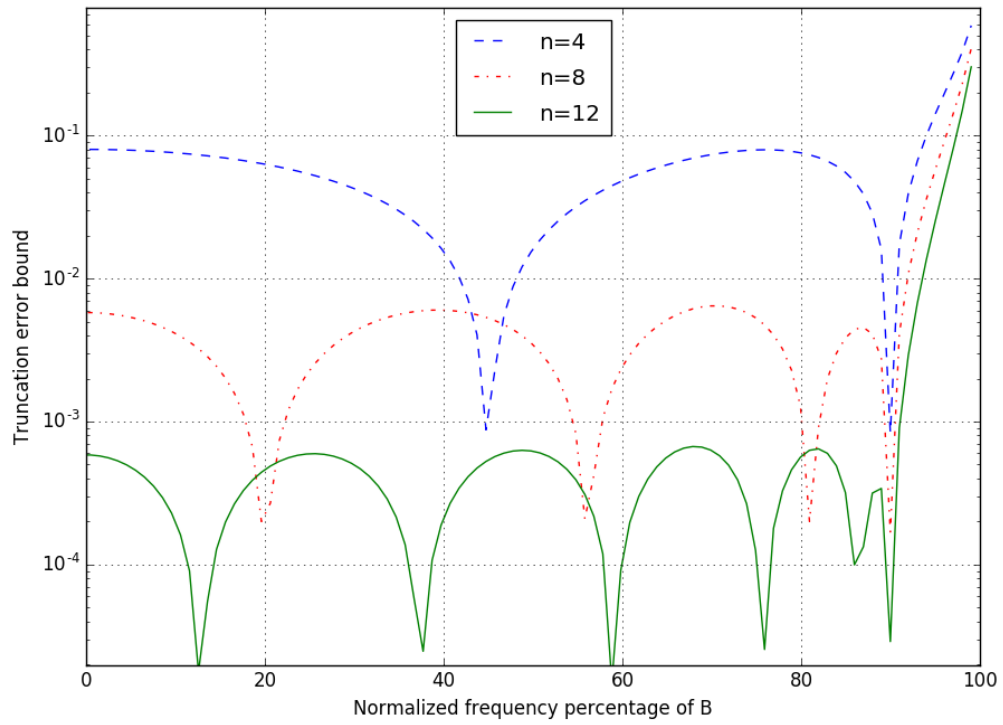


Figure 4.1: Truncation error bound vs. normalized angular frequency with $\epsilon = 0.1$

4.3 Reconstruction Operation

Due to discrete nature of the band-limited data, direct application of Hilbert Transform produces erroneous results. Therefore, a modified version of Hilbert Transform is adopted in literature which takes the nature of the data into account. As given in equations (4.2a)-(4.2b), this technique uses a number of anchor points to apply the Hilbert kernel on the frequency samples. A generalized reconstruction operator R_n is defined that maps the data onto itself if the data is causal. If there exists violation of causality, the reconstruction generates large error. The error threshold can be specifically determined that allows us a check whether the test reports causality violation or not. The reconstructed output $H_n(j\omega)$ can be obtained from the original sampled frequency domain data $H(j\omega)$ as [10, 72]:

$$H_n(j\omega) = R_n H(j\omega) = \mathcal{L}_H(j\omega) + \frac{\prod_{q=1}^n (\omega - \bar{\omega}_q)}{j\pi} \times \int \frac{H(j\omega') - \mathcal{L}_H(j\omega')}{\prod_{q=1}^n (\omega' - \bar{\omega}_q)} \frac{d\omega'}{(\omega - \omega')} \quad (4.5)$$

Here, the term $\mathcal{L}_H(j\omega)$ refers to the Lagrange interpolation polynomial for $H(j\omega)$ [73]. It can be mathematically expressed as:

$$\mathcal{L}_H(j\omega) = \frac{1}{\pi} \sum_{q=1}^n H(j\bar{\omega}_q) \prod_{q=1}^n \frac{\omega - \bar{\omega}_q}{\bar{\omega}_p - \bar{\omega}_q} \quad (4.6)$$

Here, the subtraction points are used as interpolation knots. The detailed proof of the reconstruction operation can be found in references [10, 74]. Equation (4.5), also known as generalized Hilbert transform [75], defines a generalized reconstruction operator R_n . Only causal frequency responses are mapped onto themselves by the reconstruction operator R_n . This generalized reconstruction operator has two major advantages. First advantage is generality, since results well defined for any frequency response having a polynomial growth up to ω^{n-1} . Second, its sensitivity to the high-frequency behavior of $H(j\omega)$ results drastically reduced. This is essentially due to the presence of the polynomial at the denominator in

(4.5), which acts as a sort of "low-pass" filter.

However, Integration in equation (4.5) is performed over the whole real line. Application to band-limited responses imposes a restriction of the integration interval to Ω defined as:

$$\Omega = [-\omega_{max}, \omega_{max}] \quad (4.7)$$

In practical cases, we have band-limited response available to us, therefore only an approximate reconstruction $\hat{H}_n(j\omega)$ can be evaluated. The modified reconstruction equation can be expressed as:

$$\begin{aligned} \hat{H}_n(j\omega) = \mathcal{L}_H(j\omega) &+ \frac{\prod_{q=1}^n (\omega - \bar{\omega}_q)}{j\pi} \int_{\Omega} \frac{H(j\omega') - \mathcal{L}_H(j\omega')}{\prod_{q=1}^n (\omega' - \bar{\omega}_q)} \frac{d\omega'}{(\omega - \omega')} \\ &+ \frac{\prod_{q=1}^n (\omega - \bar{\omega}_q)}{j\pi} \int_{\Omega^c} \frac{-\mathcal{L}_H(j\omega')}{\prod_{q=1}^n (\omega' - \bar{\omega}_q)} \frac{d\omega'}{(\omega - \omega')} \end{aligned} \quad (4.8)$$

Here, the integration is split into two parts, the first part containing the bandwidth where frequency samples are available, and where the singular nature of the integral exists (which accounts for the first integral term of equation (4.8)). The process to determine this singular integral is discussed in a later section. The last term of the integral in equation (4.8) accounts for the bandwidth beyond the maximum available frequency. Since the frequency sample beyond this point is not available, it is assumed to be zero. If this contribution is not included in the computation, the result turns out to be very inaccurate, thus wasting the effort in using the more sophisticated generalized dispersion relations.

4.4 Numerical Integration

The reconstruction equation as described in equation (4.8), can be interpreted as the application of the original dispersion relation with the auxiliary frequency response by subtracting the polynomial trend $\mathcal{L}_H(j\omega')$ from $H(j\omega)$ and dividing by the polynomial normalization

factor at the denominator:

$$G(j\omega) = \frac{H(j\omega') - \mathcal{L}_H(j\omega')}{\prod_{q=1}^n (\omega - \bar{\omega}_q)} \quad (4.9)$$

The first integral of equation (4.8) contains singularities and special care should be taken so that the discretization error does not become unbounded. To regularize the integral, we adopt a singularity extraction procedure [76]. The singular part of the integrand function is subtracted from the integral and added separately, as shown in the following equation:

$$\begin{aligned} \int_{\Omega} \frac{G(\omega')}{\omega - \omega'} d\omega' &= \int_{\Omega} [G(\omega') - G(\omega)] \frac{d\omega'}{\omega - \omega'} + G(\omega) \int_{\Omega} \frac{d\omega'}{\omega - \omega'} \\ &= \int_{\Omega} \frac{[G(\omega') - G(\omega)]}{\omega - \omega'} d\omega' + G(\omega) \ln \left| \frac{\omega_{max} + \omega}{\omega_{max} - \omega} \right| \end{aligned} \quad (4.10)$$

The first term in equation (4.10) still contains the singularity. If we assume that the function $\phi(\omega', \omega)$ is of class C^1 for fixed ω and variable ω' , where

$$\phi(\omega', \omega) = \frac{G(\omega') - G(\omega)}{\omega - \omega'} \quad (4.11)$$

we can write $\phi(\omega, \omega) = G'(\omega)$, and the integral has no difficulties associated with it [77–80]. For evaluating the first derivative, we have used the center difference formula to determine $G'(\omega)$. Alternatively, we can use Taylor series expansion to evaluate the derivative more accurately, but in our case we have adopted the center difference formula for simplicity. Since the center difference formula requires two neighboring sample values to determine the derivative, we were not able to reconstruct exactly at the edge of the spectrum. Instead, we continued the reconstruction operation till the point immediately before last the available sample.

As stated before, the last part of equation (4.8) accounts for the contribution of the Lagrange interpolation polynomial beyond the available bandwidth. Since the Lagrange

polynomial is known analytically, the quantity that accounts for the last integral (which we denote as $C_n(j\omega)$) can be evaluated by the following equation:

$$C_n(j\omega) = \sum_{q=1}^n \frac{H(j\bar{\omega}_q)}{j\pi} [L(\omega) - L(\bar{\omega}_q)] \prod_{\substack{p=1 \\ p \neq q}}^n \frac{\omega - \bar{\omega}_p}{\bar{\omega}_q - \bar{\omega}_p} \quad (4.12)$$

Therefore, the total reconstruction operation can be taken as the sum of three individual components: the Lagrange interpolation term, numerical integral term and the $C_n(j\omega)$ term, that can be summarized as follows:

$$\hat{H}_n(j\omega) = \mathcal{L}_H(j\omega) + I_n(j\omega) + C_n(j\omega) \quad (4.13)$$

Where $I_n(j\omega)$ refers to the numerical integration of samples within the available bandwidth.

4.5 Error Thresholds

Because of the numerical approximations and band-limited, truncated nature of the data, the reconstruction will not match the original. However, the reconstruction operation should be contained within a definite threshold value which is well defined in literature if the original response is causal. The total error consists of two main parts: truncation error and discretization error. We can determine accurate formulation for both the error terms.

4.5.1 Truncation Error

A rigorous upper limit of the truncation error made the reduction of truncation error possible. The truncation error term depends on the number of subtraction points used for the reconstruction operation. It also depends on the location of the subtraction points. If we obtain Chebyshev distribution and span the entire bandwidth of the frequency spectrum, we obtain our desired truncation error bound. The formulation is given in equation (4.4). Since

the equation is independent of frequency response, it can be determined solely based on the locations of the subtraction points and frequency spectrum spanned for the reconstruction.

4.5.2 Discretization Error

The discretization error arises from the numerical evaluation of the integral in equation (4.8). The discretization error may be very large if no special care is taken in handling the singular kernel of the Hilbert transform. A detailed procedure for handling the singular integral was described in section 4.4. For estimating the discretization error introduced by numerical integration, we can choose between two different strategies, depending on the application. We have opted the method which involves taking the difference of result in two different methods of numerical integration (namely, Simpson's rule and Trapezoidal rule). Mathematically we can express the error as:

$$\tilde{D}_n(\omega) = \left| \tilde{H}_n^{\nu_1}(j\omega) - \tilde{H}_n^{\nu_2}(j\omega) \right| \simeq |D_n(j\omega)| \quad (4.14)$$

Here, we assume $\nu_1 < \nu_2$, which are the order of the quadrature routine. For our analysis, we have selected the Simpson's rule as the higher order numerical integration technique and Trapezoidal rule as the lower order integration technique. We further assume that the higher order quadrature rule provides a much better result, which can be used as the reference for the error estimate.

4.6 Numerical Simulation and Discussion

In this section, we present the numerical simulations and experiments with this technique. We have performed causality verification and enforcement both on analytic transfer functions and sampled S-parameter data. We have tested different specification parameters and found the optimal values of these parameters for successful implementation of the algorithm.

4.6.1 Analytic Example

We construct a fictitious transfer function in rational form to identify causality easily and do the test on the sampled version of this function. Let the analytic function be $H_c(j\omega)$ which is described as:

$$\begin{aligned}
 H_c(j\omega) &= \frac{-20 + 180j}{j\omega - (-1200 + 15000j)} + \frac{-20 - 180j}{j\omega - (-1200 - 15000j)} + \frac{60 + 450j}{j\omega - (-3000 + 35000j)} \\
 &+ \frac{(60 - 450j)}{j\omega - (-3000 - 35000j)} \tag{4.15}
 \end{aligned}$$

The transfer function is sampled in the range $\omega = [-50000, 50000]rad/s$ with 100 sampled points. Then the transfer function is normalized by dividing it with the maximum absolute value of $H_c(j\omega)$ too keep consistency with the error thresholds as S-parameters. The real and imaginary parts of the transfer function is depicted in figure 4.2. Since real part of all the poles of $H_c(j\omega)$ are negative, the system should be causal. If we perform the reconstruction operation on this system, the reconstructed real and imaginary parts should be limited to the error threshold value specified in the previous section. This result is shown in figure 4.3, 4.4. For performing these reconstructions, we chose $\epsilon = 10^{-4}$ and the number of subtraction points, $n = 12$.

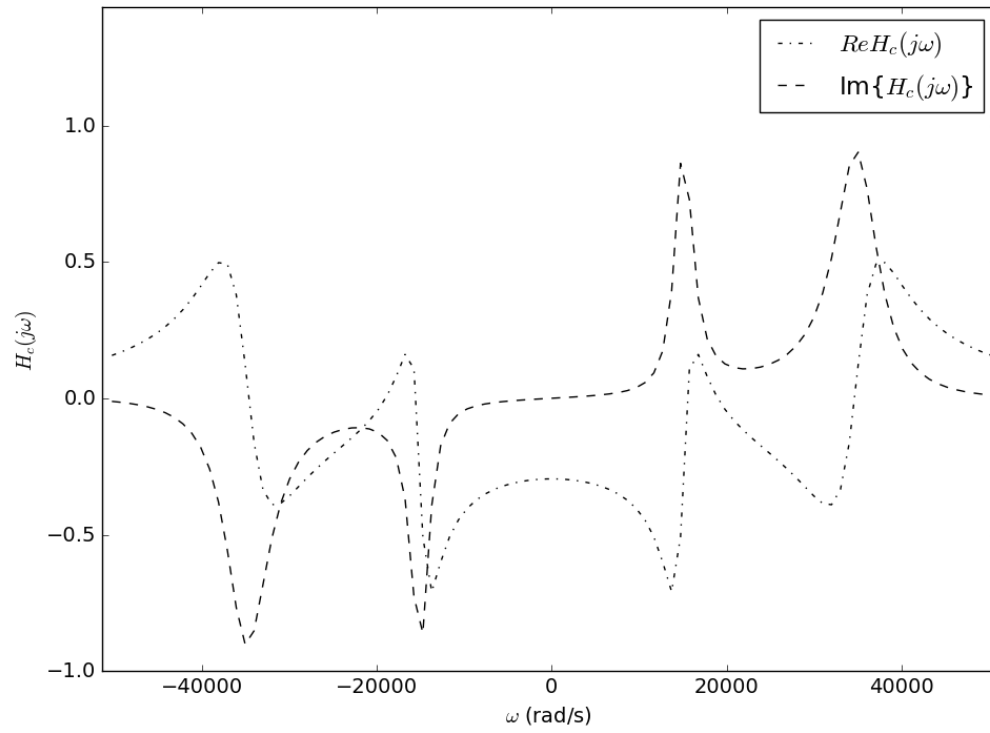


Figure 4.2: Real and Imaginary part of the input transfer function

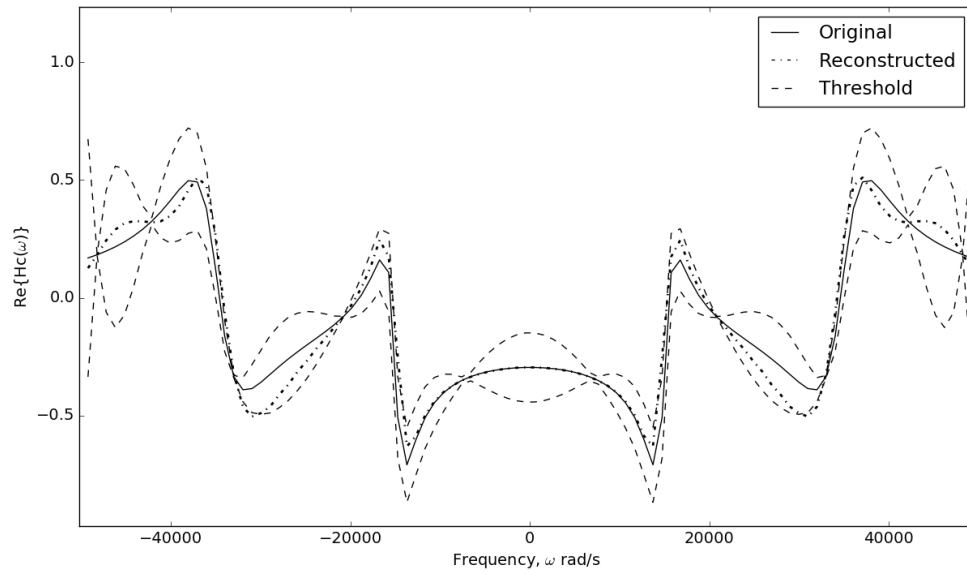


Figure 4.3: Reconstructed Real part of the input transfer function. Since the reconstructed output stays within the threshold, the system is causal

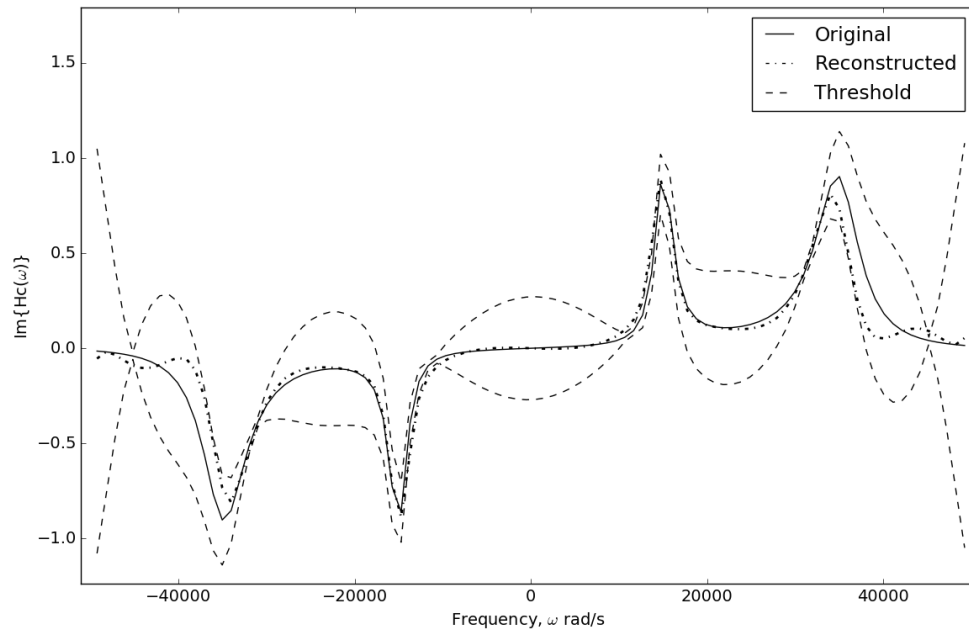


Figure 4.4: Reconstructed Imaginary part of the input transfer function. Since the reconstructed output stays within the threshold, the system is causal

To check whether this method could detect violation, we introduce Gaussian perturbation to the transfer function of the following form:

$$P(j\omega) = A \exp \left\{ - \left(\frac{\omega - \omega_0}{2\pi B} \right)^2 \right\} \quad (4.16)$$

For our simulation, we set $A = 0.05$, which is a fairly small amplitude for perturbation. The Gaussian is centered at the lower frequency region and the value of B is 0.064. The perturbation adds an uncorrelated component to the real part of $H_c j\omega$. Therefore, the real and imaginary part no longer follows the dispersion relations. We can see the result is figure 4.5. Since the real part was perturbed, the reconstructed imaginary violated the causality condition. If we consider the reconstructed real part as the causality enforced response, then the effect of the Gaussian perturbation is removed. These effects are depicted in figure 4.5 and 4.6. In figure 4.5, the deviation in the real part of the transfer function can be seen clearly. In figure 4.6, the reconstruction based on the imaginary part corrects the deviation due to the perturbation, thus causality enforcement has been achieved.

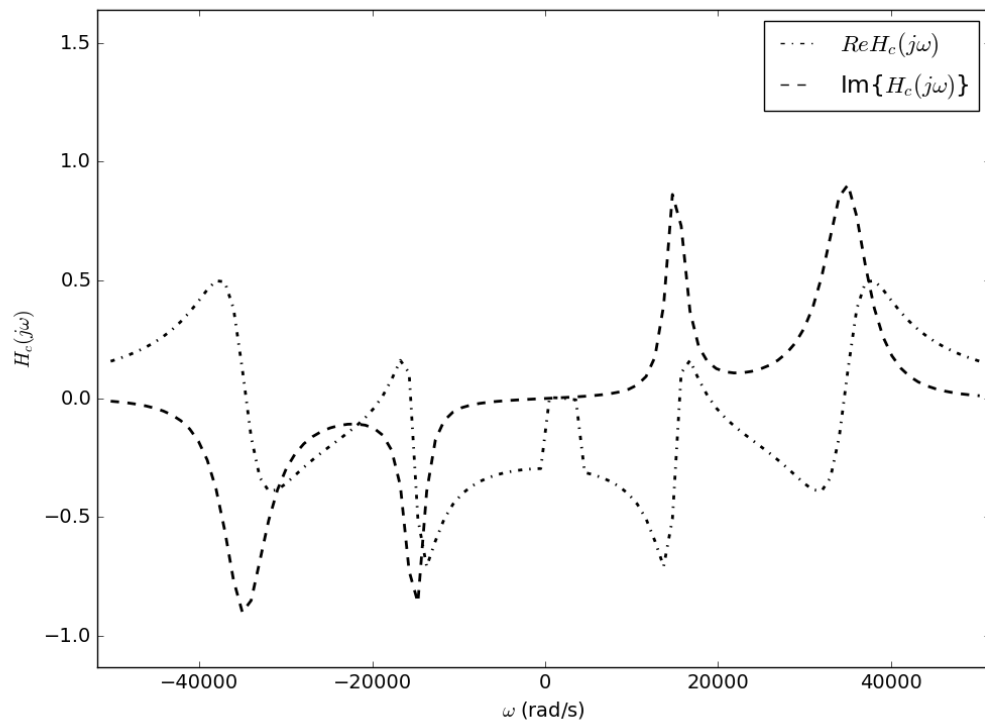


Figure 4.5: Real and Imaginary part of the input transfer function, with Gaussian perturbation

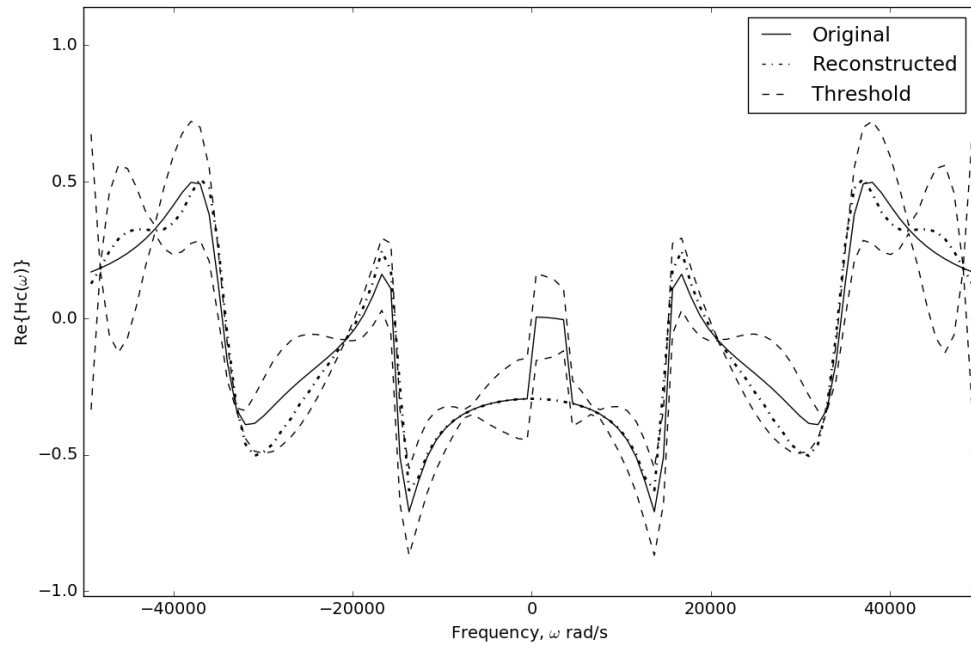


Figure 4.6: Reconstructed Real part of the input transfer function. Since the reconstructed output goes beyond the threshold, the system is non-causal

Now we perform the test on S-parameters (courtesy of Micron Technology). We ran the causality test on a 6 port S-parameter with samples available from 1Hz to 10GHz, with 3 samples per decade. On our test, we set $\epsilon = 10^{-4}$ and number of subtraction points $n = 12$. In this configuration, we performed our test on the S_{11} response of the S-parameter. The test results are shown in figure 4.7, 4.8.

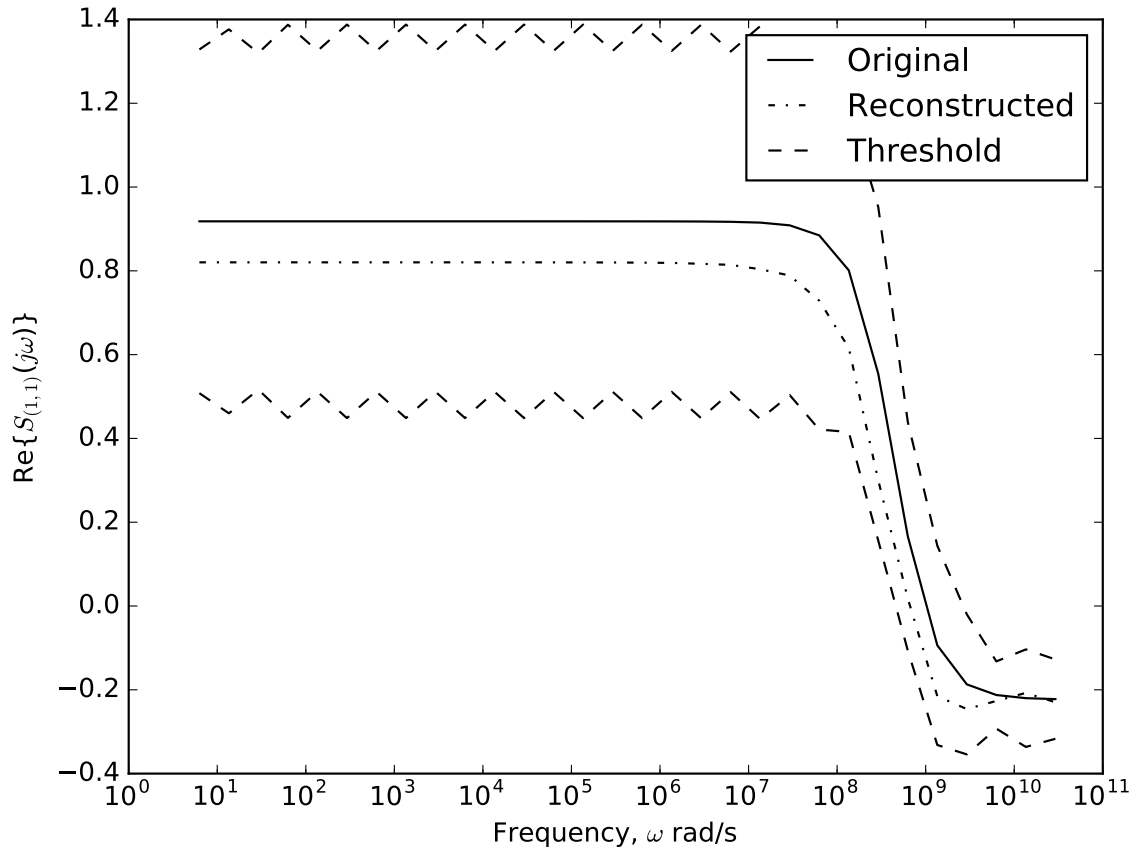


Figure 4.7: Reconstructed Real part of the input transfer function (in log scale). Since the reconstructed output does not go beyond the threshold, the system is causal

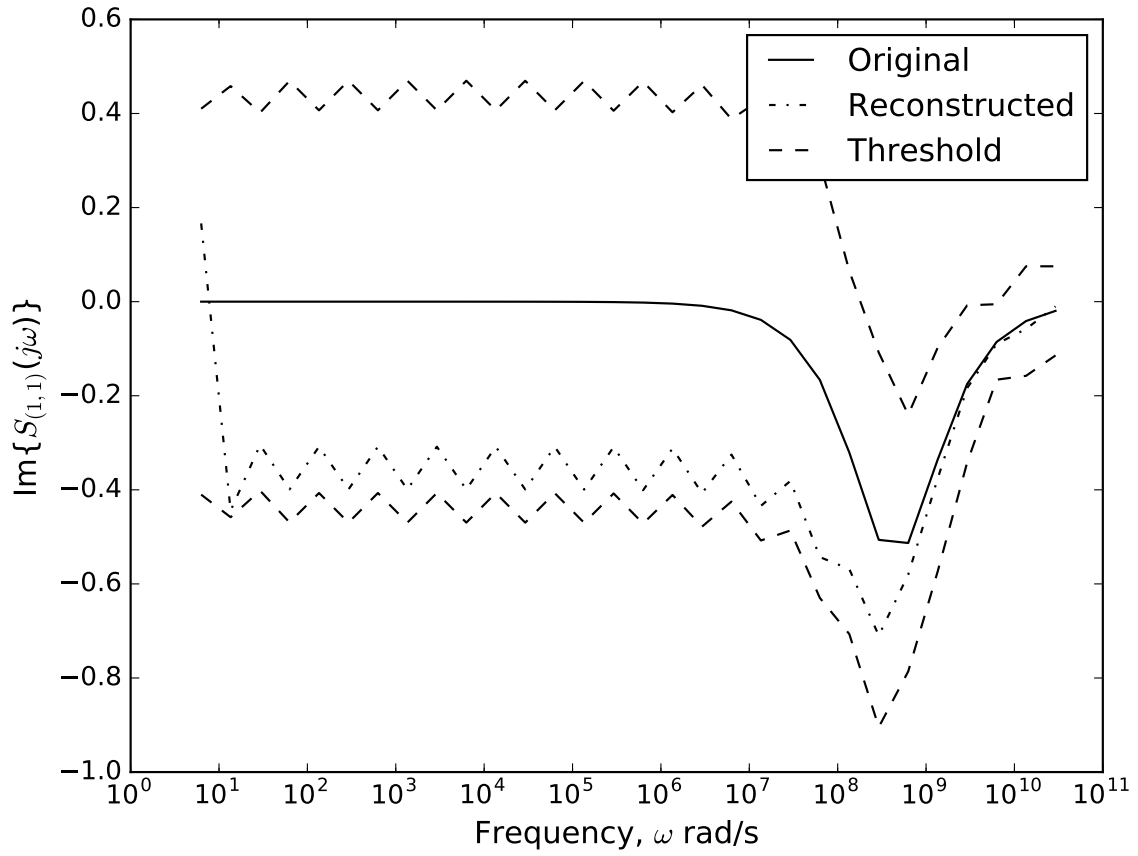


Figure 4.8: Reconstructed imaginary part of the input transfer function (in log scale). Since the reconstructed output does not go beyond the threshold, the system is causal

As before, if we introduce causality violation into the sampled S-parameter, the reconstructed output goes beyond the threshold value. However, depending on which part of the reconstruction violates causality, we can enforce by replacing the original input with the reconstructed output, as shown in previous example. In this case also, we add similar perturbation for manually injecting causality violation. The reconstructed outputs are given in figure 4.9 and figure 4.10.

These tests show the validity and the advantage of causality detection and enforcement for high-speed interconnect models. Although, we need to carefully choose different parameters to run the test smoothly and accurately. Proper use of the variables can ensure useful application of this technique in large scale.

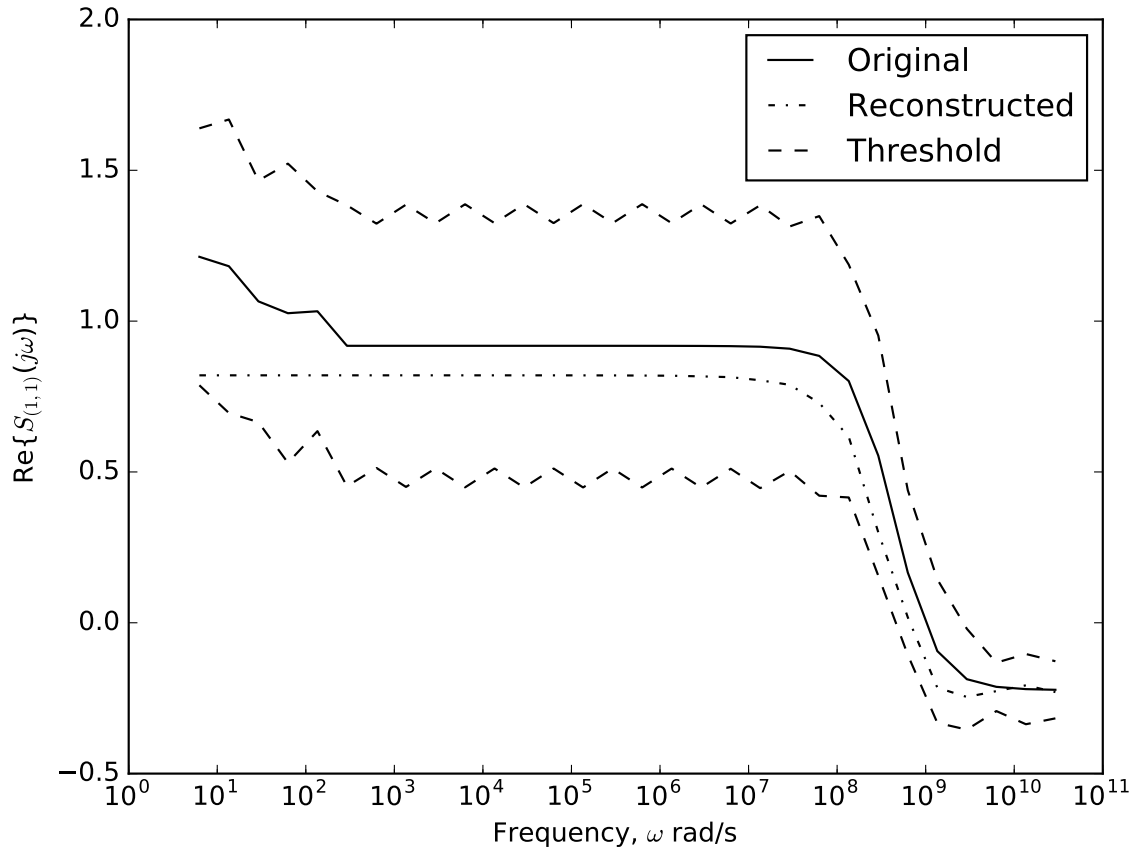


Figure 4.9: Reconstructed Real part of the input transfer function (in log scale) with the perturbation. The reconstructed output can be used as the causality enforced response

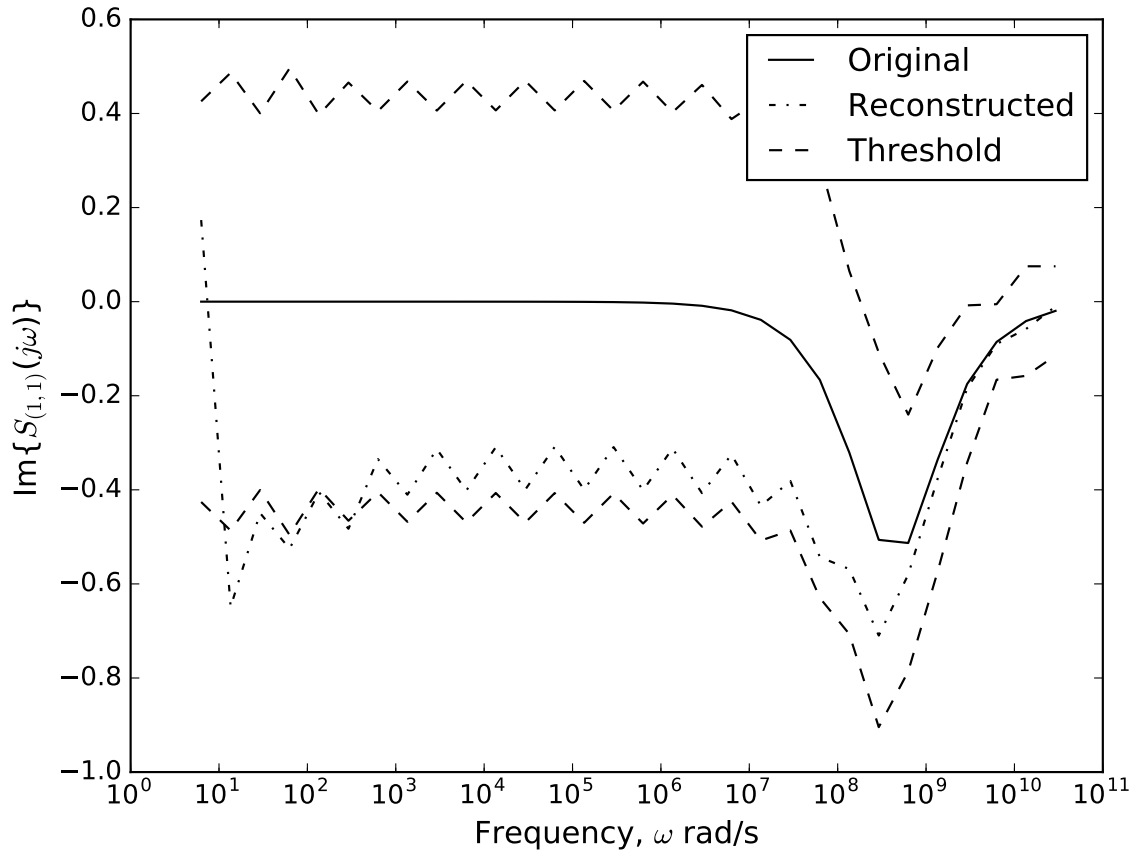


Figure 4.10: Reconstructed imaginary part of the input transfer function (in log scale) which shows causality violation.

4.7 Summary

In this chapter, we discuss and analyze the frequency-domain causality verification and enforcement techniques based on the Generalized Hilbert Transform with subtractions. The method is fairly complicated and difficult to implement. Moreover, the detection threshold is largely dependent on the number and location of the subtraction points. Increasing number of subtraction points makes the threshold value become too narrow, which may report false-positive outcome. On the other hand, as the bandwidth spanned by subtraction points go closer to the actual bandwidth, the threshold becomes wider, which may declare all systems as causal. Therefore, the parameters have to be carefully chosen. Additionally, the computation time for running the test increases exponentially with number of frequency samples. For larger systems with dense frequency samples, the use of this technique becomes impractical. In the following chapter, we introduce a method which is much simpler and faster compared to this technique, and is able to detect causality violation with good precision.

CHAPTER 5

Causality Verification and Enforcement of Signal Power Integrity Models by Filtered Hilbert Transform on Extrapolated Systems

In this chapter, we propose a method for checking causality in frequency-domain by applying direct Hilbert Transform on the system; however, using direct Hilbert Transform on sampled transfer functions may result in significant detection errors. To address these issues, we develop a frequency-domain method based on Hilbert Transform that apply a minimum phase filter on extrapolated data beyond maximum sampled frequency. We demonstrate that a minimum phase low-pass filter with suitable parameters reduces the error and provides a definite threshold which may be used to accurately determine the causality of the system under consideration. Also, we demonstrate two ways to enforce causality using this technique, and provide several examples that highlight the strengths and weaknesses of the proposed method.

5.1 Introduction

In this chapter, we propose a technique that overcomes the issues associated with both time-domain [50] and frequency-domain method [41] discussed above. We take a a minimum-phase low-pass filter and set the cutoff frequency to the maximum available frequency that has a sampled value (ω_{max}), so that no valuable frequency response is attenuated. We also extrapolate the sampled frequency response to a certain extent so that after applying the filter, the response becomes asymptotically decaying in nature. On the filtered response, we apply direct Hilbert Transform to compare: a) the real part of the sampled response with the reconstructed real part (Hilbert Transform of the imaginary part); b) the imaginary part of the sampled response with the reconstructed imaginary part (Hilbert Transform of the real part). Since we are using finite number of samples to apply the Hilbert Transformation, an

error will be introduced. We analytically find an expression for determining the error, which acts as the detection threshold for verifying causality. The technique is tested with different filter configurations (filter order and pass-band ripple) and we declare an appropriate range for the method to be effective. Numerical examples are shown both for causal and non-causal frequency responses. The main contributions of this work can be summarized as:

a) We propose that the cutoff frequency of the filter to be equal to the maximum frequency, which removes the sensitivity of the filter cutoff frequency. Also, the analysis is done in frequency-domain, so no error is introduced for frequency-domain to time-domain conversion.

b) In this work, we use direct Hilbert Transform instead of the dispersion relation with subtractions [41]. As a result, the dependency on the location of the subtraction points are removed. Also, the proposed technique is much faster and simpler to implement.

c) We derive an analytic expression for estimating error that arises from performing direct Hilbert Transform, which to the best of our knowledge has not been developed before. We demonstrate the effectiveness of this threshold value in the numerical examples.

The chapter is organized into several sections to describe the method. Section 5.2 describes the methodology for Hilbert transform and its utility in detecting causality violations. In Section 5.3, we introduce a minimum-phase low-pass filter for improved results. Section 5.4 shows the utility of extrapolating the data and then applying the filter. Here, we determine the error bound for detecting causality violations. Section 5.5 shows few more analysis and examples related to the technique. In the following section (section 5.6), we discuss the effect of different filter parameters and their effect on the causality test. In section 5.7 we discuss how the proposed technique can be used to enforce causality on non-causal system. We have a concluding discussion and probable future prospects of this technique in section 5.8.

5.2 Dispersion Relations and the Hilbert Transform

The close relationship of causality and dispersion relations has been discussed previously in chapter 2. In this chapter, we primarily focus on the effect of applying the K-K relation directly on sampled frequency-domain data. For causal systems, the dispersion relations should be validated. One way of checking the causality of the system under consideration is to validate the dispersion relations on them.

Reference [17] addressed the Hilbert transformation as a means of verifying causality of measured continuous-wave data. In this paper, a numerical formulation of the Hilbert transformation is demonstrated with several examples. Assuming spectral symmetry, $\text{Re}\{H(j\omega)\} = U(\omega)$ is an even function of ω and $\text{Im}\{H(j\omega)\} = V(\omega)$ is an odd function of ω . As a consequence of these relations, if only one part of the transform is known, the other may be determined. However, these relations only hold for square-integrable functions as they asymptotically decay to zero as frequency increases, which may not occur for general S-parameters. To show the kind of error that arises from direct Hilbert transform of sampled functions, we take a fictitious system $H_c(j\omega)$ of the following form:

$$H(s) = \sum_{n=1}^N \left(\frac{c_n}{s - p_n} + \frac{c_n^*}{s - p_n^*} \right) \quad (5.1)$$

Where, the Laplace variable $s = \sigma + j\omega$; for our analysis we assume that the real part of the frequency parameter $\sigma = 0$ and ω is the angular frequency in the units of *rad/sec*. c_n, c_n^* refers to the complex conjugate pair of residues and p_n, p_n^* refers to the complex conjugate pairs of poles. N refers to the total number of pairs; in our example we have $N = 3$. The three pairs of causal complex conjugate sets of poles and residues listed in Table 5.1:

By observing the poles of the system, we can confirm that the system is causal. Now, we take sample values of $H(s)$ upto $\omega_{max} = 8000 \text{ rad/s}$ with 1000 equidistant frequency points to obtain the frequency response H_s and normalize the function to obtain a causal sampled version of $H(s)$. The reason for normalizing will be apparent in the following discussion

Table 5.1: Poles and residues for realizing the causal system $H(s)$

n	c_n	p_n
1	$-20 \pm 180j$	$-120 \pm 1500j$
2	$-10 \pm 160j$	$-140 \pm 2000j$
3	$60 \pm 450j$	$-300 \pm 6500j$

about error estimation. Then, using the spectral symmetry described in equation (5.2), we obtain the double sided frequency response H_{ds} that is defined in the range $[-\omega_{max}, \omega_{max}]$. After normalizing H_{ds} with respect to its absolute value, we finally obtain $H_c(j\omega)$ that is ready for Hilbert transform:

$$H_s(j\omega) \xrightarrow{\text{extend}} H_{ds}(j\omega) \xrightarrow{\text{normalize}} H_c(j\omega)$$

After obtaining the normalized sampled causal function, we perform the Hilbert transform using equations (2.1a)-(2.1b). There are numerous methods of performing numerical evaluation of the Hilbert Transform in literature [81, 82]. As expected, the Hilbert transform of the real part of $H_c(j\omega)$ does not match with the imaginary part of the same transfer function. This result is shown in Figure 5.1.

Similarly, the Hilbert transform of the imaginary part of $H_c(j\omega)$ does not match with the real part, which is depicted in Fig. 5.2. We see a violation of the K-K relation even when the transfer function is clearly causal.

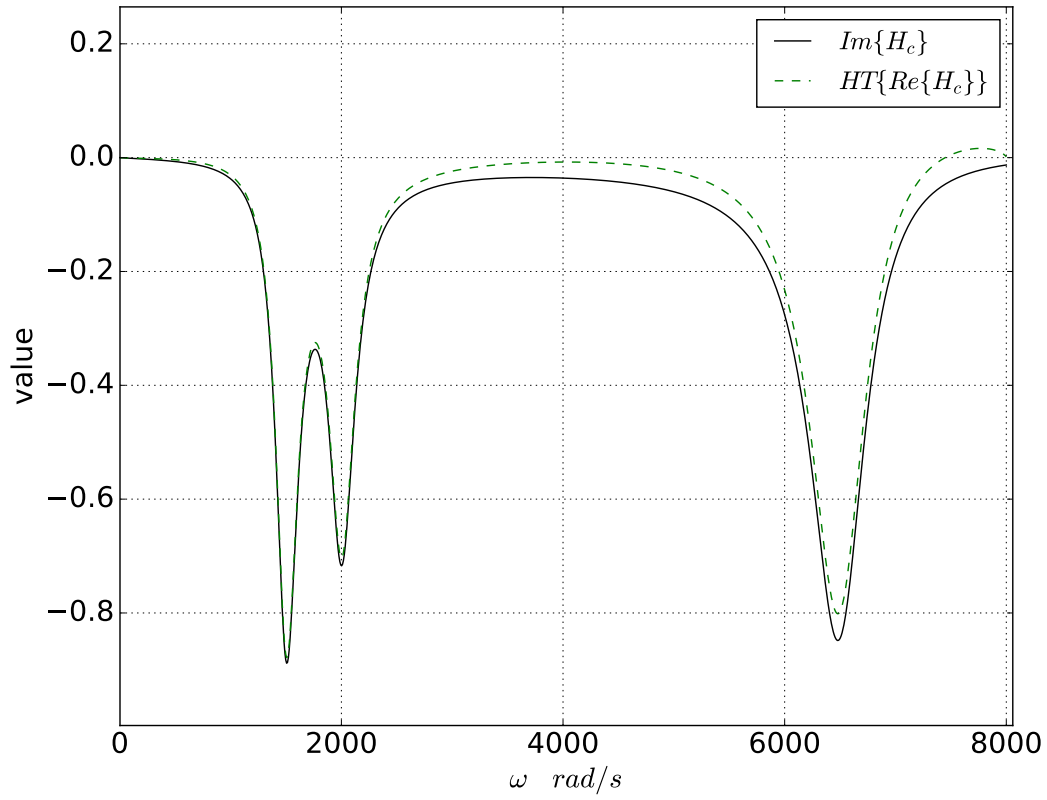


Figure 5.1: Comparison of imaginary part of $H_c(j\omega)$ and the Hilbert Transform of the real part of $H_c(j\omega)$. Although the function is causal, reconstructed imaginary does not match with the original.

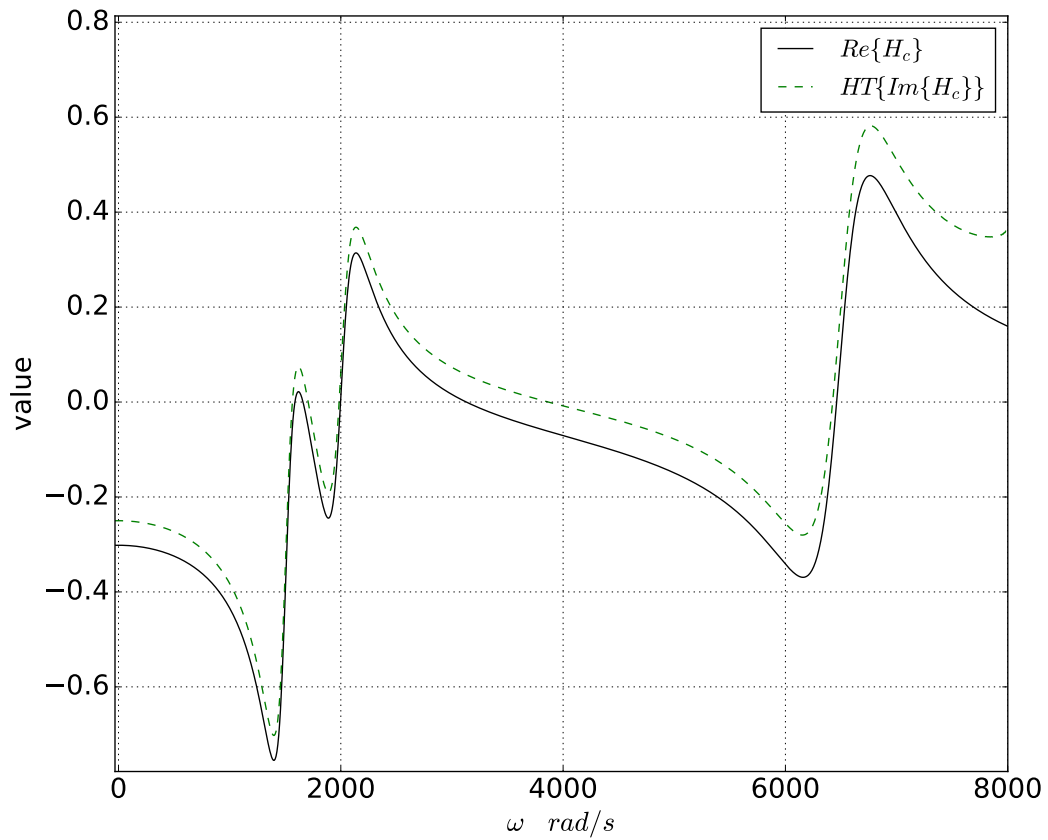


Figure 5.2: Comparison of real part of $H_c(j\omega)$ and the Hilbert Transform of the imaginary part of $H_c(j\omega)$. Although the function is causal, reconstructed real does not match with the original.

Although, from the figure we can visualize that the reconstructed output follows the variations and trends of the original response. The mismatch occurs because of the finitely truncated signal at ω_{max} . But there is no quantitative measure of how much error can we expect from the direct Hilbert transform of such a band-limited signal. Since we know that the K-K relations are valid for square-integrable functions, for the functions that does not decay as $\omega \rightarrow \infty$, direct Hilbert transform produces large error. In the following section, we discuss a possible way of reducing the error of this nature.

5.3 The Low-pass Filter Approach

5.3.1 Minimum Phase Filter

Previously, in reference [50], a theorem is provided that stated that applying a minimum-phase filter preserves the causality characteristic of the original signal. The method described in [50] uses a low-pass filter on the sampled response and performs inverse Fourier Transform to find the impulse response in time-domain. However, performing inverse Fourier Transform on a finite sequence introduces error. Additionally, the technique is heavily dictated by the filter parameters, which are described in details in reference [53]. Another ambiguity of this method is that, there is no definite limit on how much in negative time the impulse response should be determined.

In order to alleviate the ambiguity with the negative time, we decided to stay in the frequency-domain for the causality test. The most dominant filter parameter is the cutoff frequency of the filter, hence we have fixed the cutoff frequency equal to the maximum available sample frequency ($\omega_{cutoff} = \omega_{max}$). Therefore, the sensitivity due to the variation of cutoff frequency goes away.

Therefore, our approach is to apply a minimum-phase low-pass filter on the transfer function. The filter will tend to drive the signal into a decaying nature after the cutoff frequency. According to the theorem described in [50], the filtered version will still retain

the causality characteristic of the original signal. To demonstrate the effectiveness of applying a filter, we apply a low-pass Chebyshev type-I filter with order, $nn = 3$ and pass-band ripple $rp = 3 \text{ dB}$ on $H_c(j\omega)$ and then perform Hilbert Transform on the real and imaginary part of the signal. The results are shown in Fig 5.3 and 5.4. The filter operation can be shown as follows:

$$H_{cf}(j\omega) = H_c(j\omega)F(j\omega) \quad (5.2)$$

Here, H_{cf} is the filtered transfer function and $F(j\omega)$ is the frequency response of the low-pass filter.

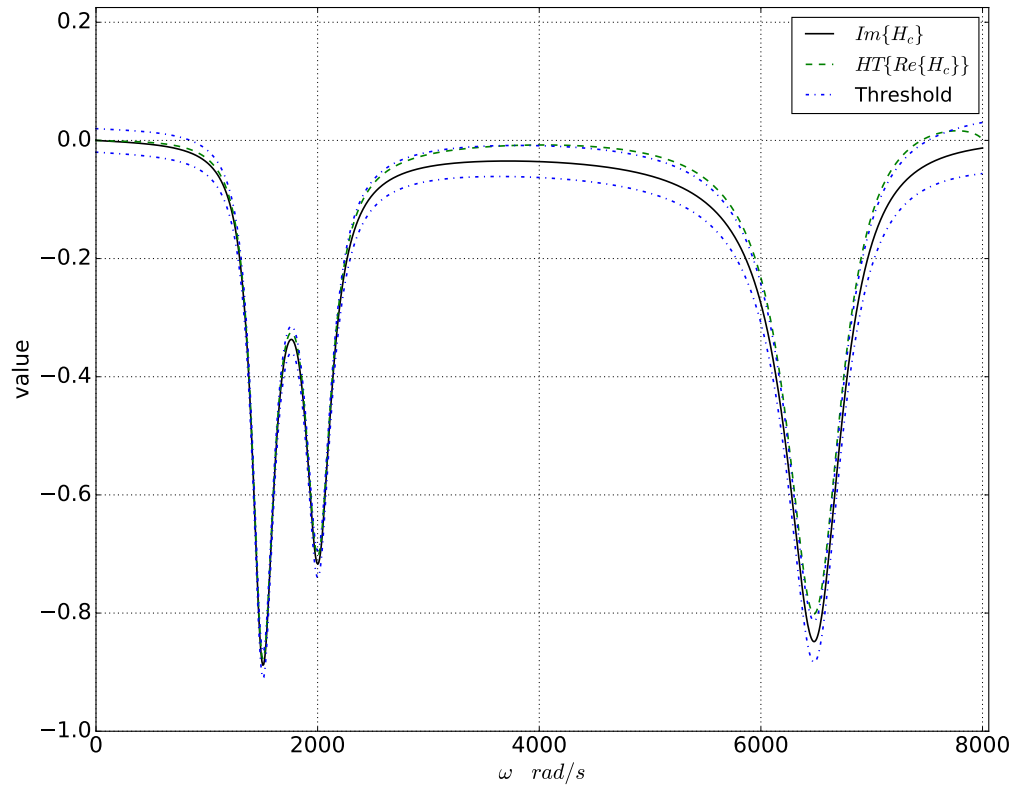


Figure 5.3: Comparison of imaginary part of $H_c f(j\omega)$ and the Hilbert Transform of the real part of $H_c f(j\omega)$. The reconstruction error is much less than Fig. 5.2, but still significant close to ω_{max} . Here, $nn = 3$ and $rp = 3$ dB.

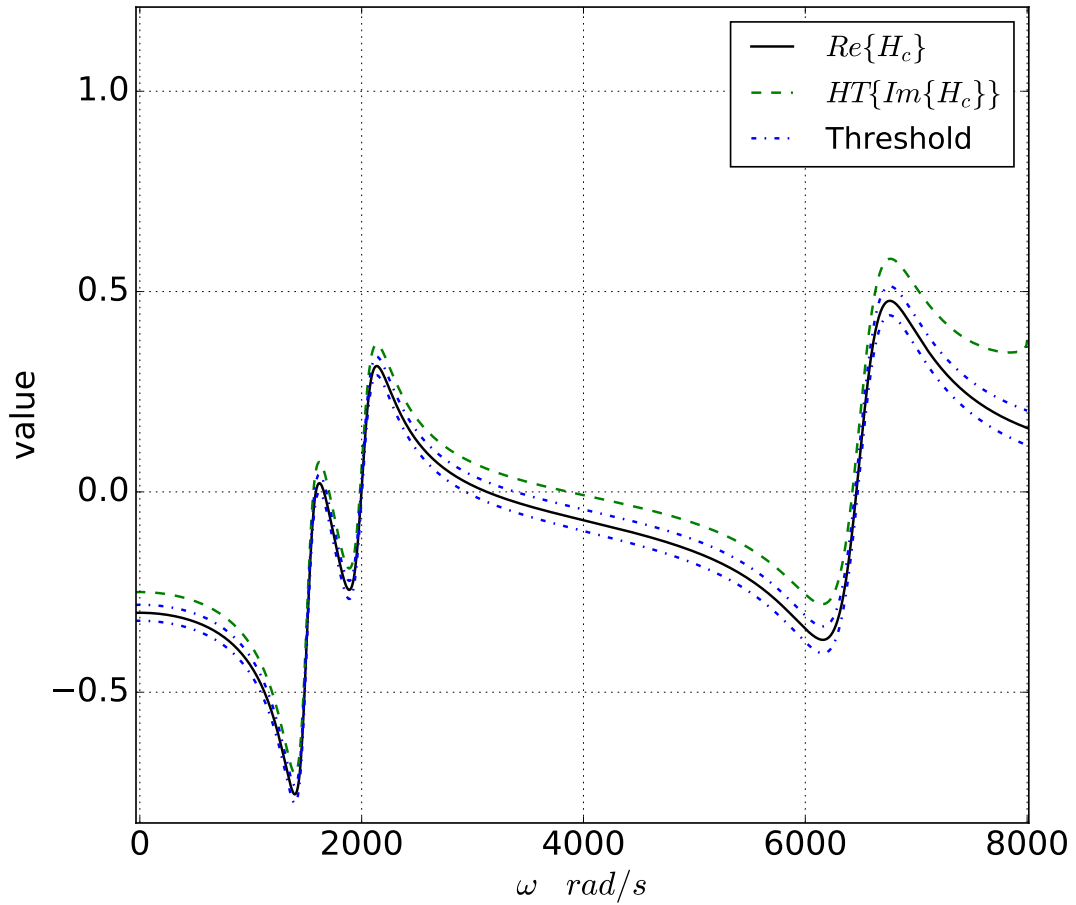


Figure 5.4: Comparison of imaginary part of $H_c(j\omega)$ and the Hilbert Transform of the imaginary part of $H_c(j\omega)$. Here, $nn = 3$ and $rp = 3$ dB.

5.3.2 Error Estimation

The use of a low-pass filter allows us to estimate the truncation error accurately. Since we are normalizing the system before applying the filter, the individual real or imaginary part of the signal is restricted between $[-1,1]$. The following analysis helps us to determine the maximum error bound that may occur upon using the Hilbert Transform. Let us assume that:

$$H_c(j\omega) = U(\omega) + jV(\omega)$$

$$F(j\omega) = F_r(\omega) + jF_i(\omega)$$

Here, $U(\omega)$ and $V(\omega)$ are the real and imaginary parts of the input system $H_c(j\omega)$, respectively. Similarly, $F_r(\omega)$ and $F_i(\omega)$ are the real and imaginary parts of the minimum phase filter $F(j\omega)$. From equation (5.2), we can determine the filtered response $H_{cf}(j\omega)$ as:

$$\begin{aligned} H_{cf}(j\omega) &= H_c(j\omega)F(j\omega) \\ &= (U(\omega) + jV(\omega))(F_r(\omega) + jF_i(\omega)) \\ &= F_r(\omega)U(\omega) - F_i(\omega)V(\omega) \\ &\quad + j(F_r(\omega)V(\omega) + F_i(\omega)U(\omega)) \end{aligned} \tag{5.4}$$

Now, we consider the original Hilbert Transform as provided in equation (2.1a), with the imaginary part of $H_{cf}(j\omega)$ as input, we can obtain the reconstructed filtered real part $U_f(j\omega)$ as follows:

$$\begin{aligned}
U_f(j\omega) &= HT\{Im\{H_{cf}(j\omega)\}\} \\
&= \frac{1}{\pi} \int Im\{H_{cf}(j\omega')\} \frac{d\omega'}{\omega - \omega'} \\
&= \frac{1}{\pi} \underbrace{\int_{-\omega_{max}}^{\omega_{max}} Im\{H_{cf}(j\omega')\} \frac{d\omega'}{\omega - \omega'}}_{r_F(\omega)} \\
&\quad + \frac{1}{\pi} \underbrace{\int_{|\omega'| > \omega_{max}} Im\{H_{cf}(j\omega')\} \frac{d\omega'}{\omega - \omega'}}_{e_F(\omega)}
\end{aligned} \tag{5.5}$$

Here, $r_F(\omega)$ refers to the reconstructed real part that is calculated by applying equation (2.1a) numerically. The term $e_F(\omega)$ refers to the associated error after applying the filter, which accounts for the frequencies beyond ω_{max}). We can further simplify the expression of the absolute error associated with the filtering as follows:

$$e_F(\omega) = \frac{1}{\pi} \int_{|\omega'| > \omega_{max}} \frac{F_r(\omega)V(\omega) + F_i(\omega)U(\omega)}{(\omega - \omega')} d\omega'$$

We have already normalized $H_c(j\omega)$, therefore $U(\omega)$ and $V(\omega)$ can not exceed 1. At the worst case, we can assume $U(\omega)$ and $V(\omega)$ equal to 1 when $|\omega'| > \omega_{max}$. We also notice that the real part of the filter is even symmetric and imaginary part of the filter is odd symmetric. Therefore, the integral reduces to:

$$e_F(\omega) = \frac{2}{\pi} \int_{\omega_{max}}^{\infty} \frac{F_r(\omega')}{\omega - \omega'} d\omega' \tag{5.6}$$

Throughout our analysis, we use the above derived expression of maximum error bound for causality detection using direct Hilbert Transform. If the reconstructed output stays within the original value added with the error threshold, the system can be regarded as causal. If the reconstructed output goes beyond the threshold at any point, then we can decide that the real and imaginary part of the system is not related by the K-K relations, therefore the sample has causality violation.

However, in figure 5.3 and 5.4, although the input is causal, the reconstructed output

has significant mismatch at the extreme end of the spectrum, where it should be within the maximum error limit defined by the error threshold. The reason for this mismatch is the abrupt truncation at the end of the spectrum. For the direct Hilbert Transform to converge, the data needs to be asymptotically decay, which is not guaranteed when we abruptly truncate the samples at ω_{max} . In the following section, we try to provide a possible solution for this issue.

5.4 Numerical Extrapolation

One way to ensure that the system goes into decaying nature is to apply a low-pass filter. But applying a low-pass filter raises the probability of losing valuable information of the signal at high frequency. Primarily for this reason, we have selected the cutoff frequency of the filter being used to be at the maximum frequency. However, the abrupt truncation causes the Hilbert Transformation to diverge at the high frequency end. One possible solution would be to extrapolate the original data to some extent and then applying the filter. This ensures the preservation of information up to ω_{max} and only the extrapolated data will be attenuated by the filter. In this section we discuss two possible extrapolation techniques that can be used.

5.4.1 Linear Extrapolation

For our first approach, we use simple linear extrapolation technique on the original sampled response to get the result. We have used the same filter to conduct this test. The data was extrapolated up to 50% of the original data, therefore the last sample point of the new data would be $\omega_{ex} = 1.5 \times \omega_{max}$. Applying the filter and then taking the Hilbert Transform yields the results depicted in the following figures.

We can observe from these plots that for the causal case, the reconstructed response stays within the error threshold, therefore detecting a causal system appropriately.

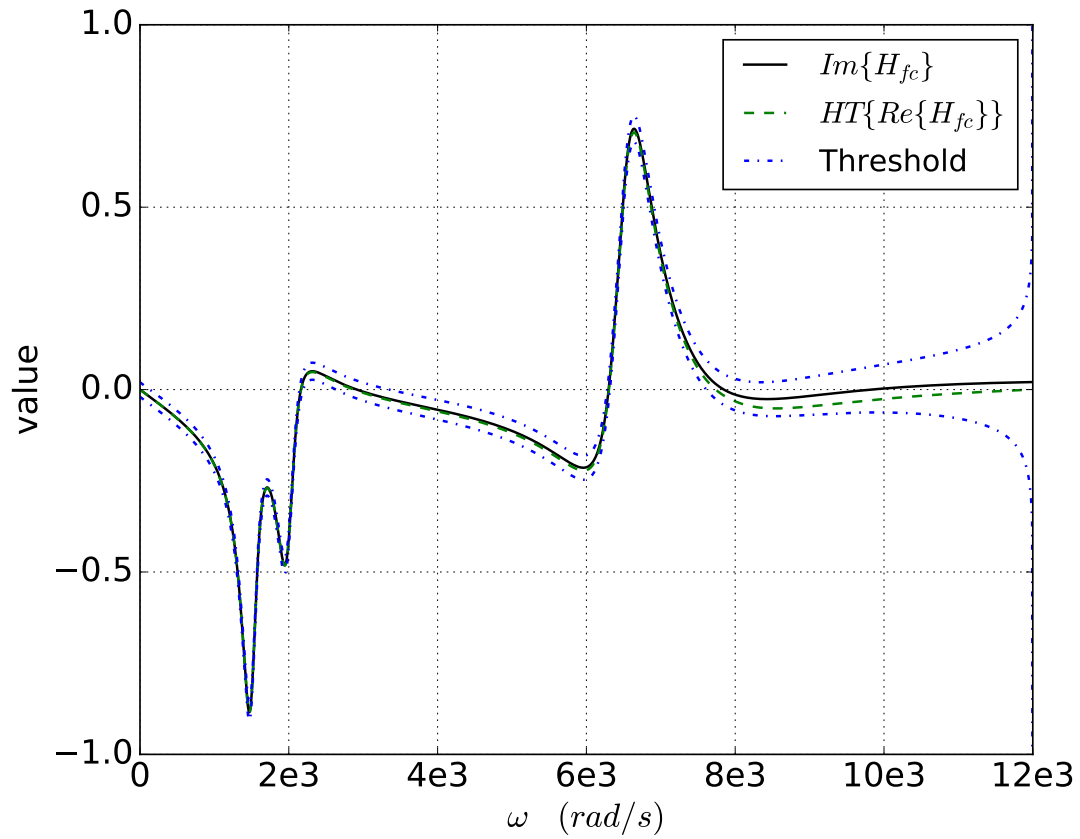


Figure 5.5: Comparison of imaginary part of $H_{cf}(j\omega)$ and the Hilbert Transform of the real part of $H_{cf}(j\omega)$ using Linear extrapolation. The reconstruction error in the vicinity of ω_{max} is removed. Filter parameters: $nn = 3$ and $rp = 3$ dB. Here, $\omega_{max} = 8000$ rad/s, $\omega_{ex} = 12000$ rad/s

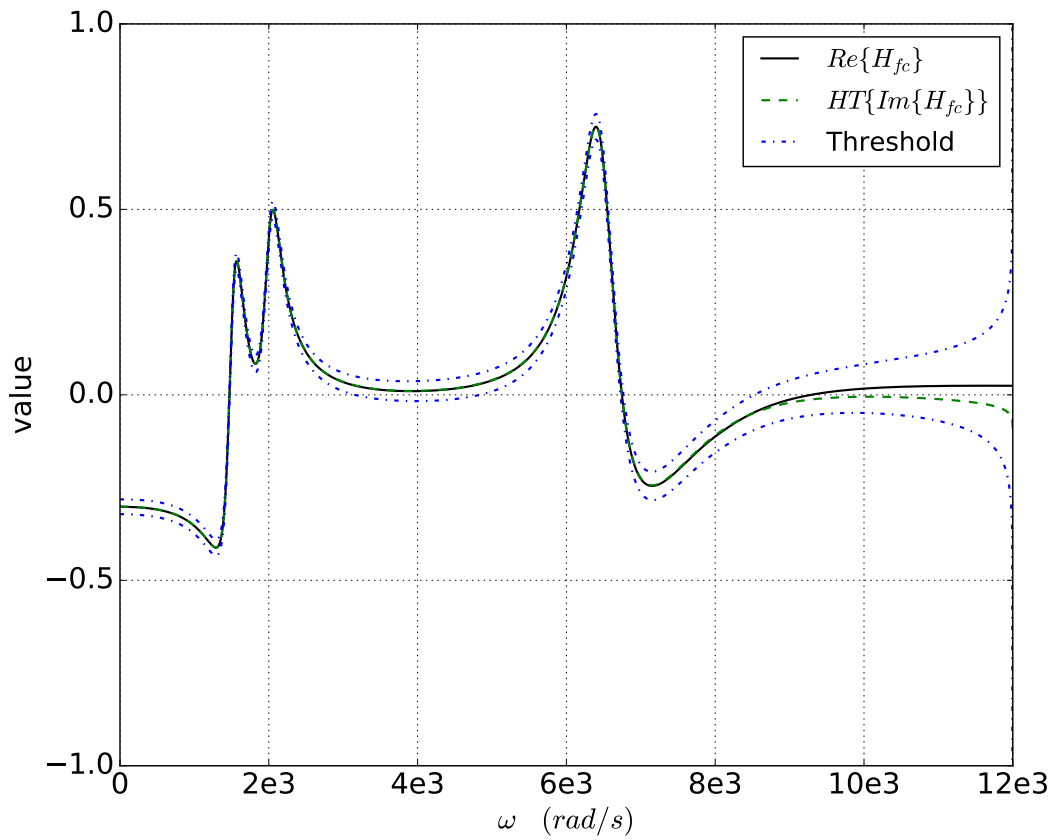


Figure 5.6: Comparison of imaginary part of $H_{cf}(j\omega)$ and the Hilbert Transform of the real part of $H_{cf}(j\omega)$ using Linear extrapolation. Here, $nn = 3$ and $rp = 3$ dB and $\omega_{max} = 8000$ rad/s, $\omega_{ex} = 12000$ rad/s.

5.4.2 Three Point Extrapolation

We have implemented another technique for extrapolating the original system, which is referred to as *Three point frequency-domain extrapolation*. An elaborate approach to obtain high frequency extrapolated data could be a rational polynomial to curve-fit the tabulated data [83], which implicitly extrapolates the data beyond the original range. We use the algorithm provided in reference [83] to fit the last three points of the available frequency response to obtain a rational function with complex conjugate pair of poles and residues. Details about the formulation of the fitted response can be found in reference [84]. The fitted polynomial is attached to the original response beyond the maximum frequency (ω_{max}) and up to the extrapolated frequency (ω_{ex}). Using the updated frequency response, the reconstruction operation is again performed to verify causality. The filter parameters are kept the same as before. The results are shown in Fig. 5.7, 5.8.

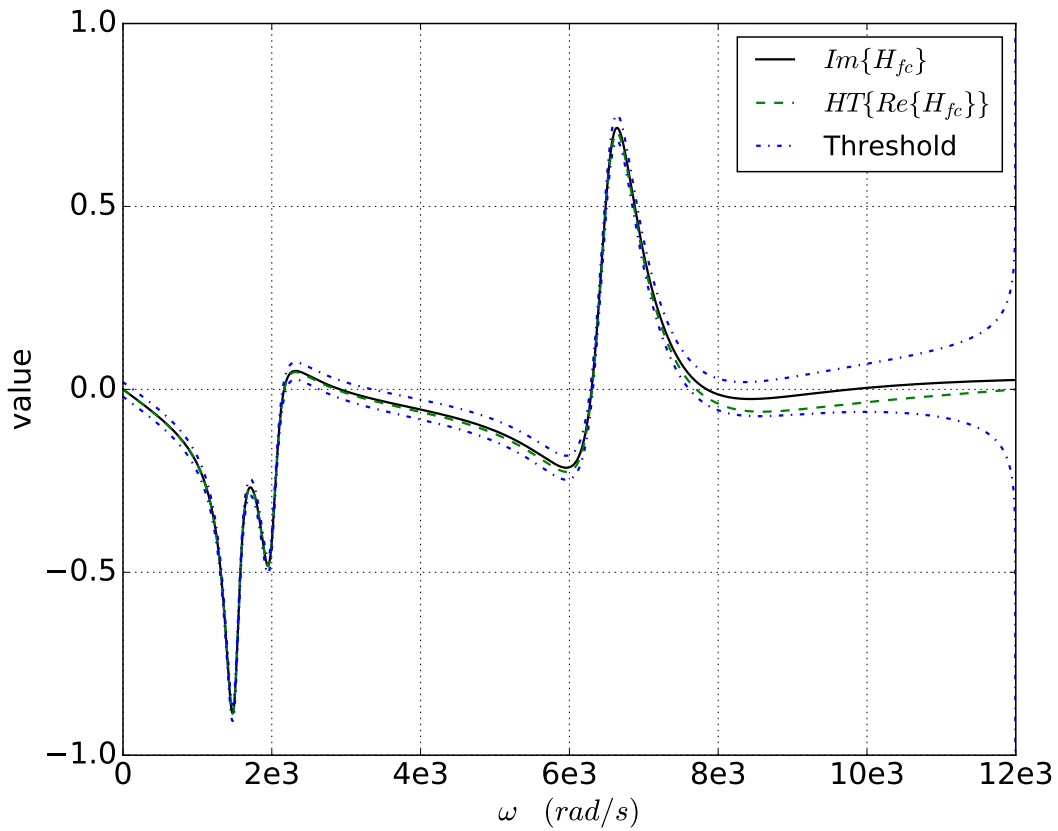


Figure 5.7: Comparison of imaginary part of $H_{cf}(j\omega)$ and the Hilbert Transform of the real part of $H_{cf}(j\omega)$ using Three-point extrapolation. The reconstruction error in the vicinity of ω_{max} is removed. Filter parameters: $nm = 3$ and $rp = 3$ dB. Here, $\omega_{max} = 8000$ rad/s, $\omega_{ex} = 12000$ rad/s

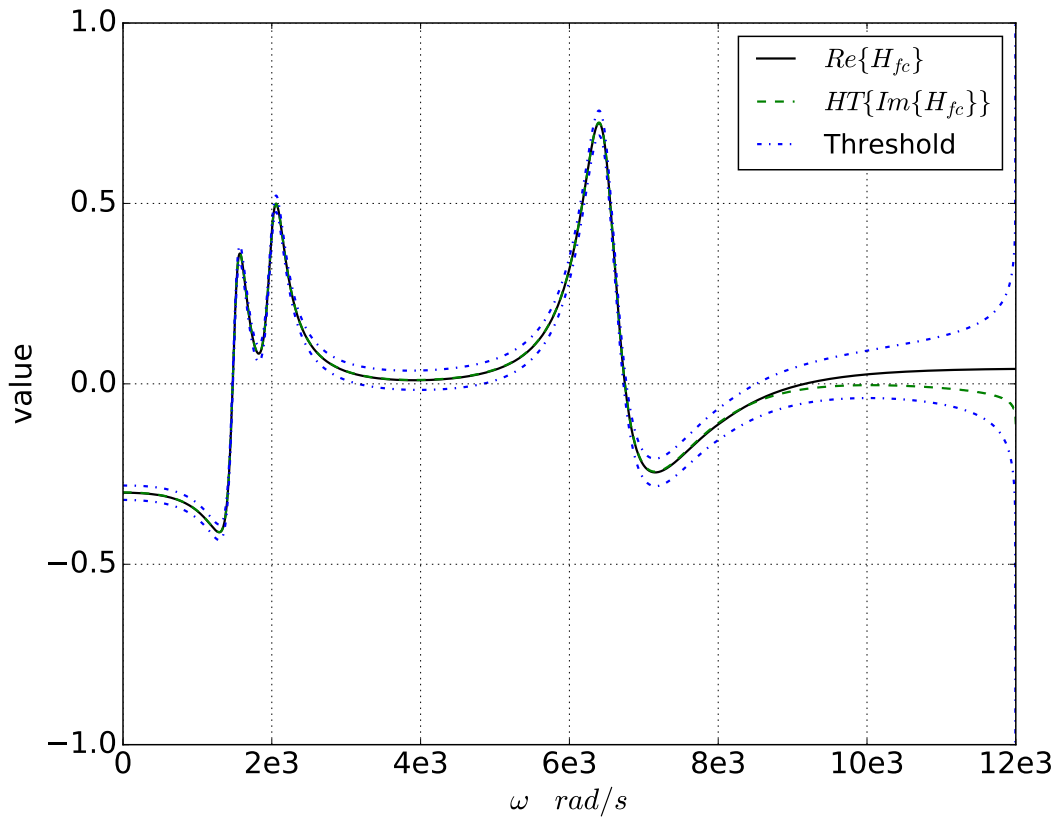


Figure 5.8: Comparison of imaginary part of $H_{cf}(j\omega)$ and the Hilbert Transform of the real part of $H_{cf}(j\omega)$ using Three-point extrapolation. Here, $nn = 3$ and $rp = 3$ dB and $\omega_{max} = 8000 \text{ rad/s}$, $\omega_{ex} = 12000 \text{ rad/s}$.

From these figures, it is evident that this extrapolation technique improves the causality detection from detection without using extrapolation.

5.5 Detecting Causality Violation

So far, we have shown the validity of our proposed technique for causal examples and it appears that when using a low-pass filter and extrapolation, the above described technique detects causal responses correctly. For our next analysis, we take a pair of non-causal pole/residue to show whether the method can detect causality violations. For this purpose, we make modification to the existing system by adding the non-causal part as follows:

$$H_x(j\omega) = \left(\frac{-30 + 150j}{j\omega - (-170 + 2500j)} + \frac{-30 - 150j}{j\omega - (-170 - 2500j)} \right) \times 0.1e^{0.03\omega} \quad (5.7)$$

Because of the presence of the exponential anticipatory term $e^{0.03\omega}$, which in time-domain accounts for a negative delay, $H_x(j\omega)$ becomes non-causal, although the amplitude of the non-causal poles and residues are multiplied by a factor of 0.1. When added with $H_c(j\omega)$, the result becomes non-causal as well:

$$H_{nc}(j\omega) = H_c(j\omega) + H_x(j\omega) \quad (5.8)$$

If we apply the same 3rd order filter with cutoff frequency at $\omega_{max} = 8000 \text{ rad/s}$ and extrapolate up to $\omega_{ex} = 12000 \text{ rad/s}$, we obtain the results depicted in the following figures.

These results show that the non-causality can be detected based on the technique proposed in this work. From the examples we clearly observe that it reports violation only where we added the non-causal pole, which provides effectiveness of this technique.

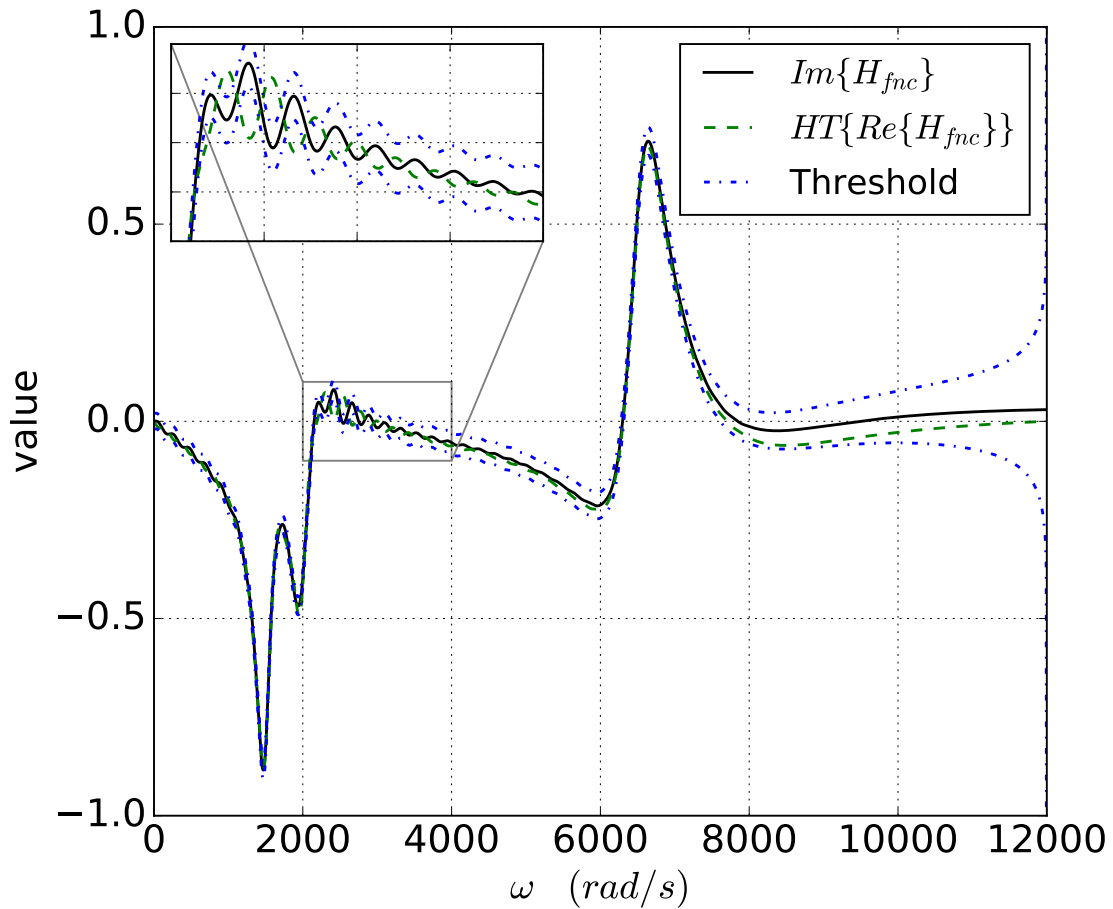


Figure 5.9: Comparison of imaginary part of $H_{ncf}(j\omega)$ and the Hilbert Transform of the real part of $H_{ncf}(j\omega)$ using linear extrapolation. The reconstruction goes beyond the threshold around 2500 rad/s, where the non-causal pole location is located. It is more clearly visible in the zoomed box. Filter parameters: $nn = 3$ and $rp = 3$ dB. Here, $\omega_{max} = 8000$ rad/s, $\omega_{ex} = 12000$ rad/s

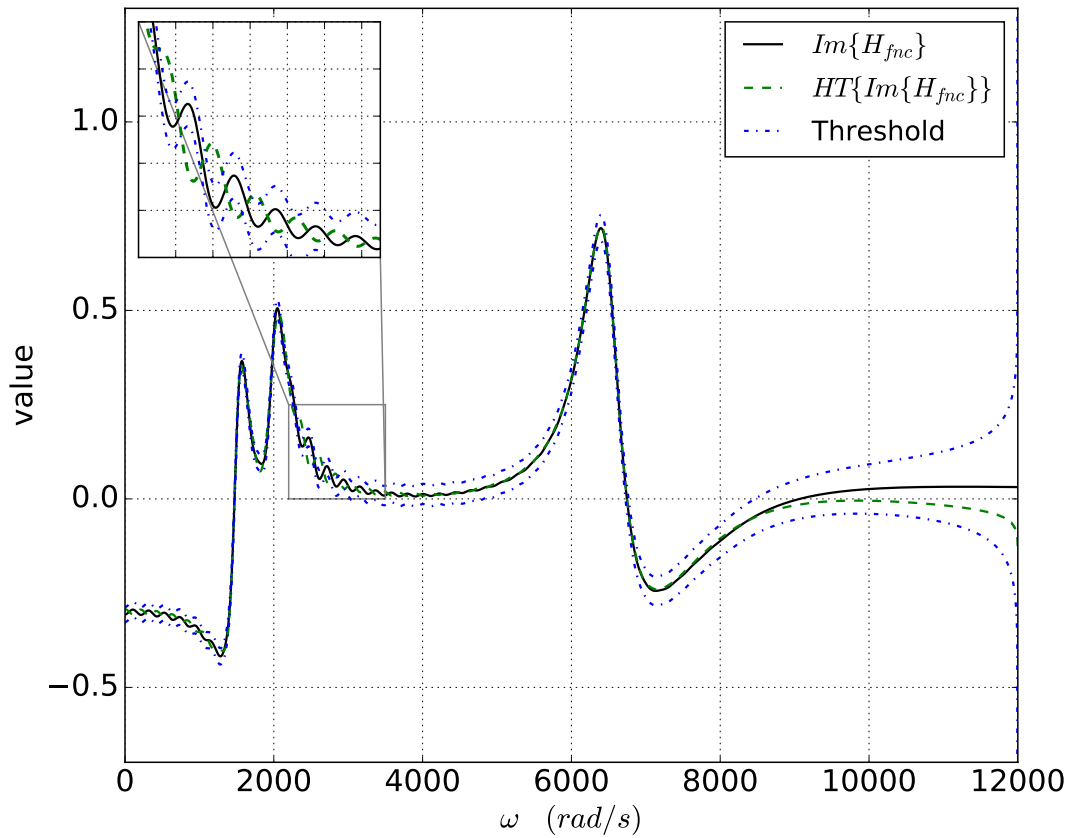


Figure 5.10: Comparison of real part of $H_{ncf}(j\omega)$ and the Hilbert Transform of the imaginary part of $H_{ncf}(j\omega)$ using linear extrapolation. The reconstruction goes beyond the threshold around 2500 rad/s, where the non-causal pole location is located. It is more clearly visible in the zoomed box. Filter parameters: $nn = 3$ and $rp = 3$ dB. Here, $\omega_{max} = 8000$ rad/s, $\omega_{ex} = 12000$ rad/s.

5.6 Effect of Filter Parameters

One of the major contribution of this work is reducing the sensitivity of filter parameters. Since we have set the cutoff frequency at the maximum available frequency, the sensitivity due to different cutoff frequencies are removed [53]. However, there are still two important filter parameters that may drive the test over-sensitive: filter order and pass-band ripple. In our experiments, we have seen that by increasing the filter order, the roll-off becomes steeper making the error threshold narrower, which may declare a causal system as non-causal. Such a case is illustrated in Fig. 5.11, where we used a 6th order type-I Chebyshev low-pass filter with 6 dB ripple. The threshold becomes very narrow which may produce false positive results. Although the response $H_{fc}(j\omega)$ is causal, the reconstructed imaginary part goes beyond the threshold value at several points.

On the other hand, if filter order and ripple is reduced to a very low level, the roll-off gets much slower causing the threshold value to become very large. This way, small causality violations could be impossible to detect, as shown in Fig. 5.12, where a 2nd order type-I Chebyshev low-pass filter with 3 dB ripple is used on the non-causal response $H_{fnc}(j\omega)$. It is clearly visible that the threshold value becomes too large to detect the violation in the input.

Therefore, we have to select a suitable filter order and ripple in order to make the technique work accurately. Upon our experiments, we have selected filter order $nn = 3$ and $rp = 3 \text{ dB}$, which was able to generate consistent results. For all other simulations and plots, this configuration of the filter was used.

5.7 Causality Enforcement

We have demonstrated that we can use our Filtered Hilbert Transform technique to detect causality violation. An important task after detecting violation would be to enforce causality on the original sample, which ensures that the modified system response will be causal. We

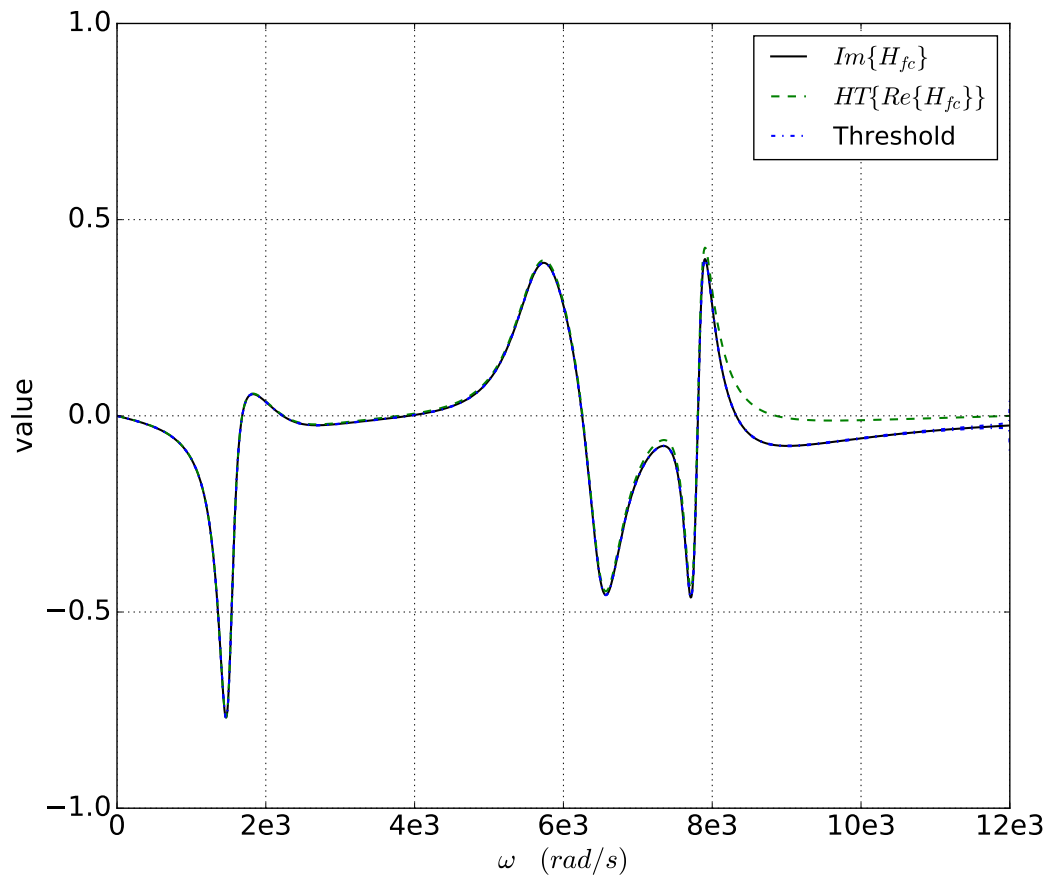


Figure 5.11: Hilbert Transform performed on real part of $H_{fc}(j\omega)$ with filter parameters: $nm = 6$ and $rp = 6$ dB. Here linear extrapolation is used with $\omega_{max} = 8000$ rad/s, $\omega_{ex} = 12000$ rad/s.

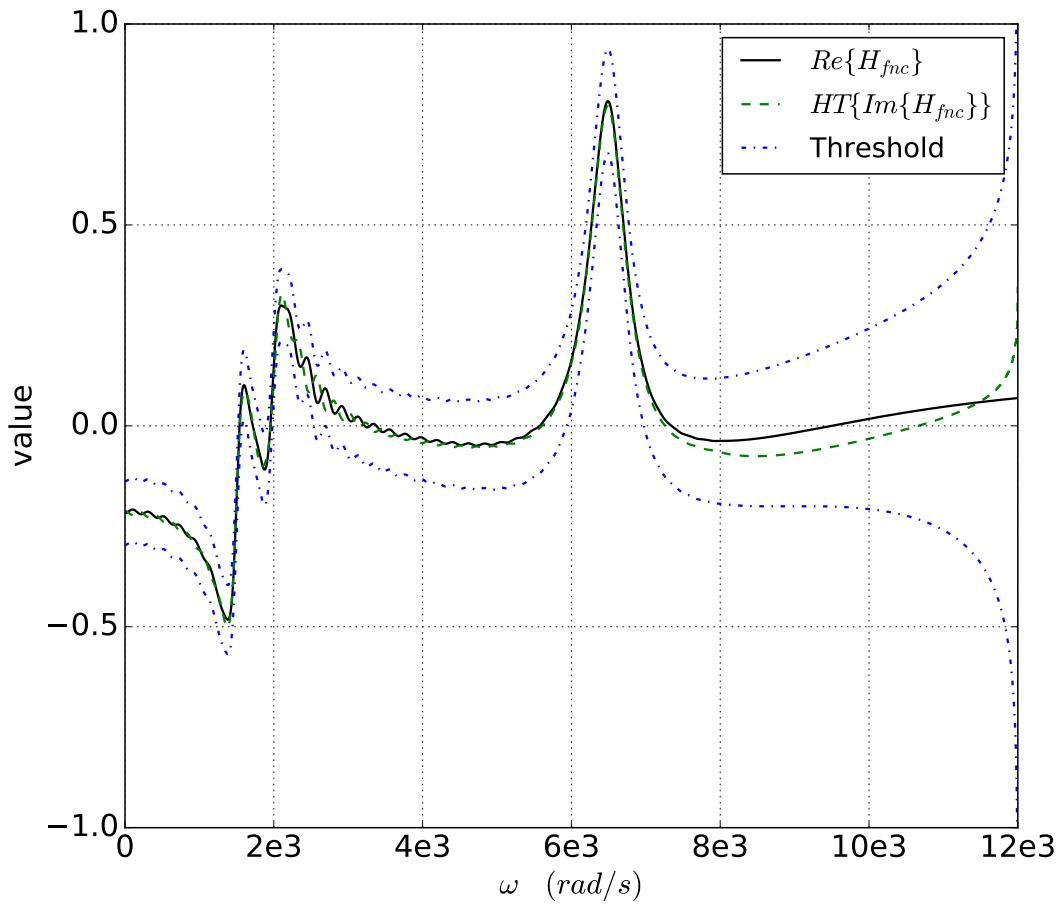


Figure 5.12: Hilbert Transform performed on real part of $H_{fnc}(j\omega)$ with filter parameters: $nn = 2$ and $rp = 3$ dB. Here linear extrapolation is used with $\omega_{max} = 8000$ rad/s, $\omega_{ex} = 12000$ rad/s.

propose two techniques on enforcing causality on frequency responses if there is causality violation found, which are:

Option A) Perform Hilbert Transform on the real part and Enforce causality by replacing the imaginary part with the reconstructed imaginary part (illustrated in Fig. 5.13 and 5.14)

Option B) Perform Hilbert Transform on the imaginary part and Enforce causality by replacing the real part with the reconstructed real part (illustrated in Fig. 5.15 and 5.16)

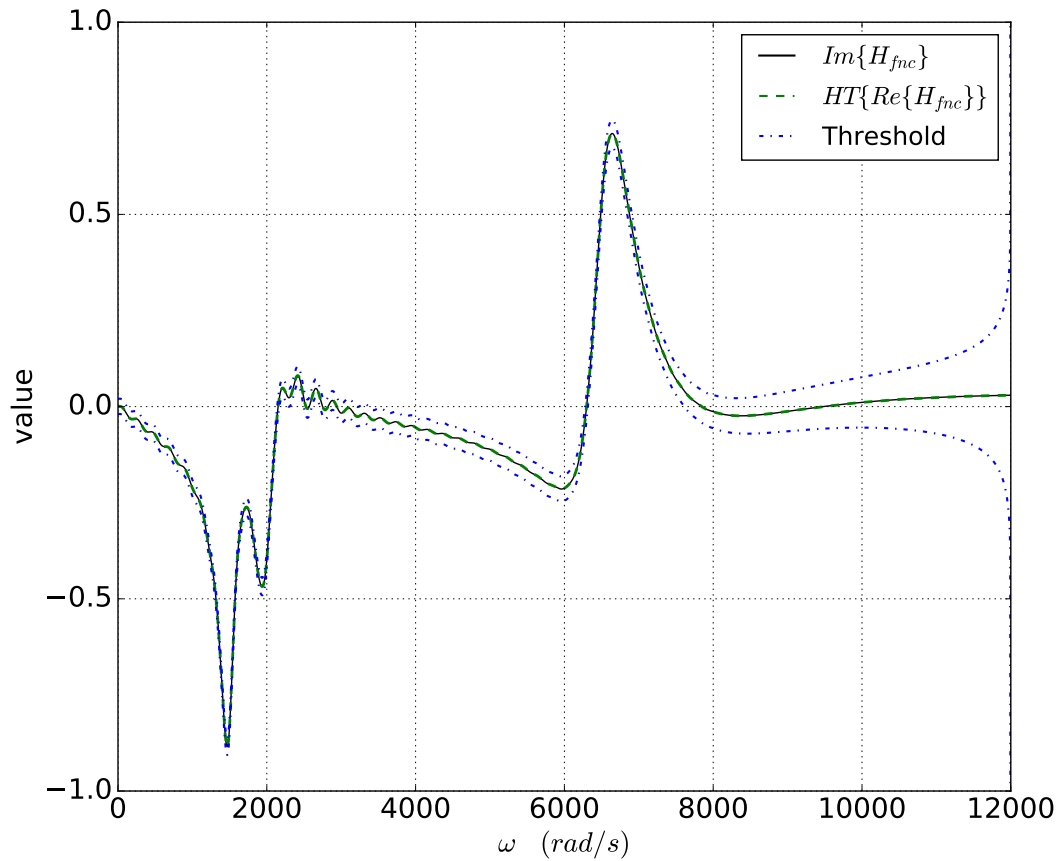


Figure 5.13: Enforcing causality by Option A using Linear Extrapolation. That imaginary part is again used for generating the real part, which is shown here and we observe a full match. Filter parameters: $nn = 3$ and $rp = 3$ dB. Here, $\omega_{max} = 8000$ rad/s, $\omega_{ex} = 12000$ rad/s.

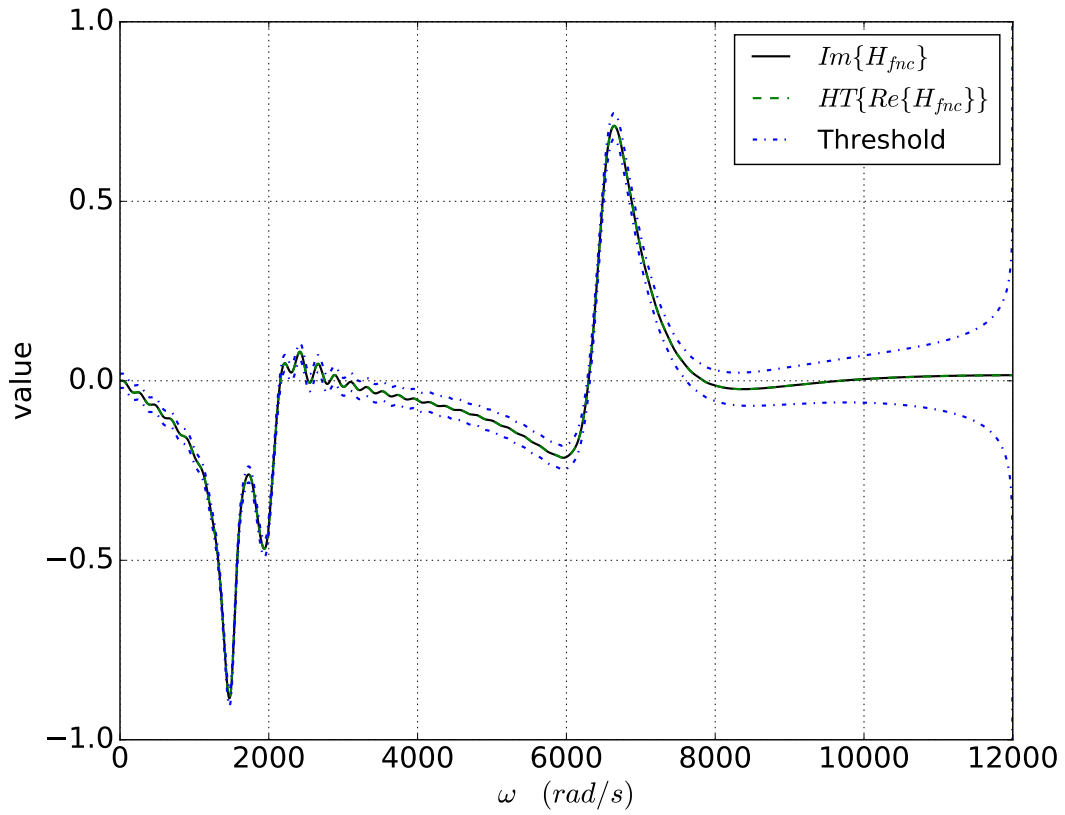


Figure 5.14: Enforcing causality by Option A using Three-point Extrapolation. That imaginary part is again used for generating the real part, which is shown here and we observe a full match. Filter parameters: $nn = 3$ and $rp = 3$ dB. Here, $\omega_{max} = 8000$ rad/s, $\omega_{ex} = 12000$ rad/s.

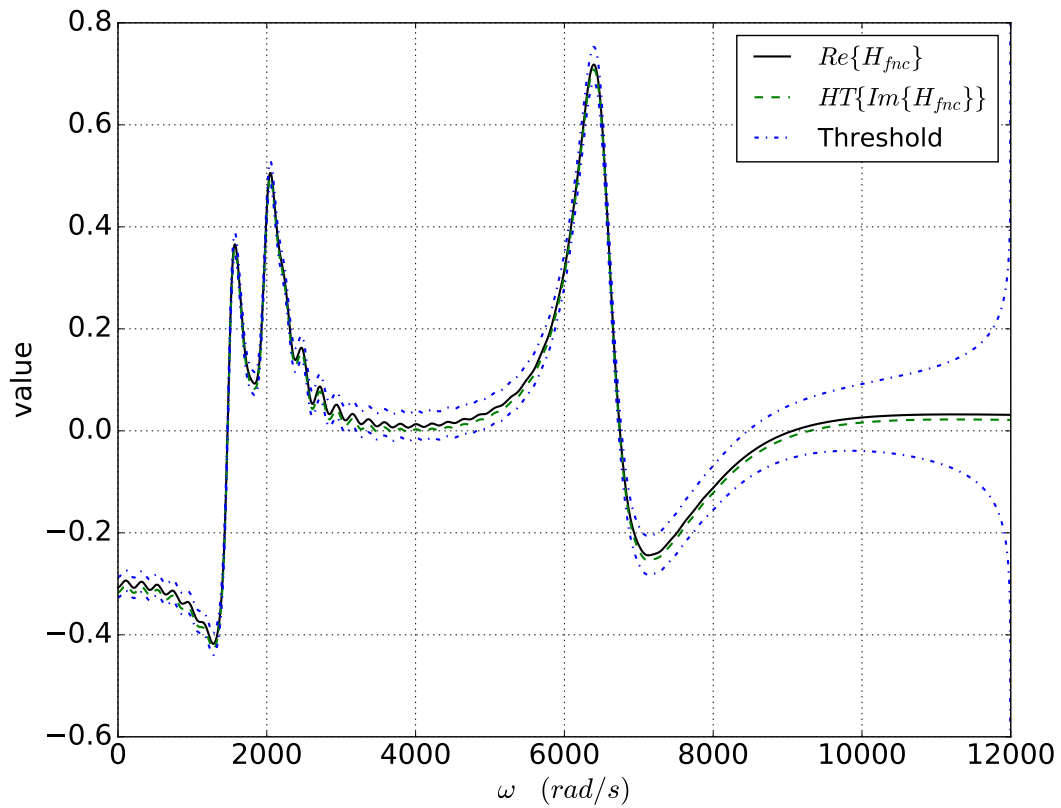


Figure 5.15: Enforcing causality by Option B using Linear Extrapolation. Here, the reconstruction does not fully match, but stays within the threshold limit. Filter parameters: $nn = 3$ and $rp = 3$ dB. Here, $\omega_{max} = 8000$ rad/s, $\omega_{ex} = 12000$ rad/s.

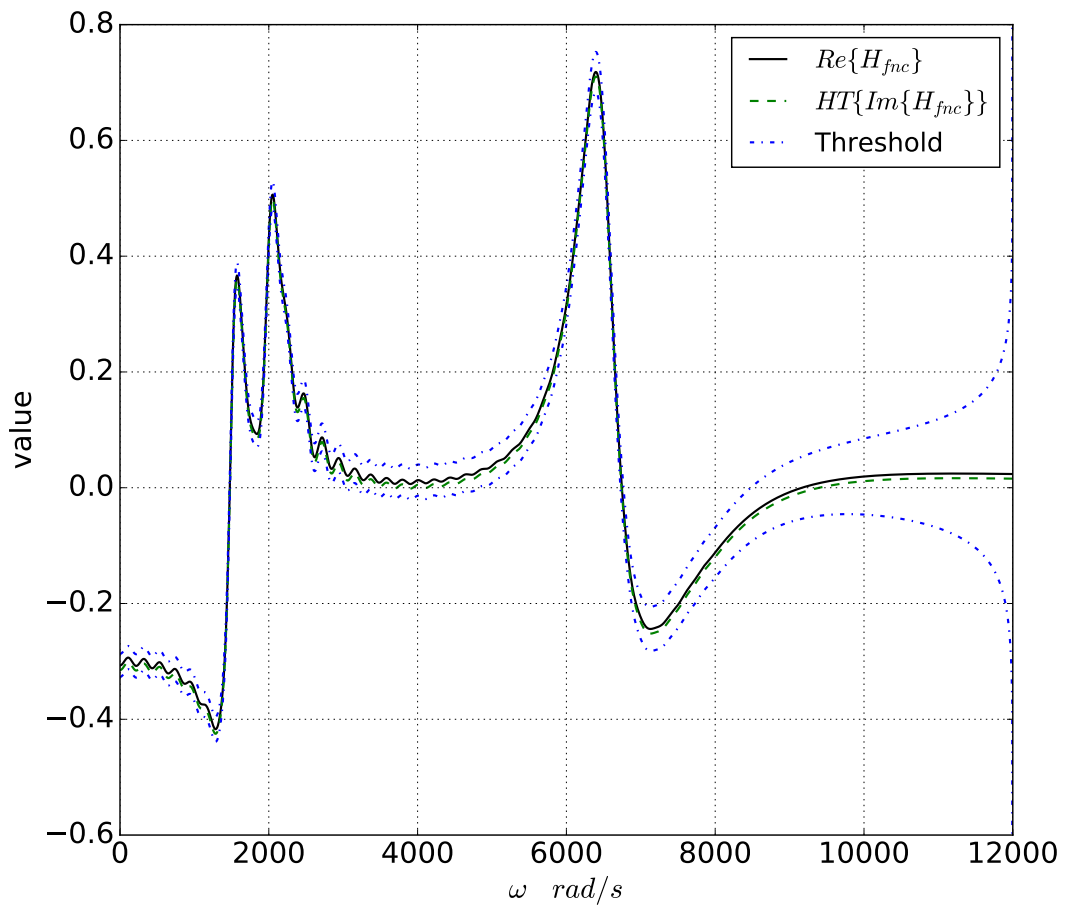


Figure 5.16: Enforcing causality by Option B using Three-point Extrapolation. Here, the reconstruction does not fully match, but stays within the threshold limit. Filter parameters: $nn = 3$ and $rp = 3$ dB. Here, $\omega_{max} = 8000$ rad/s, $\omega_{ex} = 12000$ rad/s.

Both the options generate a modified system that is causal according to the methodology described in our paper so far. However, our experiments show that if we follow option A, the reconstructed imaginary part matches perfectly with the original real part. Since we are replacing either the original real or imaginary part of the non-causal response, an amount of error will be introduced. The magnitude of the error depends on the amount of non-causality existing in the system. We can represent the error due to the enforcement graphically for option A (see Fig. 5.17) and option B (see Fig. 5.18). We can see from the plots that the error is maximum around $\omega = 2500 \text{ rad/s}$, which is the location of the non-causal pole.

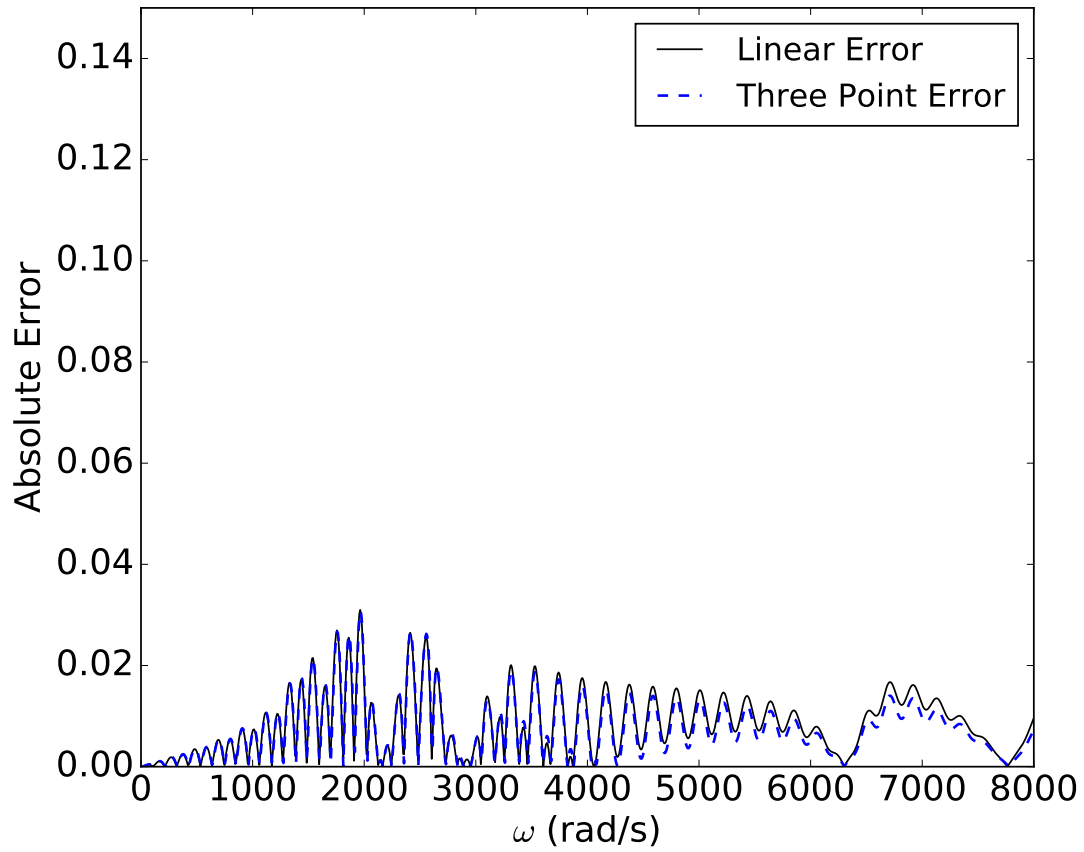


Figure 5.17: Absolute error reported from Enforcing causality by Option A (Both linear and three-point extrapolation. Filter specification are as in Fig. 5.15.

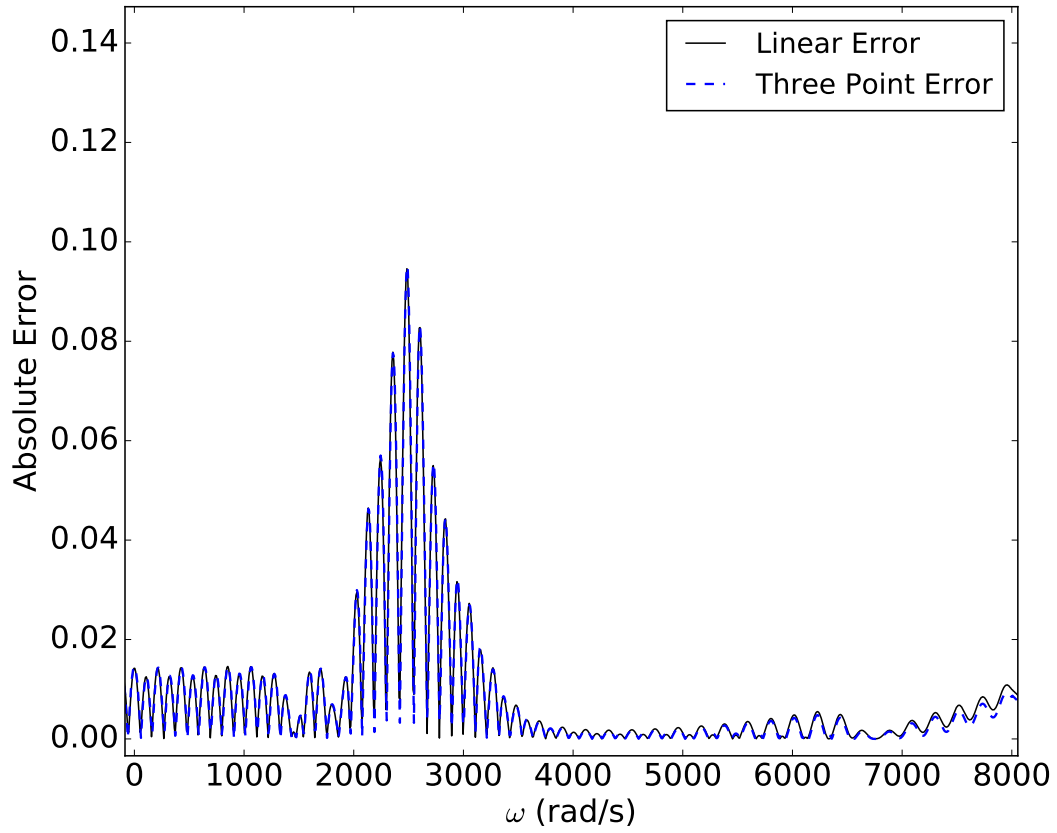


Figure 5.18: Absolute error reported from Enforcing causality by Option B (Both linear and three-point extrapolation). Filter specification are as in Fig. 5.16.

5.8 Summary

In this chapter, we present a novel technique for causality verification and enforcement in the frequency-domain. Previous works have been shown to be sensitive on certain parameters, especially in time-domain technique involving inverse Fourier Transform suffers from over-sensitivity of filter parameters. The proposed technique suffers less from filter parameters, as the cutoff frequency is set at a fixed point (at the maximum available frequency), which also prevents valuable data attenuation. Generalized Hilbert transformation using subtraction points also suffer from the sensitivity of the location of subtraction points, whereas the proposed technique does not require any subtractions points. The subtraction method is fairly complicated to implement, whereas our proposed technique is simple and easy to implement. Moreover, the complexity of operation is significantly reduced in this technique. Additionally, it provides a useful way to perform causality enforcement as well. However, the method is still sensitive to filter order and pass-band ripple, which can be considered as a drawback of this technique. Although for most cases, the configuration that we specified in this chapter should produce accurate results. Full automation of the filter specification is a topic for future research.

CHAPTER 6

Summary and Conclusions

In this thesis, I have addressed an important characteristic for signal/power integrity for high speed digital circuits. Verification of causality for macro-models is an important task for ensuring convergent transient simulation. An actual physical system is bound to possess causality, although several issues may compromise the construction of a successful model such as error in measurement or numerical simulation inaccuracy.

We have tested several techniques and discussed their advantages/disadvantages in detecting causality violations. Specially, the newly proposed filtering technique has been analyzed in details. The main drawback of this technique is the dependency of the threshold value on the cutoff frequency of the filter. Additionally, it is not clear how far back in negative time the impulse response must be checked to conclusively demonstrate causality. Moreover, the effect of maximum frequency available for sampled data can significantly affect the detection of non-causality. The fundamental issues associated with this technique has to be addressed in order to apply this technique effectively.

We have analyzed the frequency-domain causality verification and enforcement techniques based on the Generalized Hilbert Transform with subtractions thoroughly. For this method, the detection threshold is largely dependent on the number and location of the subtraction points. The threshold value is largely dependent on the number and location of subtraction points. These parameters have to be carefully chosen in order to correctly implement this work. Due to the complexity of the algorithm, long run time of this method makes it impractical for large systems.

The newly proposed method, which is the main contribution of this thesis, provides effective solutions to some of the issues of the existing methods of causality testing. It has less dependency on filter parameters, and the threshold value is more stable than the previous methods. The method is simpler and faster compared to the subtraction method,

which makes it suitable to apply on large systems. The method also provides a way to enforce causality on non-causal systems with minimum error introduced. Although, the threshold value may become too narrow or too wide if filter order and ripple are chosen inappropriately.

It is worth noting that, there is still scope for future extension to this work. In this work, we show that the proposed method is free from the sensitivity that arises from the filter cutoff frequency. The order and ripple has a strong impact on the threshold value as well. Although we demonstrate that for most cases, the method is effective for the specified range of filter parameters. Further research is needed to fully automatize these parameters.

We also explain in details why we use extrapolation for producing accurate results. Other extrapolation methods can be tested to see which method produces better result in detecting causality. Upon our investigation, we have identified that when the extrapolated data is decaying, direct Hilbert Transform converges. One can certainly utilize this property of the transform to ensure convergence of simulation.

Bibliography

- [1] M. Tsiklauri, M. Zvonkin, N. Dikhaminjia, J. Fan, and J. Drewniak, “Stable recursive convolution for channel response calculation with causality enforcement,” in *Proc. IEEE Electrical Design of Advanced Packaging and Systems Symposium (EDAPS)*, 2015, pp. 31–34.
- [2] S. Min and M. Swaminathan, “Construction of broadband passive macromodels from frequency data for simulation of distributed interconnect networks,” *IEEE Transactions on Electromagnetic Compatibility*, vol. 46, pp. 544–558, 2004.
- [3] R. Achar and M. S. Nakhla, “Simulation of high-speed interconnects,” *Proceedings of the IEEE*, vol. 89, pp. 693–728, 2001.
- [4] P. Triverio, S. Grivet-Talocia, M. Nakhla, F. Canavero, and R. Achar, “Stability, causality, and passivity in electrical interconnects models,” *IEEE Trans. Adv. Packag.*, vol. 30, pp. 795–808, 2007.
- [5] M. Doyle, R. Mandrekar, and J. Morsey, “Techniques and considerations for verification of model causality,” in *IEEE 61st Electronic Components and Technology Conference (ECTC)*, Lake Buena Vista, FL, June 2011, pp. 488–494.
- [6] T. R. Arabi, A. T. Murphy, T. K. Sarkar, R. F. Harrington, and A. R. Djordjevic, “On the modeling of conductor and substrate losses in multiconductor, multielectric transmission line systems,” *IEEE transactions on microwave theory and techniques*, vol. 39, no. 7, pp. 1090–1097, 1991.
- [7] J. He, N. Nahman, and S. Riad, “A causal skin-effect model of microstrip lines,” in *Microwave Symposium Digest, 1993., IEEE MTT-S International*. IEEE, 1993, pp. 865–868.

- [8] S. Hall, T. Liang, H. Heck, and D. Shykind, "Modeling requirements for transmission lines in multi-gigabit systems," in *IEEE 13th Topical Meeting on Electrical Performance of Electronic Packaging*. IEEE, 2004, pp. 67–70.
- [9] B. Young and A. S. Bhandal, "Causality checking and enhancement of 3d electromagnetic simulation data," in *19th Topical Meeting on Electrical Performance of Electronic Packaging and Systems*. IEEE, 2010, pp. 81–84.
- [10] H. M. Nussenzveig, *Causality and Dispersion Relations*. New York: Academic Press, 1972.
- [11] L. Brillouin, *Wave Propagation in Periodic Structures Electric Filters and Crystal Lattices*. 2nd ed. New York: Dover, 1953.
- [12] T. H. Havelock, *The Propagation of Disturbances in Dispersive Media*. Cambridge. UK: Univ. Press, 1914.
- [13] R. Krönig, "On the theory of dispersion of x-rays," *J. Opt. Soc. Amer.*, vol. 12, pp. 547–557, 1926.
- [14] H. A. Kramers, "La diffusion de la lumière par les atomes," in *Collected Scientific Papers*, Amsterdam, The Netherlands: North-Holland, 1956.
- [15] E. C. Titchmarsh, *Introduction to the Theory of Fourier Integrals*. London, U.K: Oxford Univ. Press, 1948.
- [16] G. Antonini, A. Orlandi, and V. Ricchiuti, "Causality check for si data validation," in *Proceedings. 9th IEEE Workshop on Signal Propagation on Interconnects*, 2005, pp. 155 – 158.
- [17] F. M. Tesche, "On the use of the hilbert transform for processing measured cw data," *IEEE Transactions on Electromagnetic Compatibility*, vol. 34, pp. 259–266, 1992.

- [18] M. M. Rao, T. K. Sarkar, T. Anjali, and R. S. Adve, "Simultaneous extrapolation in time and frequency domains using hermite expansions," *IEEE Transactions on Antennas and Propagation*, vol. 47, no. 6, pp. 1108–1115, 1999.
- [19] H. Boche and M. Protzmann, "A new algorithm for the reconstruction of bandlimited functions and their hilbert transform," *IEEE transactions on instrumentation and measurement*, vol. 46, no. 2, pp. 442–444, 1997.
- [20] B. Gustavsen and A. Semlyen, "Rational approximation of frequency domain responses by vector fitting," *IEEE Transactions on power delivery*, vol. 14, no. 3, pp. 1052–1061, 1999.
- [21] J. D. Jackson, *Classical Electrodynamics*. 2nd ed. New York: Wiley, 1975.
- [22] H. W. Bode, "Relations between attenuation and phase in feedback amplifier design," *Bell Sys. Tech. J.*, vol. 19, pp. 421–454, 1940.
- [23] E. Feenberg, "The scattering of slow electrons by neutral atoms," *Phys. Rev.*, vol. 40, pp. 40–54, 1932.
- [24] G. E. Pake and E. M. Purcell, "Line shapes in nuclear paramagnetism," *Phys. Rev.*, vol. 74, pp. 1184–1188, 1948.
- [25] V. L. Ginzberg, "Concerning the general relationship between absorption and dispersion of sound waves," *Sov. Phys. Acoust.*, vol. 1, pp. 32–41, 1955.
- [26] V. Mangulis, "Kramers-kronig or dispersion relations in acoustics," *J. Acoust. Soc. Amer.*, vol. 36, pp. 211–212, 1964.
- [27] W. Heisenberg, *Z. Phys.*, vol. 120, p. 513, 1943.
- [28] J. Wheeler, "On the mathematical description of light nuclei by the method of resonating group structure," *Phys. Rev.*, vol. 52, p. 1107, 1937.

- [29] W. Schützer and J. Tiomno, “On the connection of the scattering and derivative matrices with causality,” *Phys. Rev.*, vol. 83, p. 249, 1951.
- [30] N. G. van Kampen, “S matrix and causality condition. ii. nonrelativistic particles,” *Phys. Rev.*, vol. 91, p. 1267, 1953.
- [31] D. K. Cheng, *Analysis of Linear Systems*. Reading, MA: Addison-Wesley, 1959.
- [32] E. A. Guillemin, *The Mathematics of Circuit Analysis*. MIT Press, 1949.
- [33] F. M. S-PARAMETERS and H. KONDOH, “Microwave technology division santa rosa, ca 95401,” 1986.
- [34] M. Sugawara and A. Kanazawa, “Subtractions in dispersion relations,” *Physical Review*, vol. 123, pp. 1895–1902, 1961.
- [35] W. S. Woolcock, “Subtractions in dispersion relations,” *Physical Review*, vol. 153, pp. 1449–1454, 1967.
- [36] K. F. Palmer, M. Z. Williams, and B. A. Budde, “Multiply subtractive kramers–kronig analysis of optical data,” *Applied optics*, vol. 37, no. 13, pp. 2660–2673, 1998.
- [37] V. Lucarini, J. J. Saarinen, and K.-E. Peiponen, “Multiply subtractive generalized kramers–kronig relations: Application on third-harmonic generation susceptibility on polysilane,” *The Journal of chemical physics*, vol. 119, no. 21, pp. 11 095–11 098, 2003.
- [38] R. Ahrenkiel, “Modified kramers–kronig analysis of optical spectra,” *JOSA*, vol. 61, no. 12, pp. 1651–1655, 1971.
- [39] P. Triverio and S. Grivet-Talocia, “A robust causality verification tool for tabulated frequency data,” in *IEEE 10th Workshop Signal Propag. Interconnects*, 2006, pp. 65–68.

- [40] —, “On checking causality of bandlimited sampled frequency responses,” in *Ph.D. Research in Microelectronics and Electronics*, Otranto, Italy, 2006, pp. 501 – 504.
- [41] —, “Robust causality characterization via generalized dispersion relations,” *IEEE Trans. Adv. Packag.*, vol. 31, pp. 579–593, 2008.
- [42] W. Martin, J. Bartley, M. Doyle, R. Ericson, and G. Zettles, “Non-causal behavior: The cause for concern,” *Proc. IEEE 62nd Conf. Electr. Compon. Technol.*, pp. 1886–1892, 2012.
- [43] S. Lalgudi, “On checking causality of tabulated s-parameters,” *IEEE Transactions on Components, Packaging and Manufacturing Technology*, pp. 1204 – 1217, 2013.
- [44] B. S. Xu, X. Y. Zeng, J. He, and D. ho Han, “Checking causality of interconnects through minimum-phase and all-pass decomposition,” in *Proceedings. Conference on High Density Microsystem Design and Packaging and Component Failure Analysis*, 2006, pp. 67 – 69.
- [45] S. Asgari, S. N. Lalgudi, , and M. Tsuk, “Analytical integration-based causality checking of tabulated s-parameters,” *Proc. IEEE Conf. Electr. Perform. Electron. Packag.*, pp. 189–192, 2010.
- [46] S. N. Lalgudi, S. Asgari, and M. Tsuk, “Improved procedure to test causality of tabulated s-parameters,” *Proc. IEEE 21st Conf. Electr. Perform. Electron. Packag. Syst.*, pp. 191–194, 2012.
- [47] S. Kim, G. Luevano, K. Roselle, and T. Michalka, “Quality assurance of s-parameters and rational function models for transient simulations,” in *IEEE Symposium on Electromagnetic Compatibility and Signal Integrity*, Santa Clara, CA, Mar. 15-21, 2015.
- [48] Y. Shlepnev, “Quality metrics for s-parameter models,” in *DesignCon*, Santa Clara, CA, 2010.

- [49] M. Tsiklauri, M. Zvonkin, J. Fan, J. Drewniak, Q. B. Chen, and A. Razmadze, “Causality and delay and physics in real systems,” in *Proc. IEEE International Symposium on Electromagnetic Compatibility (EMC)*, 2014, pp. 961 – 966.
- [50] P. Triverio, “Robust causality check for sampled scattering parameters via a filtered fourier transform,” *IEEE Microw. Wireless Compon. Lett.*, pp. 72–74, 2014.
- [51] —, “Reliable detection of causality violations in tabulated scattering parameters through filtered dispersion relations,” in *22nd Conference on Electrical Performance of Electronic Packaging and Systems (EPEPS)*, San Jose, CA, Oct. 27-30, 2013.
- [52] —, “An accurate, robust and intuitive technique to detect causality violations in broadband frequency measurements,” in *IEEE International Symposium on Electromagnetic Compatibility (EMC 2014)*, Raleigh, NC, Aug. 4-8, 2014.
- [53] M. A. Hoque and A. Zadehgol, “On the sensitivity of causality filter parameters,” in *IEEE Electrical Design of Advanced Packaging and Systems (EDAPS)*, Hawaii, USA, Dec. 14-16, 2016.
- [54] R. E. Clapp, “Enforcing causality in numerical solutions of maxwell’s equations,” *Proceedings of the IEEE*, vol. 56, p. 329, 1968.
- [55] T. R. Arabi and R. Suarez-Gartner, “Time domain analysis of lossy multi-conductor transmission lines using the hilbert transform,” in *Proc. IEEE MTT-S International Microwave Symposium Digest*, vol. 2, 1993, pp. 987–990.
- [56] T. R. Arabi, A. T. Murphy, and T. K. Sarkar, “An efficient technique for the time-domain analysis of multi-conductor transmission lines using the hilbert transform,” in *Proc. IEEE MTT-S International Microwave Symposium Digest*, vol. 1, 1992, pp. 185–188.

- [57] S. M. Narayana, G. Rao, R. Adve, T. K. Sarkar, V. C. Vannicola, M. C. Wicks, and S. A. Scott, "Interpolation/extrapolation of frequency domain responses using the hilbert transform," *IEEE Trans. Microw. Theory Tech.*, vol. 14, pp. 1621–1627, 1996.
- [58] P. Triverio and S. Grivet-Talocia, "Causality-constrained interpolation of tabulated frequency responses," in *Proc. IEEE MTT-S Dig., 15th IEEE Conf. Elect. Perform. Electron. Packag.*, 2006, pp. 181–184.
- [59] R. Mandrekar and M. Swaminathan, "Causality enforcement in transient simulation of passive networks through delay extraction," in *Proc. 9th IEEE Workshop on Signal Propagation on Interconnects*, 2005, pp. 25–28.
- [60] C. Morgan, "Solutions for causal modeling and a technique for measuring, causal, broadband dielectric properties," in *Proc. of DesignCon*, 2008.
- [61] S. Roy and A. Dounavis, "Transient simulation of distributed networks using delay extraction based numerical convolution," *IEEE Transactions on Computer-Aided Design of Integrated Circuits and Systems*, vol. 30, pp. 364–373, 2011.
- [62] S. Luo and Z. Chen, "Iterative methods for extracting causal time-domain parameters," *IEEE Transactions on Microwave Theory and Techniques*, vol. 53, pp. 969–976, 2005.
- [63] E. Song, J. Cho, J. Kim, and D. G. Kam, "Causality enforcement in transient simulation of hdmi interconnects with magnitude equalization," in *Proc. IEEE International Symposium on Electromagnetic Compatibility*, 2007, pp. 1–4.
- [64] R. Mandrekar, K. Srinivasan, E. Engin, and M. Swaminathan, "Causal transient simulation of passive networks with fast convolution," in *Proc. IEEE Workshop on Signal Propagation on Interconnects*, 2006, pp. 61–64.
- [65] S. N. Lalgudi, E. Engin, G. Casinovi, and M. Swaminathan, "Accurate transient simulation of interconnect characterized by band-limited data with propagation delay enforce-

- ment in a modified nodal analysis framework,” *IEEE Trans. Electromag. Compatibility*, vol. 50, pp. 715–729, 2008.
- [66] F. Rao, C. Morgan, S. Gupta, and V. Borich, “The need for impulse response models and an accurate method for impulse generation from band-limited s-parameters,” in *DesignCon*, 2008.
- [67] F. Rao, “Optimization of spectrum extrapolation for causal impulse response calculation using the hilbert transform,” U.S. Patent 7 962 541, Jun. 14, 2011.
- [68] K. N. van Dalen, E. Slob, and C. Schoemaker, “Generalized minimum-phase relations for memory functions associated with wave phenomena,” *Geophysical Journal International*, vol. 195, pp. 1620–1629, 2013.
- [69] J. Bechhoefer, “Kramers-kronig, bode, and the meaning of zero,” *American Journal of Physics*, vol. 79, pp. 1053–1059, 2011.
- [70] A. V. Oppenheim and R. W. Schaffer, *Digital Signal Processing*. 3rd ed. NJ: Prentice Hall, 1975.
- [71] E. W. Matthews, “The use of scattering matrices in microwave circuits,” *IRE Trans. Microw. Theory Techn*, vol. 3, pp. 21–26, 1955.
- [72] M. Wohlers and E. Beltrami, “Distributions and the boundary values of analytic functions,” DTIC Document, Tech. Rep., 1967.
- [73] M. Abramowitz, I. A. Stegun *et al.*, “Handbook of mathematical functions,” *Applied mathematics series*, vol. 55, no. 62, p. 39, 1966.
- [74] E. J. Beltrami and M. R. Wohlers, *Distributions and the boundary values of analytic functions*. Academic Press, 2014.

- [75] W. Güttinger, “Generalized functions in elementary particle physics and passive system theory: recent trends and problems,” *SIAM Journal on Applied Mathematics*, vol. 15, no. 4, pp. 964–1000, 1967.
- [76] P. J. Davis and P. Rabinowitz, “Methods of numerical integration,” 1984.
- [77] E. H. Bareiss and C. P. Neuman, “Singular integrals and singular integral equations with a cauchy kernel and the method of symmetric pairing,” Argonne National Lab., Ill., Tech. Rep., 1965.
- [78] N. Ioakimidis, “One more approach to the computation of cauchy principal value integrals,” *Journal of Computational and Applied Mathematics*, vol. 7, no. 4, pp. 289–291, 1981.
- [79] I. Longman, “A method for the numerical evaluation of finite integrals of oscillatory functions,” *Mathematics of Computation*, vol. 14, no. 69, pp. 53–59, 1960.
- [80] C. E. Stewart, “On the numerical evaluation of singular integrals of cauchy type,” *Journal of the Society for Industrial and Applied Mathematics*, vol. 8, no. 2, pp. 342–353, 1960.
- [81] X. Wang, “Numerical implementation of the hilbert transform,” Ph.D. dissertation, Citeseer, 2006.
- [82] V. Cizek, “Discrete hilbert transform,” *IEEE Transactions on Audio and Electroacoustics*, vol. 18, no. 4, pp. 340–343, 1970.
- [83] V. Avula and A. Zadehgol, “Pole residue equivalent system solver (press),” in *Signal and Power Integrity (SPI), 2016 IEEE 20th Workshop on*. IEEE, 2016, pp. 1–4.
- [84] A. Zadehgol, “A semi-analytic and cellular approach to rational system characterization through equivalent circuits,” *International Journal of Numerical Modelling: Electronic Networks, Devices and Fields*, 2015.